



Technische Universität München

TUM School of Medicine and Health

Role of CD44 in the regulation of oncogenic YAP in Hepatocellular carcinoma

Saumya Sukumary Manmadhan

Vollständiger Abdruck der von der TUM School of Medicine and Health
der Technischen Universität München zur Erlangung einer

Doktorin der Naturwissenschaften (Dr. rer. nat.)
genehmigten Dissertation

Vorsitz: Prof. Dr. Marc Schmidt-Supprian

Prüfende der Dissertation:

1. Priv.-Doz. Dr. Ursula Ehmer, Ph.D.
2. Prof. Dr. Gabriele Multhoff

Die Dissertation wurde am 18.04.2024 bei der Technischen Universität
München eingereicht und durch die TUM School of Medicine and Health am
07.08.2024 angenommen.

Contents

List of Tables.....	6
List of Figures.....	7
List of Acronyms.....	9
1. Abstract	12
2. Zusammenfassung	14
3. Introduction.....	16
3.1 Cancer – a long and continuous fight.....	16
3.2 International trends in the epidemiology of HCC	16
3.3 Staging of HCC	18
3.4 Therapeutic strategies to treat primary liver cancer	19
3.5 Major Hallmarks of HCC	20
3.6 Molecular classification of HCC.....	21
3.7 Role of cancer stem cells in liver cancer	21
3.8 Signaling pathways regulating CSCs in HCC.....	23
3.9 CD44 and liver cancer.....	25
3.10 Hippo signaling in the liver	27
3.11 Role of YAP/TAZ in liver tumorigenesis	29
3.12 Hippo signaling co-operates with other major cellular biological mechanisms to regulate YAP/TAZ.....	30
3.13 Hippo-independent regulation of YAP	31
3.13.1 Tyrosine phosphorylation.....	31
3.13.2 Nuclear-cytoplasmic YAP/TAZ distribution by regulation of nuclear export and import.....	31
3.14 YAP/TAZ regulation by deubiquitination.....	32
3.15 Regulation of YAP mediated by CD44	33
3.16 Pre-clinical or translational research on HCC.....	34
3.16.1 <i>In -vitro</i> HCC models	34
3.16.2 Animal Models of Human HCC.....	34

3.16.3	Genetically engineered mice	35
3.16.4	Chemically induced models	37
3.16.5	Engrafted mouse models of HCC	38
3.17	Background data associated with the project	38
3.17.1	Rb family conditional triple knock-out (<i>TKO</i>) HCC mouse model	38
4	Aim and hypothesis	41
4.1	Elucidating the role of CD44 in regulating oncogenic YAP in liver cancer cells <i>in vitro</i>	41
4.2	The role of CD44 in the HCC development <i>in vivo</i>	41
4.3	Relevance of the CD44-YAP axis in murine and human hepatocellular carcinoma	41
5	Materials	43
5.1	Technical equipment	43
5.2	Consumable supplies	45
5.3	Reagent	46
5.4	PCR Primers for genotyping	48
5.5	Primers for quantitative real-time PCR (qPCR)	49
5.6	Primer list for Cd44 CRISPR constructs	50
5.7	Antibodies	50
5.8	Molecular biology kits	51
5.9	Cell Culture	52
6	Methods	54
6.1	Mice	54
6.1.1	Mouse models	54
6.1.2	Mouse breeding and genotyping	55
6.1.3	Intrasplenic injection of adenovirus	55
6.2	Cell culture	56
6.2.1	Cryopreservation of cells	56
6.2.2	Lentivirus-mediated transduction with CRISPR constructs	56
6.2.3	Plasmid DNA isolation	57
6.2.4	Midi and Maxi preparation	58
6.2.5	Single colony isolation from infected cells	58

6.2.6	Proliferation assay using MTT	58
6.2.7	Colony formation assay (clonogenic assay)	59
6.3	Immunofluorescence staining.....	60
6.4	Molecular Biology.....	61
6.4.1	Genomic DNA isolation.....	61
6.4.2	Polymerase chain reaction (PCR)	61
6.4.3	Detection of DNA bands by agarose gel electrophoresis	62
6.4.4	Gel extraction and PCR purification.....	63
6.4.5	RNA extraction and cDNA synthesis	63
6.4.6	Quantitative real-time PCR (qPCR)	63
6.5	Biochemistry.....	64
6.5.1	Protein extraction.....	64
6.5.2	Protein Concentration Estimation	64
6.5.3	SDS Polyacrylamide gel electrophoresis (SDS-PAGE)	65
6.5.4	Western blot	66
6.5.5	Statistical analysis	67
7	Results.....	68
7.1	Positive correlation between CD44 and YAP in the <i>TKO</i> mouse model and other human HCC mouse models.....	68
7.2	CRISPR/Cas9-based <i>Cd44</i> inactivation reduces <i>TKO</i> liver cancer cell proliferation	69
7.3	<i>Cd44</i> ablation in <i>TKO</i> cell lines negatively regulates YAP expression	74
7.4	<i>Cd44</i> -mutant <i>TKO</i> cells showed nuclear exclusion of YAP	76
7.5	<i>Cd44</i> mutation increased expression of senescence marker p16.....	78
7.6	Mechanism of action within the CD44-YAP axis	81
7.7	Rho-A is crucial for CD44-mediated YAP regulation.....	83
7.8	CD44 mutation in <i>TKO</i> liver cancer cells induces changes in cell morphology and adhesion	86
7.9	The chemical induction of HCC in <i>Cd44</i> ^{-/-} mice demonstrated reduced tumor burden.....	88
7.10	Adeno-Cre injection into <i>TKO</i> and <i>TKO</i> ; <i>Cd44</i> ^{-/-} mice	91
7.11	Correlation of CD44 and YAP expression in human HCC samples	92
8	Discussion	94

9	Conclusions	100
	Acknowledgments	101
	References	102

List of Tables

Table 1: Technical equipment	43
Table 2: Consumable supplies	45
Table 3: Reagents	46
Table 4: Genotyping PCR primers	48
Table 5: Primers for qPCR	49
Table 6: Primer list for <i>Cd44</i> guide RNA (<i>gRNA</i>) constructs	50
Table 7: Primary and secondary antibodies used in this study.....	50
Table 8: Kits used for molecular biology.....	51
Table 9: Cell culture medium and medium composition	52
Table 10: Lentiviral transfection mixture.....	52
Table 11: TENSV Buffer- 60 ml recipe	53
Table 12: HBS 2x (HEPES Buffered saline) Buffer	53
Table 13: Cell lysis buffer	53
Table 14: Immunofluorescence assay primary antibody dilution	61
Table 15: Immunofluorescence assay secondary antibody dilution	61
Table 16: Genotyping PCR recipe.....	62
Table 17:Composition of running gel.....	66
Table 18: Composition of stacking gel.....	66

List of Figures

Figure 1: Bar graph showing HCC incidence worldwide stratified by gender	17
Figure 2 : Overview of the BCLC staging system in HCC	19
Figure 3: Regulatory mechanisms of liver cancer stem cells.....	23
Figure 4: Model of HCC progression from Cancer stem cells (CSCs).....	25
Figure 5 : Schematic representation of Hippo signaling pathway components in drosophila and mammals	28
Figure 6 : HCC induction in TKO mouse model	39
Figure 7: Immunohistochemistry staining of tumor precursor lesion near the portal triad in TKO livers 4-5 weeks after tumor induction.....	40
Figure 8: Microarray analysis of TKO tumor.....	68
Figure 9: Immunohistochemistry staining of HCC mouse models	69
Figure 10 : MTT assay in mixed population of <i>TKO</i> liver cancer cell line after <i>Cd44</i> CRISPR edition.	70
Figure 11: Schematic representation of single cell clone derivation from <i>Cd44</i> mutant mixed populations.	71
Figure 12: <i>Cd44</i> inactivation in TKO2.1 cells derived from <i>TKO</i> tumor	72
Figure 13: Cell viability analysis of <i>Cd44</i> -mutant cells by MTT assay	73
Figure 14: <i>Cd44</i> inactivation downregulates YAP expression	74
Figure 15: Relative mRNA expression of YAP target genes	75
Figure 16: Immunofluorescence staining of YAP in <i>Cd44</i> mutant cells and control TKO2.1 cell lines	77
Figure 17: Quantification of YAP staining.....	78
Figure 18: Immunofluorescence staining for p16 in control and <i>Cd44</i> -mutant TKO2.1 cells	80
Figure 19: Candidate signaling pathways are downregulated in <i>Cd44</i> -mutant cells	81
Figure 20: Proliferation analysis of TKO control cells and <i>Cd44</i> -mutant cells after inhibitor treatments.....	82
Figure 21 : Rhosin treatment in TKO2.1 liver cancer cells in varied concentrations.....	84

Figure 22: CD44 mediated YAP regulation is Rho-A dependent.....	85
Figure 23: YAP protein expression analysis after rhosin treatment in TKO liver cancer cells.....	86
Figure 24: Cell morphology of TKO control cells and Cd44-mutants cells.....	87
Figure 25: Chemical induction of HCC in C57/Bl6 and Cd44 ^{-/-} mice using DEN.....	89
Figure 26: IHC Staining of CD44 and YAP in liver extracted from DEN mice.....	90
Figure 27: Quantification of liver tumor burden in livers of DEN-treated mice.....	91
Figure 28 : Histological staining of liver sections of Ad-Cre injected mice.....	92
Figure 29: Hematoxylin-eosin (H&E) staining and immunohistochemical staining of human HCC tissue.....	93

List of Acronyms

°C	Degree celcius
µg	Microgram
µl	Microlitre
µM	Micromolar
µm	Micrometer
AGE	Agarose gel electrophoresis
Amotl2	Angiomotin like 2
ANKRD1	Ankyrin repeat domain-containing protein 1
APS	Ammonium persulphate
BCA	Bicinchoninic acid
Bp	Base pair
BSA	Bovine serum albumin
Cas9	CRISPR-associated 9 endonuclease
Cd44	Cluster of differentiation 44 gene/protein
cDNA	Complementary DNA
CreER	Inducible Cre recombinase
CRISPR	Clustered regularly interspaced short palindromic repeats
CTGF	Connective growth factor
cTKO	Conditional triple knockout Rblox/lox; p130lox/lox; p107-/-
Cyr61	Cysteine-rich angiogenic inducer 61
DAPI	4',6-diamidino-2-phenylindole
DEN	Di-ethyl nitrosamine
DMEM	Dulbecco´s modified Eagle medium
DMSO	Di-methyl sulphoxide
DNA	Deoxyribonucleic acid
<i>E. coli</i>	Escherichia coli
ECL	Enhanced chemiluminescence
EDTA	Ethylenediaminetetraacetic acid
EtOH	Ethanol
FCS	Fetal Calf serum
g	Gram
GAPDH	Glyceraldehyde 3-phosphate dehydrogenase
GFP	Green fluorescent protein
GSEA	Gene set enrichment analysis
h	Hours

H&E	Hematoxylin and eosin stain
HCC	Hepatocellular carcinoma
HEK	Human embryonic kidney
HRP	Horseradish peroxidase
i.p.	Intraperitoneal
IF	Immunofluorescence
IHC	Immunohistochemistry
Kda	Kilodalton
Kg	Kilogram
L	Liter
LATS1/2	Large tumor suppressor 1 and 2
LB	Luria bertani
M	Molar
MASLD	Metabolic dysfunction-associated steatotic liver disease
mg	Milligram
min	Minute
min	Minute
ml	Milliliter
mRNA	Messenger ribonucleic acid
MST1/2	Mammalian Ste20-like 1 and 2
MTT	3-(4,5-dimethylthiazol-2-yl)-2,5-diphenyl-2H-tetrazolium bromide
MW	Molecular weight
NAFLD	Non-alcoholic fatty liver disease
nM	Nanomolar
nm	Nanometer
OD	Optical density
PAGE	Polyacrylamide gel electrophoresis
PAM	Protospacer adjacent motif
PBS	Phosphate buffered saline
PCR	Polymerase chain reaction
PenStep	Penicillin streptomycin
PFA	Paraformaldehyde
pH	Power of hydrogen
PVDF	Polyvinylidene fluoride
qPCR	Quantitative real-time PCR
RB	Retinoblastoma gene
RIPA	Radioimmunoprecipitation assay buffer
RNA	Ribonucleic acid
RNA-Seq	RNA sequencing
RPM	Revolutions per minute

RPMI	Roswell Park memorial institute medium
RT	Room temperature
SD	Standard deviation
SDS	Sodium dodecyl sulphate
SEM	Standard error mean
SgRNA	Single guide RNA
Src	Rous sarcoma oncogene
STAT-3	Signal transducer and activator of transcription-3
SYBR	Synergy bands inc
TAE	Tris-acetate-edta
TAM	Tamoxifen
TBST	Tris-buffered saline Tween 20
TCGA	The cancer genome atlas
TEMED	Tetra-methylethylenediamine
temp	Temperature
TIDE	Tracking of indels by decomposition
TKO	Triple knockout of the Rb family
TRIS	Tris (Hydroxymethyl)aminomethane
WB	Western blot
YAP	Yes-associated protein
YFP	Yellow fluorescent protein

1. Abstract

The controlled homeostasis of cellular growth-promoting signaling events is essential for normal organ function. Irregularities in signaling cross-talks and feedback loops are often associated with uncontrolled cell division and organ failure. Chronic liver damage due to heavy alcohol consumption, infections with hepatitis B or hepatitis C viruses or metabolic dysfunction-associated steatotic fatty liver disease (MASLD) may lead to hepatocellular carcinoma (HCC), the most common primary liver cancer. The prognosis of HCC in patients remains poor since most cases are diagnosed at intermediate or advanced stages of the disease with no curative treatment options. The disruption of several liver signaling pathways plays a major role in the progression of hepatocellular carcinoma. Most human HCCs express high levels of YES-associated protein (YAP), a major oncogene in different cancers. Increased YAP levels promote expression of its downstream target genes including *CTGF*, *CYR61*, and *C-MYC* amongst other genes that have established roles in cellular proliferation. However, a direct association between the genetic alterations of Hippo signaling components and increased YAP levels in the liver has been rarely identified. Therefore, alternate pathways may exist that could regulate YAP expression independent of its major upstream regulatory Hippo signaling. Using a mouse model of HCC with a conditional triple knockout (*TKO*) of the *Rb* (Retinoblastoma) gene family, we demonstrated a positive correlation between the expression of YAP and a cancer stem cell marker, CD44, in liver tumor tissue. The *TKO* mouse model, in which *p107*, *p130*, and *Rb* are genetically inactivated in the liver provides a valuable resource for studying the molecular mechanisms involved in liver regeneration and tumorigenesis. This model has been utilized to explore the effects of various genetic and environmental factors and test potential liver cancer therapies. While CD44 has previously established roles in different cancers, its association with YAP expression and development of HCC has not been extensively studied. In our study, we are exploring the role of CD44 in the regulation of YAP expression patterns and its consequence in HCC progression using various *in vitro* methodologies as well as mouse models. Our experiments

using CRISPR/Cas9 mediated inactivation of CD44 in *TKO* mouse cancer cell lines showed downregulation of YAP target genes which was associated with reduced cell proliferation. Furthermore, we were able to show an influence of *Cd44* mutations on YAP nuclear localization and the molecular drivers within the CD44-YAP axis. The chemical induction of HCC by DEN (di-ethylnitrosamine) *in vivo* also confirmed the requirement of CD44 for HCC progression. Overall, these data suggest that CD44 might be a key regulator of YAP in HCC.

2. Zusammenfassung

Eine enge Kontrolle zellulärer Signalwege mit Relevanz für das Zellwachstum sind für eine normale Organfunktion unerlässlich. Eine Dysregulation von proliferationsrelevanten Signalwegen und Feedback-Loops werden häufig mit unkontrollierter Zellteilung und Organversagen in Verbindung gebracht. Chronische Leberschäden durch starken Alkoholkonsum, Infektionen mit Hepatitis-B- oder Hepatitis-C-Viren oder mit einer metabolischen Dysfunktion assoziierte Steatohepatitiden können zu einem hepatozellulären Karzinom (HCC) führen. Die Prognose von HCC-Patienten ist jedoch nach wie vor schlecht, da die meisten Fälle erst im intermediären oder fortgeschrittenen Stadium diagnostiziert werden, in denen keine kurativen Therapieoptionen mehr bestehen. Eine Dysregulation unterschiedlicher Signalwege in der Leber spielt eine wichtige Rolle bei der Entstehung des hepatozellulären Karzinoms. Die meisten humanen HCCs weisen hohe Expression des YES-assoziierten Proteins (YAP) auf, einem wichtigen Onkogen in zahlreichen Tumorentitäten. Eine YAP-Aktivierung geht mit einer gesteigerten Expression seiner nachgeschalteten Zielgene wie *CTGF*, *CYR61* und *C-MYC* einher sowie anderer Gene, die nachweislich an der Zellproliferation beteiligt sind. Ein direkter Zusammenhang zwischen den genetischen Veränderungen der Hippo-Signalkomponenten und erhöhten YAP-Konzentrationen in der Leber ist jedoch selten. Daher könnte es alternative Wege geben, die die YAP-Expression unabhängig vom Hippo-Signalweg regulieren könnten. Anhand eines Mausmodells für HCC mit einem konditionalen dreifachen Knockout (TKO) der *Rb* (Retinoblastom)-Genfamilie konnten wir eine positive Korrelation zwischen der Expression von YAP und einem Tumorstammzellmarker, CD44, im HCC-Gewebe nachweisen. Während CD44 bei verschiedenen Tumorentitäten eine Rolle spielt, ist sein Zusammenhang mit der YAP-Expression und der Entwicklung des HCC noch nicht umfassend untersucht. In dieser Arbeit wurde mittels verschiedener *in vitro*-Methoden und Mausmodelle die Rolle von CD44 bei der Regulation des YAP-Onkoproteins und die Auswirkungen auf die HCC-Progression untersucht. Unsere Experimente mit CRIPR/Cas9-vermittelter Inaktivierung von CD44 in murinen TKO-

Tumorzelllinien zeigten eine Herabregulation von YAP-Zielgenen, die mit einer verringerten Zellproliferation einhergeht. Darüber hinaus konnten wir einen Einfluss von CD44-Mutationen auf die nukleäre YAP-Lokalisation und die molekularen Treiber innerhalb der CD44-YAP-Achse nachweisen. Die chemische Induktion von HCC durch DEN (Di-Ethylnitrosamin) *in vivo* bestätigt ebenfalls eine Relevanz von CD44 bei der HCC-Progression. Insgesamt deuten diese Daten darauf hin, dass CD44 ein wichtiger Regulator von YAP im HCC sein könnte.

3. Introduction

3.1 Cancer – a long and continuous fight

The battle against diseases has been constant threat to human lives ever since mankind. Advancements in technology and medicine drastically improved the diagnosis and early treatment of the majority of diseases. However, cancer is one of the deadliest diseases humans are still fighting to achieve a complete cure which often miserably fails in the majority of cancer patients. Among the numerous entities of human cancer, primary liver cancer has been emerging as the second leading cause of cancer related deaths worldwide over the recent years (Petrick, Florio et al. 2020).

The most common type of primary liver cancer is hepatocellular carcinoma (HCC) (Global Burden of Disease Liver Cancer, Akinyemiju et al. 2017). Survival rates of patients are high only if it is diagnosed at an early or very early stage (Farinati, Sergio et al. 2009). Patients with long-term liver diseases like cirrhosis, which is often due to hepatitis-B or hepatitis-C viral infections as well as liver damage due to excessive alcohol consumption or metabolic dysfunction-associated steatotic liver disease (MASLD) are prone to HCC. The heterogeneous nature of HCC limits the options for targeted therapy and therefore a better understanding of different aspects of HCC formation is crucial to determine stable therapeutic strategies.

3.2 International trends in the epidemiology of HCC

Primary liver cancer accounts for seventh most frequently occurring cancer and the second most causes of cancer-related deaths globally, which is more predominant in men than women (Dasgupta, Henshaw et al. 2020). The prognosis of HCC is poor throughout the world and most cases are diagnosed at intermediate or advanced, stages.

There are demographic characteristics that determine the incidence of HCC. The prominent ones are age, sex and regional prevalence of risk factors such as HBV.

The median age of HCC onset varies between populations from different continents but it is directly proportional to increased age. In most of the countries, HCC incident rates are 2 – 4-fold higher in men than women (Ang, Shields et al. 2017). In Europe, HCC incident rates in men are 4-fold greater than in women. In some countries like Colombia and Uganda, the incidence rates in men and women are equal (Fig. 1) (Tang, Hallouch et al. 2018). According to the world statistics on HCC, Asia and Africa has the highest incidence rates compared to the rest of the world, most likely due to the high prevalence of HBV in these regions.

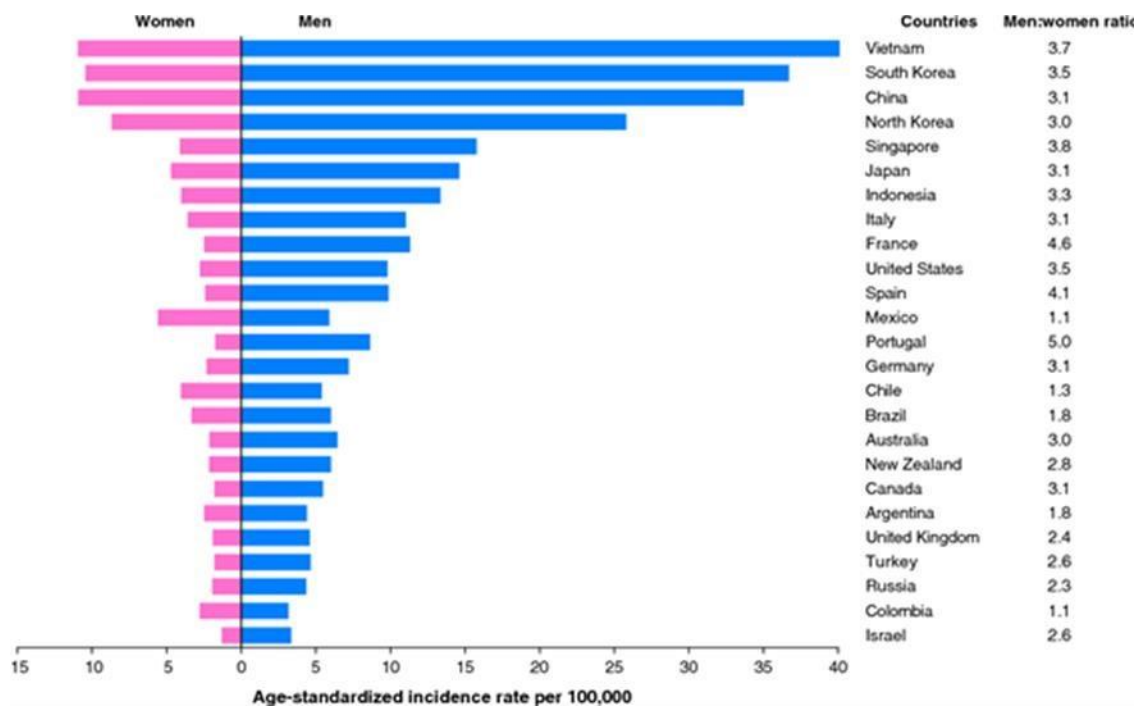


Figure 1: Bar graph showing HCC incidence worldwide stratified by gender

(Retrieved from Sirlin and Tang, 2018)

3.3 Staging of HCC

A staging system for cancer is important for the prognosis prediction in patients and for finding appropriate treatment strategies. It is also important for research and to establish a common language in clinical assessment (Bruix and Llovet 2002). Over the past decades, several staging systems have been developed for HCC. However, no staging system has been universally accepted due to the extreme heterogeneity of HCC and the existence of geographical variations across the world. In most of the other epithelial cancers, the TNM (Tumor, nodules and metastasis) staging system is widely used but only of limited use in stratifying patients with HCC for therapeutic decisions. As most HCCs develop due to underlying liver disease, the prognosis depends on multiple factors like size, number and location of tumors, the available functional reserve of the liver, the type of undergoing HCC treatment and the overall health of the patient (Marrero, Hussain et al. 2005). The ideal staging system needs to address all these aspects for an accurate prognosis. Although several staging systems have been developed over the past decades, only a few of them are widely used (Marrero, Fontana et al. 2005). The prognosis and treatment plans for HCC patients are currently made based on the Barcelona clinic liver cancer classification (BCLC) (Kinoshita, Onoda et al. 2015). The classification and parameters considered in the BCLC and staging systems are shown in Fig.2.

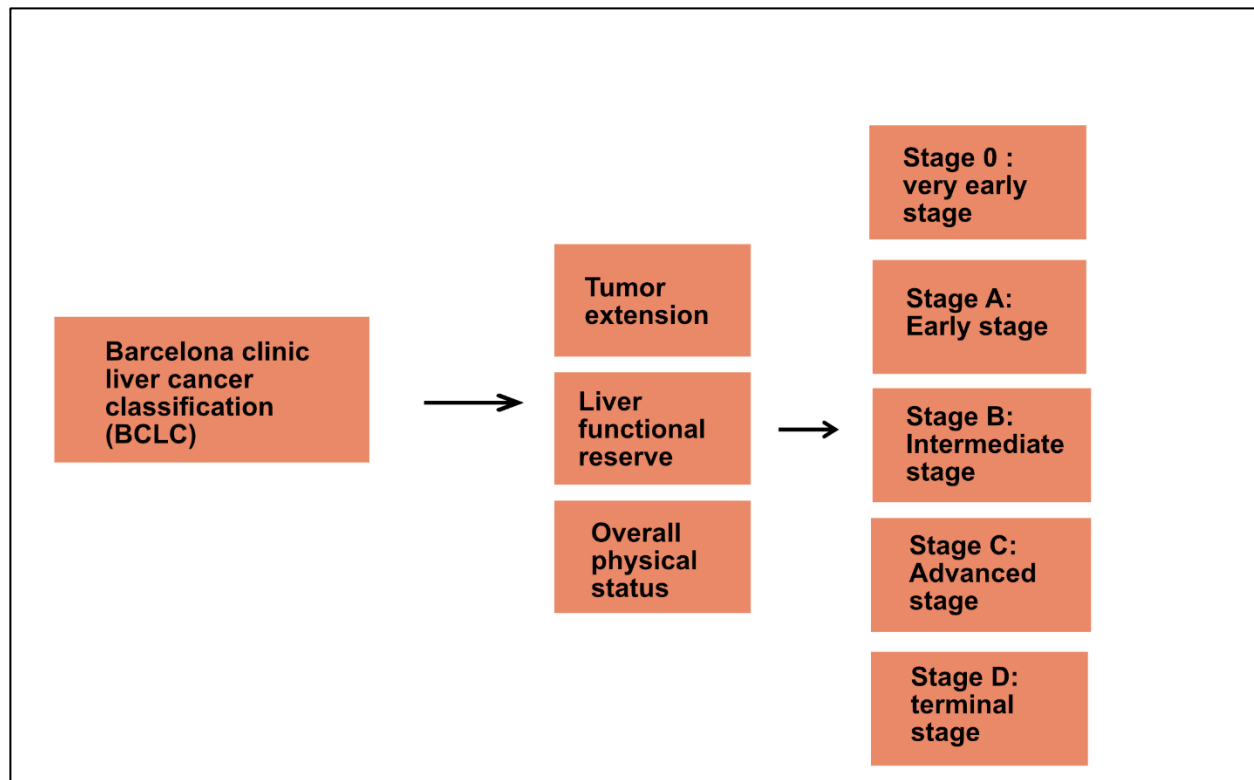


Figure 2 : Overview of the BCLC staging system in HCC

3.4 Therapeutic strategies to treat primary liver cancer

There are several treatment strategies for hepatocellular carcinoma. Based on the tumor stage, different approaches including surgical resection, percutaneous ablation, transplantation, interventional and different systemic therapies are usually performed (Reig, Forner et al. 2022). However, durable response rates in advanced tumor stages remain an exception and 5-year survival rates remain poor (Brar, Greten et al. 2020). Therefore, alternative treatment strategies are needed to improve survival rates.

3.5 Major Hallmarks of HCC

The process of progression and the different stages of any type of cancer exhibit one or more typical hallmarks. They are categorized based on six general features such as the ability to undergo: growth control escape, angiogenesis induction, continuous proliferation, tissue invasion, immunoevasion overcoming programmed cell death and unlimited replication (Hanahan and Weinberg 2011, Fouad and Aanei 2017). The hallmarks of HCC are also oriented on such typical features. However, a set of distinctive pathways is often found to be deregulated.

HCC likely occurs as a result of uninterrupted cellular proliferation through the deregulation of a series of cell cycle regulators mainly cyclin-dependent kinases (Cdks) (Malumbres, Harlow et al. 2009). Considering the regenerative ability of hepatocytes, any act leading to a bypassed cell proliferation due to the fluctuations in cyclin-dependent kinase downstream pathways, cyclin-dependent kinase inhibitors, or upregulation of cyclin-dependent kinases, could present a driver of hepatocarcinogenesis. Tumor progression mainly depends on resistance to the critical mechanisms that can limit excessive cell proliferation - apoptosis and senescence. Cirrhotic livers exhibit an impaired telomerase activity together with accelerated telomere shortening leading to hepatocyte senescence and impaired regenerative capacity. One way, hepatocytes overcome this proliferation block and regain replicative efficiency is by re-introduction of telomerase activity through aberrant mutations in the TERT promoter. However, the uncontrolled activation of telomerase can lead to unchecked cell proliferation ultimately promoting HCC (Donaires, Scatena et al. 2017, Nault, Ningarhari et al. 2019). Another factor that is associated with the poor prognosis in HCC is that tumor cells gradually attain the ability to invade different regions within the liver and spread to other organs (Shen, Dean et al. 2019). Evidence suggests that solid tumors acquire the ability to evade the immune system and reprogram immune cells from eliminating neoplasia into an immunotolerant state (Shiao, Ganesan et al. 2011, Mondal, Shivange et al. 2021).

One hallmark that is important not only for tumor growth but also for tumor metastasis, is the activation of an angiogenic switch that induces growth of novel blood vessels to sustain proliferating tumor cells, contributing to the invasive nature of HCC. In addition, the mobility of tumor cells involves the multistep process of epithelial-to-mesenchymal transition. At least to some part, this complex process is attributed to the cooperative signaling through Ras/MAPK and TGF- β pathways (Hao, Baker et al. 2019).

3.6 Molecular classification of HCC

The genetic alterations in HCC and identification of protein-altering mutations per tumor can be mapped with the help of Next-generation sequencing (Schulze, Imbeaud et al. 2015) Some mutations do not cause tumorigenesis and are called 'passenger mutations' whereas a set of few mutations referred to as 'driver mutations' involved in altering key signaling cascades beneficial for tumor progression (Budzinska, Tu et al. 2016). Common mutations in HCC are distributed among genes associated with six major biological pathways: p53/cell cycle regulation, AKT/mTOR signaling, Wnt/ β -catenin signaling, epigenetic regulators, MAP kinase signaling and oxidative stress. Genes that are frequently mutated in HCC are *TP53*, *CTNNB1*, *AXIN1*, *ARID1A* and *ARID2*, though each of these mutations occurs in less than 30% of cases and no clear driver mutations have been established in HCC (Laurent-Puig, Legoix et al. 2001, Hoshida, Nijman et al. 2009, Fujimoto, Totoki et al. 2012, Guichard, Amaddeo et al. 2012). Around 20-50% of HCC cases are influenced by epigenetic modifiers like aberrant microRNA levels, DNA methylation, histones and chromatin remodeling (Lee 2015). However, relevant targetable mutations in HCC are rare and so far, the mutational profile of HCC does not have any impact on clinical therapy.

3.7 Role of cancer stem cells in liver cancer

Cancer stem cells (CSC) are subpopulations of tumor cells that can potentially cause tumor initiation and tumor relapses. The capacity to self-renew and maintain the heterogeneous nature of tumor cells might be driven by CSCs (Batlle and

Clevers 2017). Although several studies based on identification of surface markers in HCC as well as demonstration of increased proliferative and invasive advantage in the presence of potential CSCs in HCC, the evidence is still discussed controversially. One theory suggests that pro-inflammatory TNF- α from macrophages triggers differentiation of liver progenitor cells into CSCs. However, a more commonly accepted theory suggests reprogramming of normal cells into cancer stem cells by induction of pluripotency inducers such as Oct4, Nanog, Klf4, c-Myc, and Sox2 (Li, Liu et al. 2017) (Yamashita and Wang 2013).

The role of CSCs in the initiation of HCC is still debated, but more conclusive data indicates a role of CSCs in HCC metastasis, drug resistance, and relapse (Lambert, Pattabiraman et al. 2017). There is evidence that HCC metastasis could be enhanced by CSCs through their promotion of CD90+ HCC cells to epithelial-mesenchymal transition (EMT) and cellular plasticity. Potential cancer stem cell markers in HCC include oval cell markers OV6, CD113, CD90, CD44, CD13, CD24, and the epithelial adhesion molecule (EpCAM) (Yamashita and Wang 2013). There are multiple factors that influence the regulation of CSCs. Although the detailed understanding of the mechanism of CSC regulation is still unclear, the role of several signaling pathways in CSC regulation such as Akt, TGF- β , STAT3, Notch, Wnt, and Hippo has been extensively studied (Margherita Correnti, Booiijink et al. 2018) (Fig. 3).

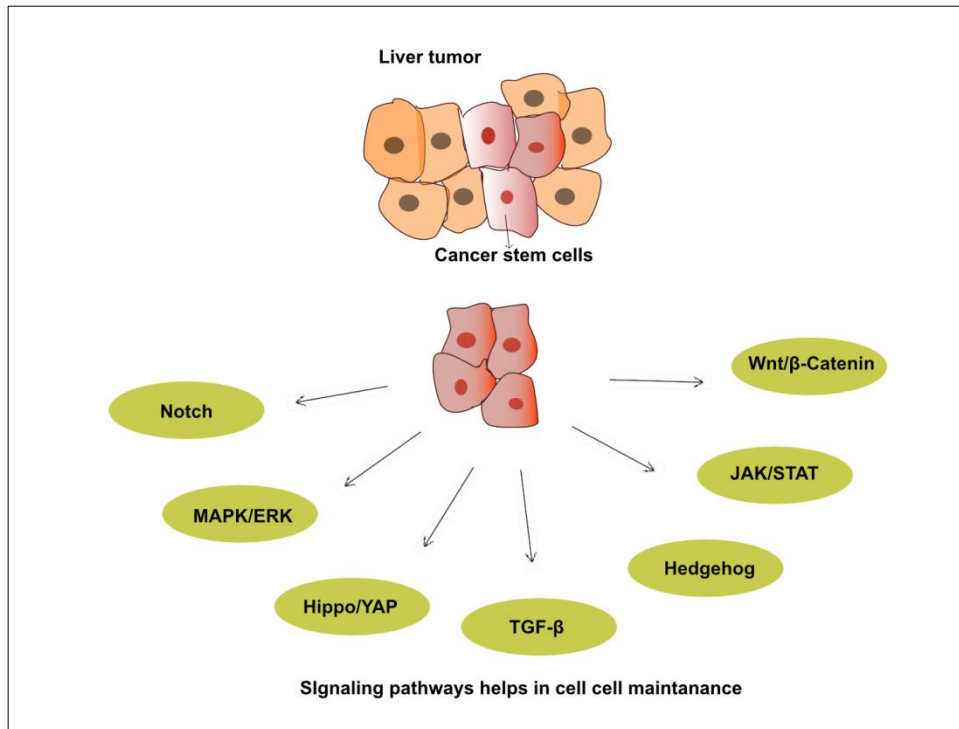


Figure 3: Regulatory mechanisms of liver cancer stem cells

Proposed model of liver cancer stem cell functions (adapted from Marra and Correnti, 2018)

3.8 Signaling pathways regulating CSCs in HCC

Wnt signaling is one pathway involved in HCC progression. One mechanism for the oncogenicity is by supporting self-renewal of CSCs which plays a role in rendering them resistant to drug treatments (Fan, Duan et al. 2019). Activating mutations in one of the major downstream molecules of Wnt-signaling, β -catenin, are commonly found in HCC (de La Coste, Romagnolo et al. 1998, Kim, Lisby et al. 2019). STAT-3 is another component downstream of Wnt signaling and the non-canonical activation of Wnt/STAT-3 signaling induces the production of CD44⁺ CSCs (Chang, Sekine et al. 2017)

The TGF- β signaling pathway has a role in the occurrence, maintenance, and differentiation of CSCs (Wang, Zhang et al. 2017, Futakuchi, Lami et al. 2019). Defective TGF- β signaling has been shown to contribute to the inherent chemotherapy resistance of HCC through STAT-3 activation mediated by IL-6 (Lin, Amin et al. 2009). Alterations in TGF- β signaling together with TNF- α signaling also promotes the differentiation of non-CSCs to CSCs (Yamashita and Wang 2013) (Fig. 4). Importantly, inhibition of the pluripotency marker Nanog in CD133⁺ CSCs reduced drug resistance and tumorigenicity that were associated with TGF- β abnormalities (Sullivan, Sasser et al. 2009).

Another pathway that has been extensively studied in the context of HCC is AKT signaling – a pathway also known to regulate CSC homeostasis and drug resistance (Xiao, Zeng et al. 2019). The AKT pathway connects to multiple other signaling hubs such as GSK-3 β , EGFR, PI3K, β -catenin signaling amongst many others that contribute to a different outcome in CSCs. (Wei, Jiang et al. 2013). There are signaling cross-talks between most signaling pathways that regulate CSCs. The identification of relevant targetable components in the maintenance of CSC might provide a major breakthrough in HCC therapy (Clara, Monge et al. 2020).

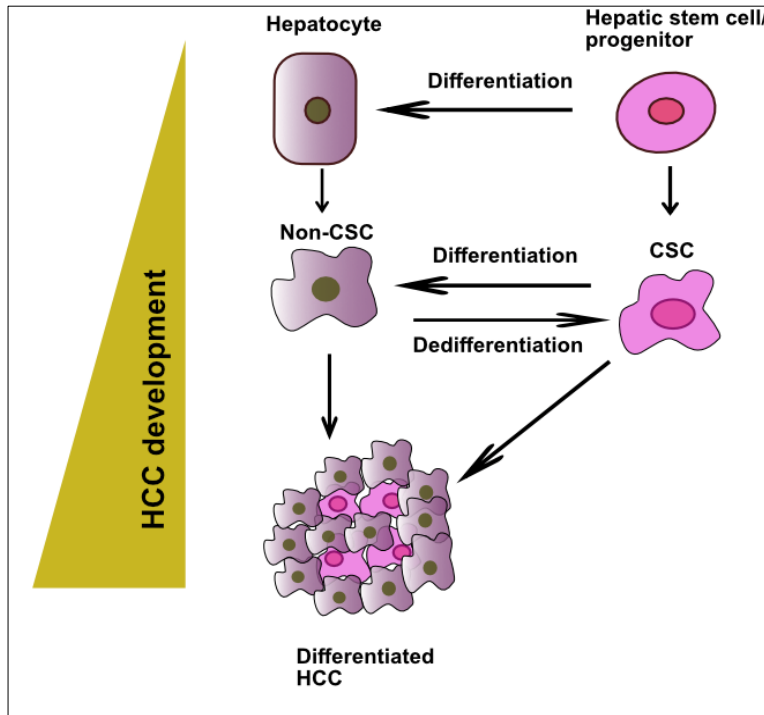


Figure 4: Model of HCC progression from Cancer stem cells (CSCs)

Accumulation of defects in signaling pathways might potentiate the activation of dedifferentiation programs leading to the formation of cancer stem cells from non-cancer stem cells (adapted from Wang and Yamashita, 2013).

3.9 CD44 and liver cancer

In HCC the existence of cells that demonstrate stem cell like properties are called liver cancer stem cells (LCSC). LCSC remain intact despite the use of conventional treatments such systemic treatments or radiotherapy (Rozeik, Hammam et al. 2017). These stem cells might have potency to develop into new tumors and their efficient targeting could offer novel treatment options. Tracing molecular markers of stemness are often the tool to identify potential cancer stem cells and Cluster of differentiation 44 (CD44) is a recognized cancer stem cell marker in a number of malignancies such as breast cancer, colorectal cancer, prostate cancer, and gastric

cancer. CD44 expression is associated with poor prognosis of hepatocellular carcinoma and the presence CD44⁺ tumor cells are correlated to its metastatic and angiogenic properties (Rozeik, Hammam et al. 2017).

CD44 is a transmembrane glycoprotein with a molecular weight of approximately 80 kDa, that is expressed in the majority of cell types including hematopoietic cells. It plays a critical role in stem cell maintenance by a spectrum of signaling cross-talks with the surrounding niche (Ponta, Sherman et al. 2003, Marhaba and Zoller 2004). It is a multifunctional molecule facilitating cell-cell interaction, lymphocyte homing and activation, tumor growth and metastasis mediated by its activation (Lokeshwar, Lokeshwar et al. 1995, Miletto-Gonzalez, Murphy et al. 2012). The main ligand of CD44 is hyaluronic acid (HA) and several other extracellular molecules such as fibronectin, laminin, collagen, osteopontin (Ishii, Ford et al. 1993). The standard form of CD44 (CD44S) consists of a short cytoplasmic tail, a transmembrane region and two extracellular domains. In addition to CD44S, there are several splice variants (v) of CD44 and the expression of them has been found in certain cancer types. In cervical cancer, the expression of v5 and v6 were strong whereas v7, v8 and v10 were completely abolished (Woerner, Givehchian et al. 1995). In the case of human cholangiocarcinoma, the expression of CD44v9 was detected (Suwannakul, Ma et al. 2018). Importantly, hepatic cells and other cell types in the gastrointestinal tract abundantly express variant 6 (v6) (Chen, Zhao et al. 2018). The increased expression level of CD44v6 was identified in the cell membranes of tumor cells in hepatocellular carcinoma. A positive correlation of Cd44v6 expression and tumor invasiveness had been established based on *in vitro* studies. However, the correlation between CD44v6 and vascular invasiveness appeared to be clinically insignificant in HCC (Mima, Okabe et al. 2012). Taken together, these data suggest that CD44 and especially its isoform CD44v6 could present a marker of LCSC.

3.10 Hippo signaling in the liver

Hippo signaling is a molecular pathway orchestrating cell proliferation and cell death. It ensures the maintenance of organ size and was first identified in *Drosophila*, similar components were later identified in mammals. The hippo signaling pathway in *Drosophila* comprises a kinase cascade of Ste-20 like kinase Hippo (Hpo) which – together with an adaptor protein called Salvador (sav) – phosphorylates and activates NDR family kinase Warts (wts). Warts then phosphorylates and inactivates the transcriptional co-activator Yorkie (Yki) leading to down regulation of Yki target genes that support cell proliferation and growth (Huang, Wu et al. 2005). The mammalian homologs of hippo pathway components are MST1/2 for Hpo, WW45 for Sav, LATS1/2 for Wts, and YAP/TAZ for Yki (Dong, Feldmann et al. 2007) (Fig. 5). In mammals, Hippo pathways kinases phosphorylate YAP and TAZ, leading to nuclear exclusion and sequestering the cytoplasmic compartment of the cell, thereby preventing its function as co-transcriptional activator. The genetic activation of *Yap1*, the gene encoding YAP increases the organ size in the liver and leads to the expansion of undifferentiated progenitor cells. (Camargo, Gokhale et al. 2007, Lu, Finegold et al. 2018).

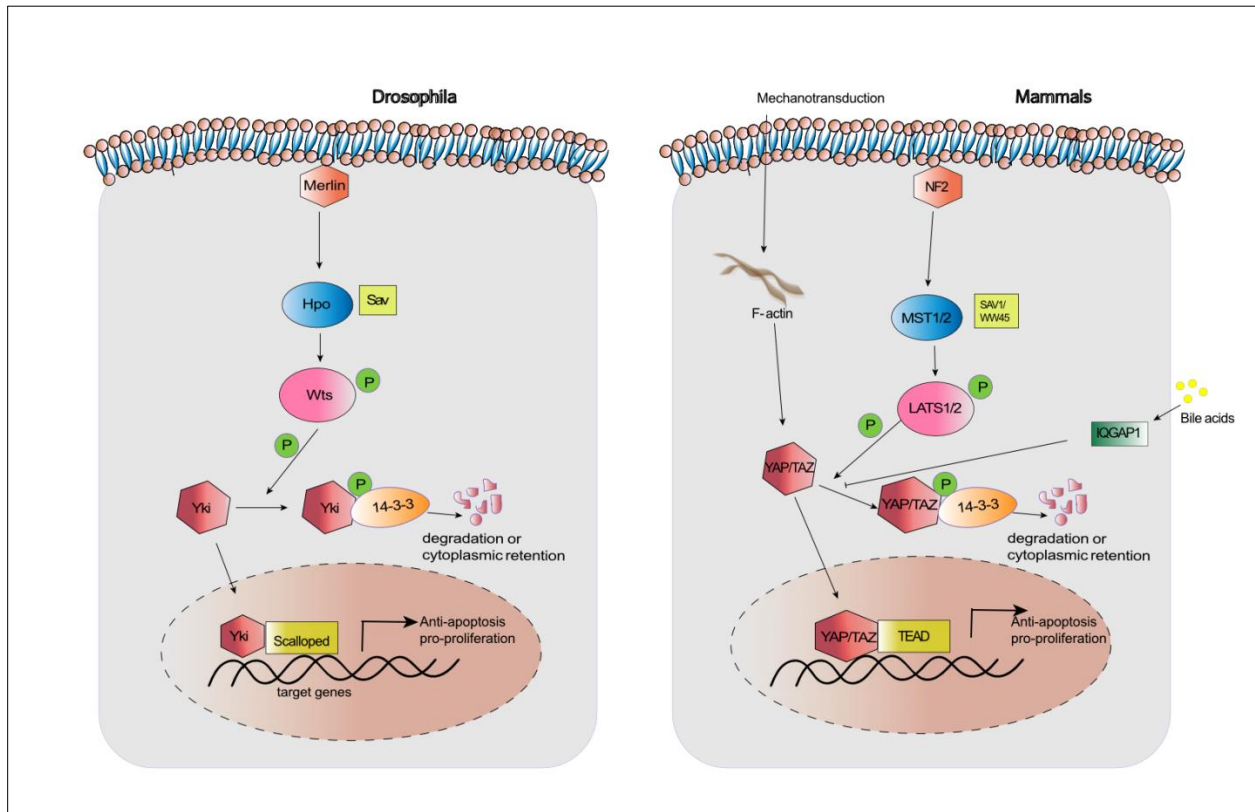


Figure 5 : Schematic representation of Hippo signaling pathway components in drosophila and mammals

(Adapted from Manmadhan and Ehmer, 2018)

The role of hippo signalling and its downstream effector YAP has been extensively studied in the context of liver regeneration. 70% partial hepatectomy in murine models showed a dynamic alteration of hippo signalling and YAP activation from day 1. The presence of elevated nuclear YAP and the decrease in activation of core kinases like MST1/2 and LATS1/2 lasted until restoration of actual liver size (Grijalva, Huizenga et al. 2014). The mechanism by which YAP/TAZ regulates regeneration and switches off automatically after achieving it is still unclear. Of note, YAP/TAZ is not completely necessary for the regulation of development of liver size but is essential for proper liver regeneration (Lu, Finegold et al. 2018). Interestingly,

overexpression of YAP in adult mouse hepatocytes induces their trans-differentiation into progenitor-like cells that could independently differentiate either into biliary epithelial cells or re-differentiate into hepatocytes (Yimlamai, Christodoulou et al. 2014). Recent evidence suggests a possible link between mechanical signals and Hippo signalling wherein the ON/OFF switch of the pathway is affected by external cues transmitted from surface of cells. The majority of such signals are believed to be caused by stress or sheer pressure of stiff extracellular matrix (ECM) leading to contact inhibition (Zhao, Wei et al. 2007). In cells susceptible to contact inhibition, sparsely growing cells *in vitro* in cell culture tend to display active YAP/TAZ in its nucleus. However, if cells grow dense or compact, YAP/TAZ are redistributed to the cytosol in its inactive form (Pavel, Renna et al. 2018).

3.11 Role of YAP/TAZ in liver tumorigenesis

There are several mechanisms by which YAP/TAZ overexpression leads to tumorigenesis in the liver. Elevated expression of active YAP regulates hepatocyte polyploidy and increased chromosomal aberrations (Weiler, Pinna et al. 2017). Additionally, YAP can induce metabolic reprogramming by increased glucose utilization that promotes liver tumorigenesis (Enzo, Santinon et al. 2015). It has also been shown that YAP and TAZ could regulate the tumor microenvironment by recruiting tumor-associated macrophages (TAM) towards the region of inflammation which secrete cytokines facilitating the proliferation of liver cancer cells (Zhang and Zhou 2019). One of the key mechanisms driving tumorigenesis downstream of activate YAP/TAZ is by unchecked proliferation caused by deregulated cell cycle genes. Studies has shown the cooperativity of YAP/TEAD complex with the transcription factor E2F downstream of retinoblastoma (Rb) signaling to support proliferation leading to cancer, including liver cancer (Ehmer, Zmoos et al. 2014, Kapoor, Yao et al. 2014, Fitamant, Kottakis et al. 2015). In addition of supporting proliferation, YAP signaling in HCC is involved in other cancer-promoting mechanisms including chromosomal instability, deregulated post-translational mechanisms and apoptotic suppression (Rosenbluh, Nijhawan et al. 2012, Weiler,

Pinna et al. 2017). Genetic ablation of *Mst1* and *Mst2* in hepatocytes that led to HCC development is outcomes of excessive Yap expression that promotes direct transcription of monocyte chemoattractant protein-1 (MCP-1). This leads to excessive tumor infiltrating macrophages that drives HCC by impairing immune clearance of transformed hepatocytes (Liu, Wang et al. 2017, Kim, Khan et al. 2018).

3.12 Hippo signaling co-operates with other major cellular biological mechanisms to regulate YAP/TAZ

Many upstream signals such as cell polarity, cell adhesion, soluble factors, and mechanical stress regulate the hippo signalling pathway through the canonical hippo kinase cascade. Although the central regulation of YAP is through hippo signaling, there are different levels of interaction between hippo signalling components and other cellular biological mechanisms influencing YAP regulation. For example, the signalling cross talk between the hippo pathway and pathways such as PI3K/AKT, Notch and Wnt contribute to the regulation of YAP/TAZ activity in liver homeostasis and regeneration (Kim, Khan et al. 2017). Abnormal activation of YAP can lead to tumorigenicity. It has previously been shown that increased p-AKT expression coincided with elevated YAP activity in liver tumors. The liver specific deletion of SAV and PTEN initiates development of liver cancer by increased activation of AKT signaling by YAP/TAZ which suggests a positive feedback loop linking hippo-YAP/TAZ and PTEN/AKT signaling (Strassburger, Tiebe et al. 2012). The double-knockout of *Mst1* and *Mst2* in mouse hepatocytes results in an enlarged liver. On the molecular level, a positive feedback loop between Notch signaling and YAP/TAZ leads to the expansion of oval/ductal cells by upregulated Notch signalling. Furthermore, β -Catenin was found to be significantly elevated in *Mst1/2* double-mutant livers indicating activation of the Wnt/ β -Catenin pathway. Importantly, deletion of β -Catenin in *Mst1/2* double-knockout hepatocytes resulted in an enormously increased liver size suggesting a negative feedback loop between the Wnt/ β -Catenin pathway and YAP/TAZ expression (Kim, Khan et al. 2017).

3.13 Hippo-independent regulation of YAP

3.13.1 Tyrosine phosphorylation

Although canonical regulation of YAP is through serine phosphorylation by hippo signaling pathway components, recent studies suggest an important role of tyrosine phosphorylation in subcellular localization and co-transcriptional functions of YAP (Reuven, Shanzer et al. 2019). For example, the role of Src family kinases (SFKs) in mediating YAP phosphorylation has been discussed in multiple studies and SFKs are getting recognized as an important regulator of YAP activity (Lamar, Xiao et al. 2019). The Src family member YES is known to regulate embryonic stem cell self-renewal through YAP-TEAD2, a mechanism facilitated by Leukemia inhibitory factor, IL-6 (Tamm, Bower et al. 2011). The SH2 domain of YES directly interacts with YAP and IL-6 through LIF receptor gp130. In colon cancer cell lines, YES/SRC can phosphorylate YAP at Tyrosine 357 residue that facilitates nuclear YAP retention and subsequent oncogenic transcriptional activity (Taniguchi, Moroishi et al. 2017). However, knockdown and rescue experiments on SRC and YES confirmed only YES could influence cell proliferation. The tyrosine phosphorylation analysis of YAP in mouse hepatocytes post partial hepatectomy also confirmed Y356-phosphorylation. The CRISPR based knockdown of different SFKs confirms a central role for LCK in the regulation of tyrosine phosphorylation of YAP and its nuclear retention in cholangiocarcinoma (Sugihara, Werneburg et al. 2018) . In all these models, the absence of any change in the LATS activity suggests YAP regulation by tyrosine phosphorylation is a hippo pathway-independent event.

3.13.2 Nuclear-cytoplasmic YAP/TAZ distribution by regulation of nuclear export and import

The nuclear export or import rate of YAP is regulated by several mechanisms causing changes in its activity based on the context. For instance, YAP is abundant in the cytoplasm of normal fibroblasts whereas it is localized in the nucleus of cancer-associated fibroblast. The shuttling of YAP in and out of the nucleus is primarily regulated by the phosphorylated state of YAP. Exportin1 (XPO1), a major

nuclear export receptor, mediates active nuclear export of YAP (Ege, Dowbaj et al. 2018) (Dupont, Morsut et al. 2011). Binding of YAP to AMOT (Angiomotin) or related proteins (AMOT1, AMOT2) is known to be independent of the phosphorylation status of YAP and primarily promotes the cytoplasmic localization of YAP (Chan, Lim et al. 2011). However, interaction of YAP with dephosphorylated AMOT promotes its nuclear localization.

Moreover, the cellular mechanical forces from the extracellular matrix play a major role in YAP/TAZ localization primarily through interactions with the cytoskeleton. For example, the actin regulator RhoA is known to promote TAZ nuclear localization independent to its phosphorylation status (Kofler, Speight et al. 2018). The mechanical force transmitted from extracellular matrix also deforms the nuclear pores facilitating the nuclear influx of YAP (Elosegui-Artola, Andreu et al. 2017).

3.14 YAP/TAZ regulation by deubiquitination

Protein ubiquitination is a fundamental mechanism by which cells trigger proteasomal degradation of damaged or unwanted proteins. Importantly, ubiquitination is a reversible process and the polyubiquitin chain can be degraded by deubiquitinating enzymes (DUB) (He, Zhou et al. 2016). A DUB enzyme, OTUB2 has been identified as a deubiquitinating agent of YAP/TAZ and thereby stabilizing the transcriptional co-factors independent of LATS1/2, a process that has been shown to promote cancer stemness (Zhang, Du et al. 2019). Another deubiquitinating enzyme, USP10 was identified as a YAP/TAZ regulator in the liver cancer cell line HepG2 (Zhu, Yan et al. 2020). Inactivation of USP10 improved proteasomal degradation of YAP/TAZ with subsequent hepatocellular carcinoma growth inhibition both *in vitro* and in xenografts. In samples from hepatocellular carcinoma patients and chemically induced mouse HCC, elevated expression of USP10 positively correlated with YAP/TAZ expression (Zhu, Yan et al. 2020).

3.15 Regulation of YAP mediated by CD44

CD44 is a cell surface glycoprotein known for its extensive expression in a wide range of malignancies, including HCC, rendering it an attractive therapeutic target. Inhibition of CD44's interaction with hyaluronan, a prominent component of the extracellular matrix, has been considered a potential strategy for therapeutic intervention in these cancers. In the context of glioblastoma, CD44 has demonstrated elevated expression levels, which have garnered particular attention. Studies employing effective CD44 knockdown approaches in both glioblastoma cell lines and murine models have shed light on its pivotal role in influencing the hippo signaling pathway. Remarkably, these investigations have unveiled CD44's capacity to safeguard glioblastoma cells from oxidative stress, chiefly originating from reactive oxygen species (ROS), as well as cytotoxic-induced stressors. ROS are chemically reactive molecular species capable of inducing cellular damage and playing a significant role in the pathophysiology of cancer (Xu, Stamenkovic et al. 2010).

Furthermore, the specific mechanisms through which CD44 exerts its influence on the hippo pathway have remained an intriguing area of exploration. Subsequent studies focusing on the lung cancer cell line A549 and the liver cancer cell line HepG2 with CD44 knockdown have indicated a notable downregulation of YAP (and its downstream target gene expression levels. (Zhang, Xia et al. 2014). Additionally, in the same study, this regulatory effect of CD44 on YAP has been found to be mediated through the involvement of a small G protein known as RhoA. The knockdown of *Cd44* resulted in the inhibition of RhoA and YAP expression. The observation remained consistent with the observation that *RhoA* knockdown mediated YAP downregulation. RhoA is a member of the Ras superfamily of GTPases and serves as a crucial regulator of various cellular processes, including cytoskeletal dynamics and gene expression, all of which contribute to the modulation of the hippo pathway (Feng, Degese et al. 2014, Li, Li et al. 2019). These findings collectively highlight the complex molecular interplay between CD44, and the hippo signaling pathway (Zhang, Xia et al. 2014).

3.16 Pre-clinical or translational research on HCC

A broad understanding of the biology, molecular mechanisms and pathogenesis in HCC is derived from preclinical experimental models. Although preclinical research models offer a detailed overview of HCC progression, no model is able to mimic human HCC due to the heterogeneous nature and complexity of this type of cancer (Blidisel, Marcovici et al. 2021). Therefore, the selection of HCC models for clinical or pre-clinical research is a crucial step and demands thorough documentation from different perspectives of disease progression. The most commonly studied pre-clinical models of HCC involve *in vitro* analysis of tumor cell lines, *in vivo* studies in HCC animal models, and computational algorithms (Blidisel, Marcovici et al. 2021).

3.16.1 *In -vitro* HCC models

Cancer cell lines are one of the most valuable *in -vitro* models in pre-clinical and drug discovery research. They provide insights into the relevance of signaling pathways, response to chemotherapies or radiotherapies as well as other compounds influencing tumor growth (Mirabelli, Coppola et al. 2019). The complexities of *in vitro* cancer cell culture vary from simple 2-dimensional (2-D) monolayers grown in cell culture dishes or a much more complex 3-dimensional (3-D) models mimicking tumor micro-environment. The 2-D models of HCC commonly utilize cell lines such as HepG2, Hep3B, Huh7, and C3A amongst many others, while 3-D models are mainly based on spheroids, co-culture models, and organoids (Katt, Placone et al. 2016).

3.16.2 Animal Models of Human HCC

Although *in -vitro* studies provide insights on drug development and crucial information on cellular sensitivity against different treatment assays, they often fails to recapitulate the tumor micro-environment, complex interactions between neighboring cells, tissues, tumor growth, angiogenesis and influence of secreted cytokines as well as hormones (Bagi and Andresen 2010). The use of animal models to understand the complexity of disease pathogenesis is therefore

established in cancer research. Widely used animal models are genetically engineered mouse (GEM) models, chemically-induced models, and engrafted models (Zhang, Henderson et al. 2019).

3.16.3 Genetically engineered mice

Genetically engineered mice are ideal models to study the genetic and molecular characteristics of HCC development. Mouse models of HCC are designed to mimic alterations in oncogenic candidates, tumor suppressor genes, and tumor microenvironments found in human HCC (Heindryckx, Colle et al. 2009).

Transgenic mouse models with the integration of hepatitis virus genes result in tumor initiation or promote liver carcinogenesis and aberrations in oncogenic or growth factor-associated genes leading to tumor development. In hepatitis B virus transgenic mice, the insertion of the hepatitis B virus X protein (HBx) coding gene directly into the germline of mice triggers inflammation leading to the proceeding of HCC development (Kim, Koike et al. 1991). Metabolic dysfunction transgenic mice are used to study early diagnostic markers of HCC. The downregulation of Glycine N-methyltransferase (GNMT) found in human HCC led to the generation of the *Gnmt*^{-/-} mouse model (Liu, Chen et al. 2003). These mice develop chronic hepatitis and fatty liver through deregulation of the PI3K/AKT pathway leading to HCC with multiple tumor nodule formations within 16 months of age (Liao, Lee et al. 2016). Multidrug resistance 2 (MDR2) is a phosphatidylcholine transporter in the bile canalicular membrane of hepatocytes and plays a role in bile formation. The human homolog *MDR3* mutation is often associated with liver pathologies and the studies on the *Mdr2*^{-/-} mouse model showed that MDR2 deficiency results in abnormal secretion of phosphatidylcholine into bile (Mauad, van Nieuwkerk et al. 1994). Hepatocyte dysplasia caused by liver inflammation and hepatotoxicity by defective bile salt secretion in *Mdr2*^{-/-} mice leads to formation of noticeable tumors within 16 months. This model offers a detailed understanding of pathogenesis of cirrhosis- and inflammation-associated HCC (Ikenaga, Liu et al. 2015) (Guicciardi, Trussoni et al. 2018).

Another strategy to induce HCC in mice is by exploiting liver-specific promoters for the expression of oncogenes. Some of the common promoters used for hepatic expression are the promoters of metallothionein, albumin and liver-activating protein among others. Transgenic mice that express liver-specific *c-Myc* have been developed using albumin promoter/enhancer. Young *c-Myc* mice developed mild to severe hepatic dysfunction and hepatoblastoma after 15 months old (Sandgren, Quaipe et al. 1989). Later, a transgenic model as an extension of *c-Myc* mice have been developed to study the interaction between *c-Myc* and transforming growth factor (TGF- α). These mice expressed *c-Myc* under the control of an albumin enhancer/promoter and TGF- α through a metallothionein-1 promoter. This model has the advantage of significantly reducing the onset time of HCC induction when compared to transgenic mice that express either *c-Myc* or TGF- α (Jhappan, Stahle et al. 1990, Murakami, Sanderson et al. 1993, Calvisi and Thorgeirsson 2005). Deletion of tumor suppressor genes is yet another method to develop transgenic mice. The phosphatase and tensin homolog (PTEN) negatively regulate the PI3K-Akt signaling pathway that regulates proliferation, energy metabolism and cell survival. The liver-specific deletion of PTEN results HCC development in mice after 44 months (Watanabe, Horie et al. 2007).

GEM models with conditional and inducible gene expression systems allow the restrained deletion/insertion of proto-oncogenes and tumor suppressor genes in a tissue-specific and time-dependent manner. The widely used inducible systems are tetracycline (Tet) controlled, Tamoxifen (Tam) controlled and virus-mediated Cre delivery (He, Tian et al. 2015). Another recently developed method to induce liver-specific mutation is by administering inducible plasmid DNA directly into the liver by hydrodynamic tail vein injection (HTVI) (Ju, Han et al. 2016). By this method, the desired plasmid DNA dissolved in a large volume of saline is injected intravenously by applying constant pressure and speed. When the injected volume exceeds the cardiac output of the animals, its backflow into the sinusoidal parenchyma of the liver leads to increased intrahepatic hydrodynamic pressure and transfection of nearby hepatocytes (Ju, Ahn et al. 2013) (Hubner, Lechler et al. 2018). HTVI

combined with *sleeping beauty*- mediated somatic gene integration of DNA encoding for constitutively active β -catenin (N-90 catenin) and YAP(YAPS127A) into livers of mice results in the development of HCC (Tao, Calvisi et al. 2014). Of note, hydrodynamic transfection of the active form of PIK3CA and YAP in mouse liver deciphered the signaling crosstalk between these two pathways in hepatocarcinogenesis (Li, Tao et al. 2015).

3.16.4 Chemically induced models

Humans are constantly exposed to a variety of chemical compounds, among them multiple carcinogens. Two broad categories of cancer-inducing agents used to generate HCC models are genotoxic and cancer-promoting compounds. These chemicals induce hepatocyte death followed by inflammation associated with development of liver fibrosis and HCC. The most widely used genotoxic agent to induce HCC in the mouse model is an intraperitoneal injection of diethyl nitrosamine (DEN). The biotransformation of nitrosamines by cytochrome P40 enzymes into alkylating metabolites causes DNA adducts leading to tumorigenesis. Usually, infant mice are administered a single low dose of DEN intra-peritoneally. They are more susceptible to HCC formation than older mice as DEN-dealkylating activity increases with age. The time of sacrifice ranges from 12-40 months depending on follow-up treatments post-DEN injection or special diets. DEN-treated mice not only develop liver tumors but also hematopoietic, gastrointestinal, and skin cancers (Mercer, Hennings et al. 2015). Carbon tetrachloride (CCl₄) is another commonly used hepatotoxin to induce fibrosis in mice, rats, and monkeys. The intraperitoneal injection of 0.5 - 2 ml per kg bodyweight twice a week can induce fibrosis within 4-6 weeks and the effect is reversible upon CCl₄ withdrawal. CCl₄ affects hepatocytes either indirectly by Kupffer cell or stellate cell-mediated inflammatory reactions or directly by oxidative damage of hepatocytes by cell membrane impairment (Xin, Cui et al. 2017).

3.16.5 Engrafted mouse models of HCC

Xenografts models are created by implanting fragments of human tumors or tumor cell lines just under the skin (ectopic) or directly into the tissue of origin (orthotopic) of the host mouse. As a direct representative of mutations associated with human cancers, a xenograft model allows studies using human tissues (Richmond and Su 2008). Xenograft mouse models can provide fast results in cancer research by rapidly growing and evaluating human tumor cells *in vivo*, making them attractive for preclinical drug development studies (Jung 2014). For instance, studies using a YAP inhibitor in xenograft model of esophageal adenocarcinoma are used to evaluate the anti-tumor effects of the inhibitor (Song, Xie et al. 2018). Another study used a YAP activator on a xenograft model of breast cancer to investigate the role of YAP in angiogenesis initiation (Yan, Song et al. 2022). The major drawback of these models is that it fails to recapitulate the process of tumorigenesis due to the lack of a tissue-specific tumor micro-environment as immunocompetent mice are used as hosts to avoid tissue rejection. However, developing a humanized version of the host mouse could overcome the limitations in future HCC studies (Day, Merlino et al. 2015, Morton, Bird et al. 2016).

3.17 Background data associated with the project

3.17.1 Rb family conditional triple knock-out (TKO) HCC mouse model

The tumor suppressor retinoblastoma (RB) is functionally inactivated in the majority of human HCC either by genetic, epigenetic, or viral mechanisms. Mice devoid of all the three *Rb* family genes in the liver (*TKO; Rb^{lox/lox}; p130^{lox/lox}; p107^{-/-}*) exhibit tumors similar to human HCC. The specific deletion of the *Rb* gene family in the liver of adult mice was achieved by performing intrasplenic injection of an adenovirus expressing the *Cre* recombinase (*Ad-Cre*) in adult *TKO* mice (Fig. 6) (Viatour, Ehmer et al. 2011). This method allows for targeted delivery of an adenovirus harboring *Cre* recombinase to the liver. These mice developed tumors within 3 - 4 months with histopathological features and gene expression profiles resembling human HCC (Fig. 6). The deletion of *Rb* and

p130 was confirmed by the RNA expression profiles from macro-dissected tumors from these mice (Ehmer, Zmoos et al. 2014).

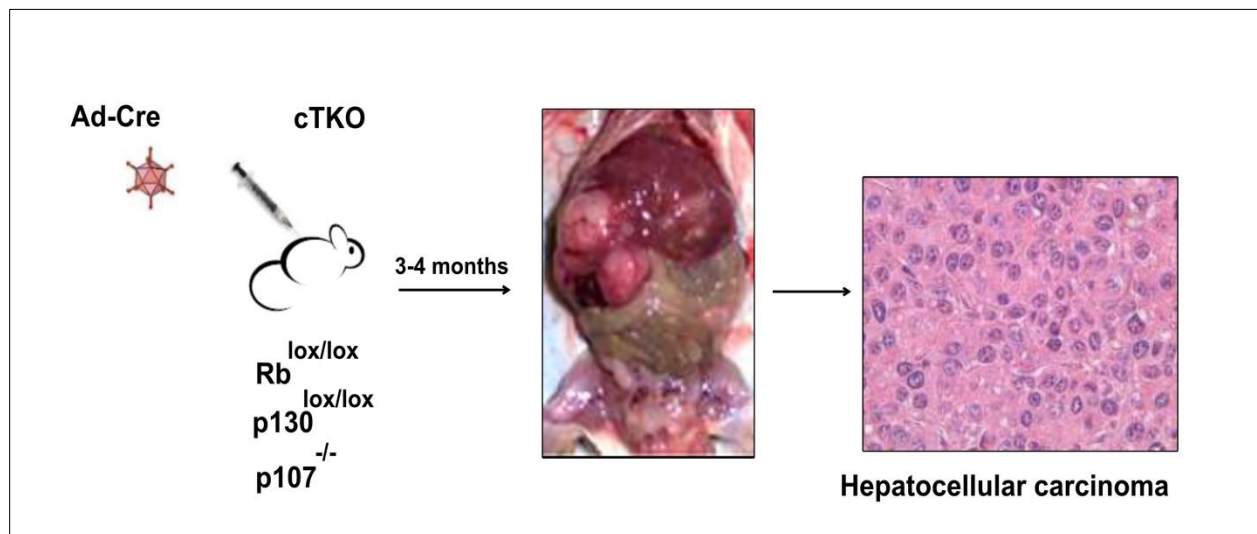


Figure 6 : HCC induction in *TKO* mouse model

Schematic representation of *Cre*-mediated activation in the *TKO* mouse model (left) and representative *TKO* mouse with liver tumors 3 - 4 months after intrasplenic injection of adenoviral *Cre* (Ad-*Cre*, middle), H&E staining (right) of liver tumor section with characteristic morphology of HCC (from Viatour et al.).

The analysis of *TKO* pre-cancerous lesions showed proliferating cells around the portal triad as represented by the proliferative marker- Ki67. Interestingly, increased nuclear expression of YAP and other progenitor cell markers such as SOX9 and A6 was found in these cells (Ehmer, Zmoos et al. 2014) (Viatour, Ehmer et al. 2011) (Fig. 7) that present tumor-initiating cells in this model. In contrast to these proliferative cells, *TKO* hepatocytes undergo cell cycle arrest upon *Rb* family knockout, likely mediated by activation of the hippo pathway resulting in downstream inactivation of pro-proliferative YAP (Ehmer, Zmoos et al. 2014). These findings suggest that YAP upregulation in tumor-initiating cells near the portal triad is controlled through a mechanism independent of hippo signaling. Among several possible YAP regulators,

overexpression of CD44v6 on the surface of YAP-expressing cells indicates a possible role of CD44 in the activation of YAP and proliferation in tumor precursor cells (Fig 6).

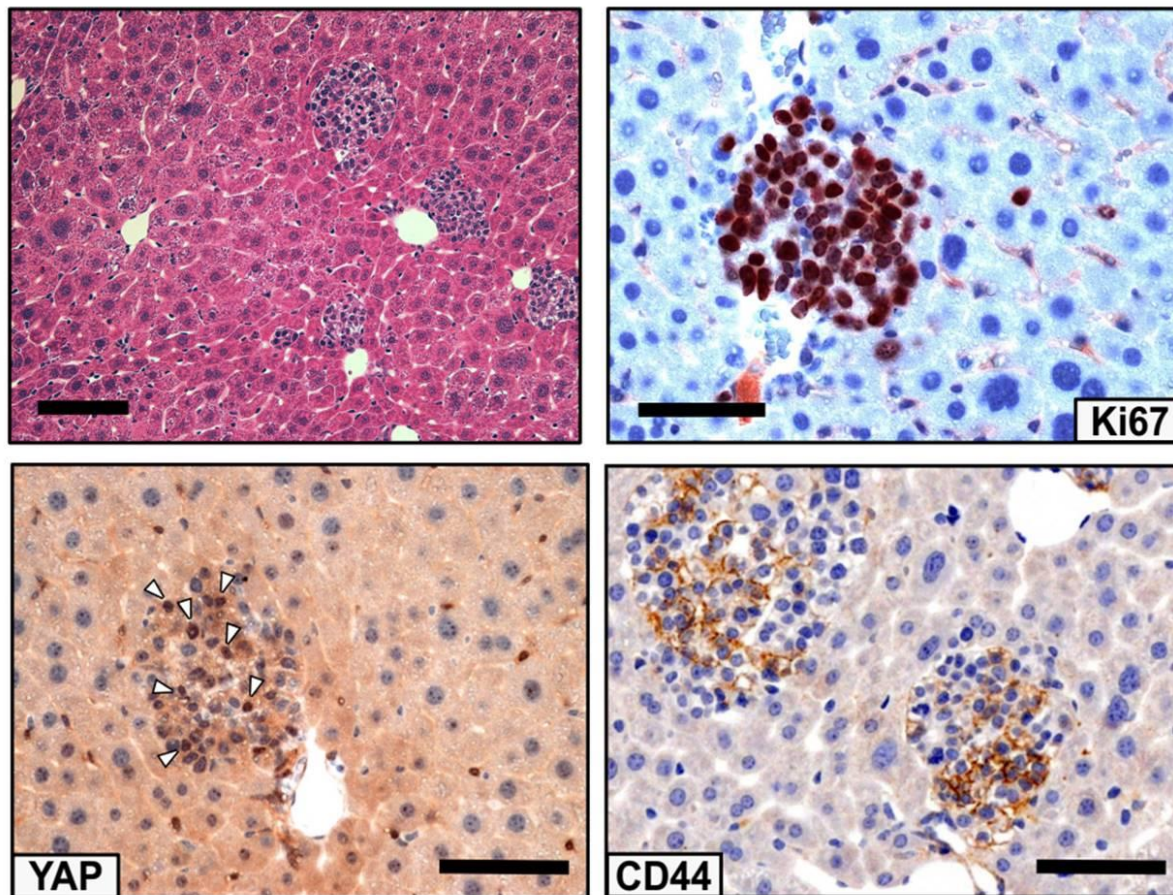


Figure 7: Immunohistochemistry staining of tumor precursor lesion near the portal triad in *TKO* livers 4-5 weeks after tumor induction.

Upper left, H&E staining of tumor precursor lesions, scale bars 100 μm , *Upper right*, staining for proliferative marker Ki67, scale bars 25 μm

Lower left, staining for expression of YAP. *Lower right*, expression of CD44v6, scale bars 100 μm .

4 Aim and hypothesis

4.1 Elucidating the role of CD44 in regulating oncogenic YAP in liver cancer cells *in vitro*

YAP expression is upregulated in *TKO* pre-cancerous lesions as well as in *TKO* hepatocellular carcinoma – likely playing an important role in driving the proliferation of tumor-initiating and cancer cells. We hypothesize that high levels of CD44 provide the basis for sustained YAP activation in these cells. To understand the role of CD44 in YAP regulation, we aimed to inactivate *Cd44* in *TKO* cell lines *in vitro* using CRISPR/Cas9-mediated gene mutation. We then aimed to analyze mutant cell lines to decipher proliferation potency as well as protein and mRNA expression levels of *Yap* and its target genes.

4.2 The role of CD44 in the HCC development *in vivo*

Early *TKO* pre-cancerous lesions show expression of both CD44 and YAP. As an extension to the *in vitro* experiments described above (4.1), we explored how the loss of active CD44 in our mouse model affects YAP expression profiles and influences the tumor progression. We also aimed to exploit DEN-induced HCC in *Cd44^{-/-}* and C57bl6 mice to understand more about the role of CD44 in tumor initiation and YAP regulation. We investigated expression of CD44 and YAP in tumors and normal tissue regions from liver extracted from test and control DEN induced mice. Moreover, we aimed to characterize CD44 and YAP levels in human HCC samples.

4.3 Relevance of the CD44-YAP axis in murine and human hepatocellular carcinoma

Here, we examined the relationship between CD44 and YAP during the progression of hepatocarcinogenesis. We conducted expression analyses of CD44 and YAP in both human and mouse hepatocarcinoma tissue samples. Observing a positive correlation between CD44 and YAP, we aimed to investigate the underlying mechanism within the CD44-YAP axis. To achieve this, we used non-transfected

TKO cell lines as well as *Cd44*-inactivated *TKO* cell lines, and analyzed the differential expression of gene sets through RNA sequencing. Subsequently, we selected a set of candidate components that showed differential expression in both groups. To further understand the CD44-YAP axis, we carried out a series of inhibitor treatments and subsequent proliferation analyses in non-transfected *TKO* cell lines.

5 Materials

5.1 Technical equipment

Table 1: Technical equipment

Device	Company
Analytical balance	KERN B1-NM
Analytical balance PCB	KERN PCB
Autoclave	Systec-VX150, neoLab Migge GmbH
AxioCam 305 Mono (Fluorescence microscope)	Carl Zeiss AG, Oberkochen
Bag sealer Folio FS 3602	Severin Elektrogeräte GmbH
Centrifuge 5424 R	Eppendorf AG
Centrifuge 5702 R	Eppendorf AG
Centrifuge 5810 R	Eppendorf AG
CO2 incubator HERAcell®	Heraeus Holding GmbH
Countess II FL automated cell counter	Life Technologies, Thermo Fischer Scientific;Inc
EcoVac	schuett-biotec GmbH
Enclosed tissue processor	Leica ASP300S, Leica biosystems
Fridge 4 degree	Siemens AG
Gel Doc™ XR+ system	Bio-Rad Laboratories GmbH, Munich
Heated paraffin embedding machine	Leica Microsystems GmbH, Germany
Heated paraffin embedding station	HistoCore Arcadia H, Leica Biosystems GmbH, Germany
Heracell™ 240 incubator	Thermo Fisher Scientific, Inc., Waltham, MA, USA
Heracell™ 240 incubator	Thermo Fisher Scientific, Inc., Waltham, MA, USA
Herasafe™ KS (NSF) Class II, Type A2 Biological Safety Cabinets	Thermo Fisher Scientific, Inc., Waltham, MA, USA
Herasafe™ Type A2 Biological Safety Cabinets	Thermofisher scientific, Inc
Horizontal shaker incubator hood	Edmund Bühler GmbH TH15
Ice machine	Ziegra Eis machinen GmbH
Liquid nitrogen tank	LS48 Taylor-Wharton
Magnetic stirrer, PC-410D	Corning®
Master Cycler™ Nexus Thermal Cycler	Eppendorf AG
Maxwell® 16 Instrument	Promega GmbH
Microbiological incubator	Kelvitron®, Heraeus Instruments

Microplate reader Anthos 2001	Anthos Mikrosysteme
Microscope Axio Imager A1	Carl Zeiss AG, Oberkochen
Microtome Microm HM355	Thermo Fisher Scientific, Inc., Waltham, MA, USA
Microwave	Sharp Corporation
Microscope AxioCam	Carl Zeiss AG
Mini -PROTEAN ®Tetra	Bio-Rad Laboratories GmbH, Germany
Mini Trans-Blot cell	Bio-Rad Laboratories GmbH, Germany
Owl™ EasyCast™ B2 mini gel-electrophoresis	Bio-Rad Laboratories GmbH
pH meter 521	WTW Wissenschaftlich-Technische Werkstätten GmbH
Pipette controller	Accu-jet® pro, BRAND GMBH + CO KG
Pipettes- 1ml, 200ul,10 ul	Eppendorf AG
Powerpac power supply	Bio-Rad Laboratories GmbH
Refrigerator -80	Forma 900 series, Thermo Scientific
Refrigerators -20	Liebherr Comfort No frost
Spectrophotometer Nanodrop 1000	Peqlab biotechnology GmbH
StepOne plus RT PCR system	Applied Biosystems, Inc
Surgical instruments	ThermoFisher scientific
Thermomixer comfort	Eppendorf AG, Hamburg
Vortex-Genie 2	Scientific Industries Inc., Bohemia, NY, USA
Western film Hyper processor	Amersham Biosciences GmbH

5.2 Consumable supplies

Table 2: Consumable supplies

Consumable	Company
Cell culture plates (10 cm, 6 well dish, 96 well dish)	FALCON® Corning Incorporated, Corning, NY, USA Frickenhausen
CHROMAFIL® Color-coded cellulose mixed ester syringe filters A-20/25	MACHEREY-NAGEL GmbH & Co. KG, Düren
Chromatography paper, 3 mm	GE Healthcare Europe GmbH, Munich
CL-XPosure™ Film	Thermo Fisher Scientific, Inc., Waltham, MA, USA
Conical tubes, 15 mL, 50 ml	Sarstedt AG & Co., Nümbrecht
Countess™ Cell Counting Chamber Slides	Thermo Fisher Scientific, Inc., Waltham, MA, USA
Coverslips	Thermo Fisher Scientific, Inc., Waltham, MA, USA
CryoPure tubes	Sarstedt AG & Co., Nümbrecht
Disposable scalpels	Feather Safety Razor Co., Ltd., Osaka, Japan
Eppendorf tubes 1.5 mL and 2 mL	Eppendorf AG, Hamburg
Glass slides Superfrost® Plus	Thermo Fisher Scientific, Inc., Waltham, MA, USA
Gloves Nitrile	Abena A/S, Denmark Egelund 35
Immobilon®-FL (PVDF transfer membrane)	Merk Millipore Ltd
MicroAmp® optical 96-well reaction plate	Applied Biosystems, Inc., Carlsbad, CA, USA
Microtome blades S35 and C35	Feather Safety Razor Co., Ltd., Osaka, Japan
PCR reaction tubes	Brand GmbH + Co. KG, Wertheim; Eppendorf AG, Hamburg
Petri dishes	Sarstedt AG & Co., Nümbrecht

Pipette tips (10ul, 20ul and 1000 ul)	Sarstedt AG & Co., Nümbrecht
Safe seal pipette tips, professional	Biozym Scientific GmbH, Hessisch Oldenburg
Serological pipettes (5 ml, 10 ml, 25 ml, 50 ml)	Sarstedt AG & Co., Nümbrecht
Single use needles Sterican® 27 gauge	B. Braun Melsungen AG, Melsungen
Single use syringes Omnifix®	B. Braun Melsungen AG, Melsungen
Tissue culture coverslips 13mm	Sarstedt, USA
Tissue embedding cassette system	Medite GmbH, Burgdorf
Watman™	GE Healthcare UK Limited

5.3 Reagent

Table 3: Reagents

Reagent	Source
2-Log DNA ladder (0.1–10.0 kb)	New England Biolabs GmbH
2-Propanol (isopropanol)	Carl Roth GmbH + Co. KG, Karlsruhe
Acetic acid (Absolute)	Carl Roth GmbH + Co. KG, Karlsruhe
Acylamide (30%)	Carl Roth GmbH + Co. KG, Karlsruhe
Ammonium persulfate	Sigma-Aldrich GmbH
Ampicillin sodium salt	AppliChem GmbH, Darmstadt
Biozym LE Agarose	Biozym Scientific GmbH
Blotting grade blocker non-fat dry milk	Serva Electrophoresis GmbH, Heidelberg
Bovine serum albumin (BSA)	Carl Roth GmbH + Co. KG, Karlsruhe
Calcium chloride dihydrate	Carl Roth GmbH + Co. KG, Karlsruhe
Complete, EDTA-free, protease inhibitor cocktail tablets	Roche Deutschland Holding GmbH
Dimethyl sulphoxide(DMSO)	Carl Roth GmbH + Co. KG, Karlsruhe
disodium phosphate (KCl)	Carl Roth GmbH + Co. KG, Karlsruhe
Dodecylsulfate Na-salt in pellets (SDS)	Serva Electrophoresis GmbH, Heidelberg

Ear lysis buffer- DirectPCR(Ear)	Viagen Biotech Inc, Los Angeles
ECL prime reagent westernblot detection reagent	GE Healthcare Amersham TM , Fischer Scientific GmbH
ECL western blotting substrate	Pierce TM , Thermofischer scientific
Ethanol (80%) denatured with Butan-2-on	BrüggemannAlcohol GmbH, Heilbronn
Ethidium bromide	Sigma-Aldrich Chemie GmbH, Munich
Ethylenediaminetetraacetic acid (EDTA)	Invitrogen GmbH
Formaldehyde solution 4 %	Carl Roth GmbH + Co. KG, Karlsruhe
Gel loading dye, purple	New England Biolabs GmbH
GeneRuler 1 kb Plus DNA Ladder	Thermo Fisher Scientific, Inc., Waltham, MA, USA
Glyceine	Carl Roth GmbH + Co. KG, Karlsruhe
Glycerol Rotipuran®	Carl Roth GmbH + Co. KG, Karlsruhe
Glycin Pufferan®	Carl Roth GmbH + Co. KG, Karlsruhe
GREENTaq® ReadyMix TM PCR reaction mix	Sigma-Aldrich Chemie GmbH
Hydrogen peroxide 30% Rotipuran®	Carl Roth GmbH + Co. KG, Karlsruhe
Incuwater-clean	PanReac Applications, AppliChem GmbH
LB agar (Luria/Miller)	Carl Roth GmbH + Co. KG, Karlsruhe
LB broth (Luria/Miller)	Carl Roth GmbH + Co. KG, Karlsruhe
Magnesium chloride	Carl Roth GmbH + Co. KG, Karlsruhe
Methanol	Carl Roth GmbH + Co. KG, Karlsruhe
MIGLYOL® 812	Caesar & Loretz GmbH
N- Nitrosodiethylamine (DNA)	Sigma-Aldrich Chemie GmbH, Munich
Nonidet® P40 (NP40)	AppliChem GmbH, Darmstadt
Ponceau S	Carl Roth GmbH + Co. KG, Karlsruhe
Potassium chloride	Sigma-Aldrich Chemie GmbH, Munich
Precision Plus Protein TM all blue standard	Bio-Rad Laboratories GmbH, Munich
Proteinase K, recombinant, PCR grade	Roche Deutschland Holding GmbH
REDTaq® ReadyMix TM PCR reaction mix	Sigma-Aldrich Chemie GmbH, Munich

Restriction endonucleases (<i>Bsm</i> 1)	New England Biolabs GmbH
Sodium acetate buffer solution	Sigma-Aldrich Chemie GmbH, Munich
Sodium chloride (NaCl)	Carl Roth GmbH + Co. KG, Karlsruhe
Sodium hydroxide solution (NaOH)	Carl Roth GmbH + Co. KG, Karlsruhe
SYBR™ Green PCR Master Mix	Applied Biosystems™
Tail lysis buffer-DirectPCR(Tail)	Viagen Biotech Inc, Los Angeles
Tamoxifen	Sigma-Aldrich Chemie GmbH, Munich
TE buffer, pH 8.0	AppliChem GmbH, Darmstadt
Tetramethylethylenediamine (TEMED)	Carl Roth GmbH + Co. KG, Karlsruhe
Tris-buffered saline 1X, pH 7.6, Tablets	Th. Geyer GmbH & Co. KG, Renningen
Tris hydrochloride Pufferan®	Carl Roth GmbH + Co. KG, Karlsruhe
Tris Pufferan®	Carl Roth GmbH + Co. KG, Karlsruhe
Triton® X-100	Merck KGaA, Darmstadt
Tween® 20	Sigma-Aldrich Chemie GmbH, Munich

5.4 PCR Primers for genotyping

Table 4: Genotyping PCR primers

Target gene	Primer name	Sequence (5' -> 3')
<i>p130</i>	p130 lox F	GTGTTGTAACATTCTCGTGGG
	p130 lox R	GACTGCTGGTATTAGAACCC
<i>p107</i>	p107- COM	TCGCTGGCAGTCTGAGTCAGAG
	p107-WT	CATGAACAGACTTGTCAATCCAC
	p107-Neo	GCACGAGACTAGTGAGACGTGC
<i>R26RLSL-YFP</i>	R26 common forward	AAAGTCGCTCTGAGTTGTTAT
	R26 WT reverse	GGAGCGGGAGAAATGGATATG
	R26-Tva-SA-mut-LP reverse	GCGAAGAGTTTGTCTCAACC
<i>Cd44</i>	Cd44 common forward	GCGACTAGATCCCTCCGTTT
	Cd44 WT reverse	ATCCCAGCTTTGCTTTGCTA

	Cd44 mut reverse	GTTTTCCCAGTCACGACGTT
<i>Rblox</i>	RB lox/ Δ forward	CTCTAGATCCTCTCATTCTTCCC
	RB lox reverse	GCAGGAGGCAAAAATCCACATAAC

5.5 Primers for quantitative real-time PCR (qPCR)

Table 5: Primers for qPCR

Target gene	Primer name	Sequence (5' -> 3')	Origin
<i>Cyr61</i>	Cyr61 forward	GGATCTGTGAAGTGCGTCCT	Mouse
	Cyr61 reverse	CTGCATTTCTTGCCCTTTTT	
<i>Ctgf</i>	Ctgf forward	TGACCTGGAGGAAAACATTAAGA	Mouse
	Ctgf reverse	AGCCCTGTATGTCTTCACACTG	
<i>Gapdh</i>	Gapdh forward	TGCACCACCAACTG	Mouse
	Gapdh reverse	CCTGCTTCACCACCTTCTT	
<i>Ankrd1</i>	Ankrd1 forward	GCTGGAGCCCAGATTGAA	Mouse
	Ankrd1 reverse	CTCCACGACATGCCCAGT	
<i>Amotl2</i>	Amotl2 forward	AGTTGGAGCTGCGTCTGC	Mouse
	Amotl2 reverse	GGTGCCTGTCTGCCTCTG	
<i>Spp1</i>	Spp1 forward	GGAAACCAGCCAAGGTAAGC	Mouse
	Spp1 reverse	TGCCAATCTCATGGTCGTAG	

5.6 Primer list for Cd44 CRISPR constructs

Table 6: Primer list for *Cd44* guide RNA (*gRNA*) constructs

Name	Gene	Exon	Position	Sequence
Guide 1	<i>Cd44</i>	1	394	GCACATCCACATCAGCAGAT
			394 fwd	CACCGGCACATCCACATCAGCAGAT
			394 rev	AAACATCTGCTGATGTGGATGTGC C
Guide 2	<i>Cd44</i>	1	364	GTGCCAGGCTCAACTGCAAG
			364 fwd	CACCGGTGCCAGGCTCAACTGCAAG
			364 rev	AAACCTTGCAGTTGAGCCTGGCAC C
Guide 3	<i>Cd44</i>	1	332	ACGCCATGGACAAGTTTTGG
			332 fwd	CACCGACGCCATGGACAAGTTTTGG
			332 rev	AAACCCAAAACCTTGTCCATGGCGTC

5.7 Antibodies

Table 7: Primary and secondary antibodies used in this study

Antibody(clone)	Host	Supplier	WB	IF/IHCC
AKT (pan) (C67E7)	Rabbit	Cell Signaling	1:1000	
AlexaFluor® 488 anti-rabbit IgG	Goat	Thermo Fisher Scientific		
Anti-CD44 standard	Rabbit	Abcam	1:1000	1:75
Anti-Mouse IgG (H+L), HRP Conjugate	Goat	Promega	1:2000	1:200
Anti-Rabbit IgG (H+L), HRP Conjugate	Goat	Promega	1:2000	
CD44 v6 (BMS145)	Rat	eBioscience		1:500

HSP 90 α/β (F-8)	Mouse	Santa Cruz Biotechnology	1:1000	
LATS1	Rabbit	Cell Signaling	1:1000	
Monoclonal anti- α -Tubulin (DM1A)	Mouse	Sigma Aldrich	1:1000	
p44/42 MAPK (Erk1/2)	Rabbit	Cell Signaling	1:1000	
p53 SC-126 (DO-1)	Mouse	Santa Cruz Biotechnology	1:500	
Phospho-AKT (Ser473)	Rabbit	Cell Signaling	1:1000	
Phospho-LATS	Rabbit	Cell Signaling	1:1000	
Phospho-p44/42 MAPK (Erk1/2)	Rabbit	Cell Signaling	1:1000	
Phospho-YAP(Ser127)	Rabbit	Cell Signaling	1:1000	
Rho-A polyclonal	Rabbit	Thermofisher Scientific	1:1000	
STAT-3 (124H6)	Mouse	Cell Signaling	1:1000	1:100
YAP	Rabbit	Cell Signaling	1:1000	1:75
YAP(H8H1X) XP	Rabbit	Cell Signaling	1:1000	

5.8 Molecular biology kits

Table 8: Kits used for molecular biology

Kit/Detection reagent	Supplier
Maxwell® 16 LEV simply RNA Purification Kit	Promega GmbH
NucleoBond® Xtra Maxi	MACHEREY-NAGEL GmbH
Pierce™ BCA Protein Assay Kit	Thermo Fisher Scientific
QIAquick Gel Extraction Kit	Qiagen GmbH, Hilden
cDNA Synthesis Kit, ProtoScript®	New England Biolabs

5.9 Cell Culture

Table 9: Cell culture medium and medium composition

Reagent/Medium	Supplier
DMEM	Gibco™, Life Technologies
RPMI	Gibco™, Life Technologies
FCS	Gibco™, Life Technologies
PenStrep	Gibco™, Life Technologies
Medium	Composition
Cell culture medium	RPMI/DMEM + 10% FCS + 1% PenStep
Freezing medium	RPMI/DMEM + 10% FCS+ 1% PenStep + 10% DMSO

Table 10: Lentiviral transfection mixture

Reagent	Volume
Lentiviral vector plasmid DNA	8 µg
pXpAX2	4 µg
pMDG2	4 µg
CaCl ₂	50 µl
ddH ₂ O	500 µl

Table 11: TENSIV Buffer- 60 ml recipe

Compound	Volume
TRIS-HCl (1M)	3 ml
EDTA (0.5 M) pH 8.0	2.4 ml
NaCl (5M)	1.2 ml
NP40	600 µL

Table 12: HBS 2x (HEPES Buffered saline) Buffer

Reagents	Amount
NaCl	274 mM
KCl	10 mM
Na ₂ HPO ₄	1.4 mM
D-Glucose	15 mM
HEPES	42 mM
H ₂ O	Adjust to 100 ml

Table 13: Cell lysis buffer

Reagent	Final concentration	Per 500 ml
1 M Tris pH 8.0	10 mM	5ml
0.5 M EDTA pH 8.0	10 mM	10 ml
10 % SDS	0.50%	25 mL
5 M NaCl	100 mM	10 ml
dH ₂ O		Adjust volume

6 Methods

6.1 Mice

All the mouse experiments in this project are carried out in accordance with the German Animal Welfare Act (Tierschutzgesetz) and all animals used were under the guidelines and protocols approved by the local authority.

6.1.1 Mouse models

There are four mouse lines used in the project. Two out of them are pure C57/Bl6 mice used as controls and *Cd44*^{-/-} mice in C57/Bl6 background, which were for chemically induced hepatocarcinogenesis. The other two lines are genetically engineered mice that allow for liver-specific deletion of the *Rb* gene family. Gene knock-out was achieved by using the conditional Cre/lox system with a mixed 129Sv/J; C57/Bl6 background. *Rb* and *p130* – two members of the Rb gene family – were engineered to contain either Lox-P sites or interspaced LoxP-stop-loxP (LSL) sites, allowing for conditional mutation with delivery of liver-specific Cre. Combined with a knock-out of *p107* – the third member of the Rb gene family – in the conditional triple knockout (*TKO*, *Rb*^{lox/lox};*p130*^{lox/lox};*p107*^{-/-}) mouse model. A detailed description of tumor development in the *TKO* mouse model is provided in the introduction section. To further investigate the role of CD44, we crossed the *TKO* mouse model with *Cd44*^{-/-} mice, resulting in the establishment of the *TKO*; *Cd44*^{-/-} mouse model. The reporters used for lineage tracing and determination of gene expression upon genetic recombination were *Rosa26*^{mTmG} reporter (*TKO* mice) or *Rosa26*^{LSL-YFP} reporter (*TKO*; *Cd44*^{-/-} mice). The *Rosa26*^{mTmG} reporter mouse is a dual-fluorescent Cre reporter strain that expresses membrane-targeted Tomato (mT) prior to Cre-mediated recombination and membrane-targeted GFP (mG) after Cre-mediated recombination. The *Rosa26*^{LSL-YFP} reporter mouse carries a loxP-flanked STOP cassette followed by the Enhanced Yellow Fluorescent Protein (EYFP) gene inserted into the *Rosa26* locus. To confirm the presence of the desired genetic variations, routine PCR analysis of tail or ear biopsies was conducted.

6.1.2 Mouse breeding and genotyping

Mouse breedings were set up to maintain the colony and for experiments. The pups from each breeding are weaned after three weeks and labelled with ear punches for later identification. Ear punch biopsies were collected for further genetic analysis. The process of genetic analysis included lysing of individual ear biopsies in ear lysis buffer for DNA extraction. The lysis was done overnight at 55 °C in a thermocycler and the next day the temperature was set to 85 °C for heat inactivation. Once the lysates are cooled down to 4 °C, 1 µl samples from the lysate are used to carry out individual PCR for different genes. The PCR-amplified products were then run against an ethidium bromide-containing agarose gel and the DNA bands were detected using a gel imager.

6.1.3 Intrasplenic injection of adenovirus

Control and test animals were anesthetized with fentanyl (0.05 mg/kg), and hair from the left upper abdominal quadrant was shaved and the mice were placed on a heated operating pad. A 5-mm subcostal incision was made and a sterile cotton swab was used to mobilize the spleen. The syringe containing 5×10^8 units of *Adeno-Cre-GFP* viral particles dissolved in 100 µl of PBS was inserted horizontally into the lower pole of the spleen. The PBS containing viral particles was stored at -80 and kept on ice few minutes prior to the injection. The contents of the syringe were injected and the injection site was compressed with a cotton swab to prevent blood loss after the needle was removed. The wound was closed with a surgical suture and the antagonists flumazenil and atipamezole, were administered subcutaneously. Buprenorphine (0.1 mg/kg) was used as a partial opioid antagonist to counteract fentanyl and at the same time functioned as pain medication. Additionally, carprofen (10mg/kg) were administered orally to control post-operative pain. The animals were monitored closely for 72 hours post-surgery and pain medication was administered in 12-hour intervals. The animals were sacrificed 4 weeks after surgery to analyze liver tissue.

6.2 Cell culture

The mouse hepatoma cell lines, TKO2.1 used in this project was isolated from *TKO* liver tumors as described before (Viatour, Ehmer et al. 2011). The culture medium to grow and maintain the cells was RPMI medium supplemented with 10% fetal calf serum and 1% penicillin/streptomycin. The cells were incubated at 37°C, 5% CO₂ and 100% humidity. The HEK293T cells used for lentiviral vector transfection procedures in this project were cultured in DMEM medium supplemented with 10% fetal calf serum and 1% penicillin/ streptomycin under standard cell culture incubation conditions.

6.2.1 Cryopreservation of cells

The cells that were grown in culture dishes were treated with trypsin to detach them from the dishes. The cells were then diluted with culture medium to inactivate trypsin and transferred to 15 ml tubes falcons for centrifugation at 1000 RPM for 5 minutes. The supernatant from the tube was discarded and the pellet was dissolved in PBS for washing. Further centrifugation was performed to pellet the cells and the pellet was dissolved in ice-cold freezing medium. The dissolved cells were then transferred to labelled cryovials and stored at -80 °C. For long-term storage, tubes were stored in liquid nitrogen.

6.2.2 Lentivirus-mediated transduction with CRISPR constructs

The CRISPR-mediated gene editing is done primarily by exploiting the LentiCRISPRV2 vector. The sgRNA corresponding to the gene of interest was designed using Benchling software. The oligos were annealed and cloned into the BsmB1 digested LentiCRISPRV2 vector backbone. The ligation mixture was then transformed into Stb13 bacteria and transformed colonies were expanded and selected for plasmid extraction. The lentiCRISPRV2 vectors were designed to express specific *sgRNA* and Cas9 for targeted gene edition. The vector system was implemented in a lentivirus that is capable of infecting the targeted cells. The lentiviral particles are produced by co-transfection of lentiCRISPRV2 plasmid along

with packaging plasmids psPAX2 and PMD2.G into HEK293T cells by conventional calcium phosphate-based transfection. HEK293T cells were seeded in DMEM medium a day before actual transfection to reach 60-70 % confluency. The medium of HEK293T cells was changed to fresh medium 1 hour before transfection. The total volume of the transfection mixture was 500 μ l and slowly dripped into 500 μ l 2xHBS buffer (Table.7 and Table.11). The contents were incubated at room temperature for 2 minutes to form calcium phosphate-DNA complexes and sprinkled dropwise to HEK293T cells. The transfected cells were incubated at 37°C and the medium was changed the next day. Simultaneously, TKO2.1 cells to be infected with lentivirus were seeded at appropriate density. The supernatant from transfected HEK293T cells was collected on Day 2 morning and centrifuged at 2000 rpm for 7 minutes to remove the debris. The supernatant was then added to the pre-seeded TKO2.1 cells. The HEK293T transfected cells were immediately replenished with fresh medium. The supernatant harvesting and infection steps were repeated twice every 12 hours. The HEK293T cells were discarded and the medium in the infected TKO2.1 cell lines were replaced with normal DMEM on the third day in the evening. The next day, the medium of infected cells was changed to a puromycin-containing RPMI medium for selection of infected cells. The concentration of puromycin (2 μ g/ml) required to eliminate uninfected cells was determined before the treatment.

6.2.3 Plasmid DNA isolation

Plasmid DNA isolation was performed for the CRISPR-Lenti viral vectors. The reaction mixture of cloning was transformed into a Stbl3 bacterial cell line by electroporation. The plasmid DNA isolation was performed by alkaline lysis and two different yielding methods were used based on the experimental requirements. For a mini preparation, single bacteria colonies were inoculated into 5 ml of LB medium containing selection antibiotics and 2 to 3 ml of the culture were used to extract plasmid DNA using a Qiagen kit according to manufacturers' protocol.

6.2.4 Midi and Maxi preparation

Single bacteria colonies were picked from LB agar plates one day after bacterial transformation and incubated overnight with 4-5 ml of LB media containing necessary antibiotics at 37°C, 200 rpm. For a midi preparation, 5 ml of starter culture was mixed with 200 ml of LB media for high-copy plasmid or 400 ml LB media for low-copy plasmid and incubated overnight at 37°C, 200rpm. The volume of secondary culture varied as 600 ml/ 1200 ml for high-copy and low-copy plasmids respectively for a maxi preparation. Bacterial cells were harvested by centrifugation at 4 °C, 4500-6000 x g for 15 minutes and plasmid DNA was isolated using the Nucleobond kit according to the manufacturer's instructions.

6.2.5 Single colony isolation from infected cells

Each cell line infected by gene-specific sgRNA constructs using the CRISPR/Cas9 method was diluted to attain a cell suspension containing 10 cells per 1 millilitre. Then 100 µl of respective cell suspensions were seeded into 96-well dishes wells to obtain cell colonies derived from a single infected cell. The plates were incubated at 37°C, 5% CO₂ and 100% humidity for approximately 2-3 weeks. The wells containing colonies were marked for further expansion. The sufficiently grown single-cell clones were then trypsinized and re-seeded into 6-well dishes for further expansion.

6.2.6 Proliferation assay using MTT

The MTT assay is a colorimetric assay used to estimate the metabolic activity of cells and indicate their viability or proliferation efficiency. The yellow tetrazolium salt, 3-(4,5-dimethyl-2-thiazolyl)-2,5-diphenyl-tetrazolium bromide, undergoes a reduction to form purple-colored formazan crystals when metabolically active cells are present. This reduction process is facilitated by the presence of NAD(P)H-dependent oxidoreductase enzymes in these cells. The optical density (OD) of dissolved purple crystals corresponds to the number of viable cells in a given sample. Therefore, the number of viable cells after a treatment can be traced and

compared with its untreated control. The *TKO* cell lines targeted with different *sgRNA* constructs to edit *Cd44* were named TKO2.1 394 (Guide 1), TKO2.1 364 (Guide 2.1), TKO2.1 332 (Guide 3). Selected single-cell clones from these different *sgRNA* constructs along with mouse non-transfected (Mouse NT) and uninfected control cells (TKO2.1) were seeded into 96 well plates at different densities (250 cells, 500 cells, 1000 cells, and 1500 cells). The cells were counted using an automatic cell counter for which 10 μ l of cell suspension was mixed with 10 μ l Trypan blue and 10 μ l of the mixture was loaded into counting chamber slides. The plates were incubated at 37°C, 5% CO₂ and 100% humidity and each plate was processed for MTT assay at specific time points. A volume of 10 μ l of MTT reagent was added into each well of the plate and kept in the incubator for 4 hours. The medium along with the spent MTT reagent was discarded from each well and 200 μ l of 1:1 ratio of dimethyl sulphoxide/ ethanol was added. The plate was shaken at room temperature for 10 min and the optical density at 595 nm was recorded by a plate reader.

6.2.7 Colony formation assay (clonogenic assay)

The CRISPR-edited TKO2.1 cell lines were monitored for their colony formation capacity. The results from each cell line were then compared to controls – TKO2.1 uninfected cell and TKO2.1 cells infected with a non-targeting *sgRNA* (Mouse NT). The cells from each line were seeded in 6 well plates at distinct cell densities (1500 cells/well and 500 cells/well) and kept inside the incubator at 37°C, 5% CO₂ and 100% humidity for 10 - 12 days until small distinguishable colonies were observed under the microscope. The plates were then washed thrice with PBS and fixed with a mixture of acetic acid and methanol (ratio acetic acid to methanol 1:7 v/v). Fixation was performed at room temperature for 20 minutes. The fixing solution was then removed to add staining solution to all the wells followed by incubation at room temperature for 1-2 hours. The staining solution was transferred for recycling and plates were immersed in a basket filled with water to remove excess stain. The process was repeated until the water remained clear. The plates were then air-dried

for future analysis by quantifying the percentage of well area covered by colonies using the ImageJ plugin colony area.

6.3 Immunofluorescence staining

Immunofluorescence staining was used to localize the distribution of proteins in cells by antibody staining and subsequent imaging by a fluorescence microscope. The cells were grown on cell culture coverslips layered on a 12-well plate in a cell density of 50,000 cells – 100,000 cells per well. For each experiment and construct, three wells with one coverslip each were used with one coverslip serving as an unstained control. The cells were grown at different time points ranging from 24 hours to 48 hours. The cells were washed thrice with PBS buffer and fixed with 4% paraformaldehyde for 20 minutes. The cells were washed thrice with PBS buffer and stained immediately or covered with parafilm to store for up to one week at 4°C. Staining of cells involved treating them with 0.4% triton-x in PBS for 20 minutes at room temperature to permeabilize cell membranes. The cells were then washed thrice with PBS buffer and blocked with 50 mM Glycine in PBS to reduce background fluorescence. Again, cells were washed thrice with PBS and coverslips were transferred to a humid chamber. The cells on the coverslips were then blocked with 5% goat serum in PBS with 0.25% tween-20 and incubated at room temperature for 45 minutes. The blocking reagent was replaced with a primary antibody in 5 % goat serum in PBS-Tween-20 according to the dilution provided in Table.14 and incubated in a 37°C incubator for 1 hour and kept at 4°C overnight. The coverslips were washed five times with PBS and incubated with fluorescent secondary antibody (1:2000) in 5% goat serum in PBS-Tween-20 for 1 hour at 37°C (Table.15). The coverslips were washed five times and mounted on a slide with Vectashield provided with DAPI to stain nuclei. The coverslips were allowed to settle at 4°C overnight and observed under a fluorescence microscope. Pictures were taken for later quantification.

Table 14: Immunofluorescence assay primary antibody dilution

Reagent	Volume
PBS + 0.25% Tween20	100 μ l
5 % goat serum	5 μ l
1:100 Yap antibody	1 μ l

Table 15: Immunofluorescence assay secondary antibody dilution

Reagent	Volume
PBS + 0.25% Tween20	1000 μ l
5 % goat serum	50 μ l
1:2000 anti-Rabbit 488	0.5 μ l

6.4 Molecular Biology

6.4.1 Genomic DNA isolation

Genomic DNA was isolated from cell culture pellets, tail biopsies, and ear biopsies for subsequent amplification of DNA using polymerase chain reaction (PCR). The lysis solution depended on the type of sample: cell lysis buffer (Table.16) was used for cell pellets, while ear lysis buffer and tail lysis buffer (Qiagen) were used according to the manufacturer. A Lysis buffer of 49.3 μ l together with 0.7 μ l proteinase-K solution was used to lyse the samples overnight at 55°C. The samples were heated at 85°C to inactivate proteinase K and cooled down to 20 °C.

6.4.2 Polymerase chain reaction (PCR)

Polymerase chain reaction (PCR) was performed for both genotyping and gel extraction. Two different Taq polymerases were used (REDTaq® and GREENTaq®) dependent on the amplicon. The suitability of these polymerases

along with each primer set was previously determined. The primers were mostly diluted to working concentration in the ratio of 1:10 and in rare cases some primers were diluted at 1:5 (Table.4). The composition of PCR mixes for both Taq polymerases are given below. A volume of 1µl of lysate from DNA lysis was added to the tube containing the reaction mixture. The reaction mixture was then subjected to PCR using a thermocycler.

Table 16: Genotyping PCR recipe

Components	GreenTaq®	RedTaq®
Primer mix	1µl	1 µl
Polymerase enzyme mix	10 µl	10 µl
Water	8 µl	8 µl
DNA lysate	1 µl	1 µl
Total	20 µl	20 µl

6.4.3 Detection of DNA bands by agarose gel electrophoresis

The percentage of agarose used for gel electrophoresis was set between 1% - 2% depending on the expected band size. Molecular biology grade agarose powder was weighed based on the required percentage and dissolved in 100 – 150 mL 1 x TAE buffer. The mixture was then melted completely by boiling in a microwave for approximately 3 minutes. The melted liquid was then stirred on a magnetic stirrer and brought to 50-55°C. The cassette for casting the gel was set with a comb and the cooled agarose mixture mixed with 5 µl of ethidium bromide solution (0.5 µg/ml) was poured into the chamber. The gel was kept for solidifying for at least 20 minutes. The gel was then immersed in the gel running chamber and subsequently, samples along with a DNA size ladder were loaded into the wells. The voltage of the chambers was set for running at 90V-110V for 45 minutes. The DNA bands in the gel were then visualized under UV light and compared to the ladder for size determination. The picture of the gel was taken using an imager for future reference.

6.4.4 Gel extraction and PCR purification

Genomic DNA isolated from cell culture pellets was used as a template for PCR. PCR was performed as described for genotyping but varied in the final reaction volume. The reaction volume for each PCR was 100 µl which was then divided into two PCR tubes. The percentage of agarose gel for gel extraction was 0.8% - 1% and the width of the comb were adjusted to fit 100 µl in one well. The band of interest from the agarose gel was detected under the UV light and carefully cut out of the gel using a fresh scalpel. The extracted piece of gel was collected in a 2-ml tube and PCR purification was performed using a PCR purification kit from Qiagen according to the manufacturer's protocol. The concentration of the extracted PCR product was determined using a spectrophotometer Nanodrop 2000 and samples were stored at -20 °C.

6.4.5 RNA extraction and cDNA synthesis

RNA was extracted from cell lines cultivated in tissue culture. The cells grown in the culture dishes were trypsinized and centrifuged to separate cells from the culture medium. The residual cell pellets were frozen at -80 °C for at least 24 hours before RNA extraction. Extraction of RNA was done using Maxwell 16 LEV simply RNA cells kit from Promega according to the manufacturer's protocol. The concentration of extracted RNA was determined by using Spectrophotometer Nanodrop 2000. RNA was either immediately taken for cDNA synthesis or stored at -80 °C for later usage. For the synthesis of cDNA, 1 µg of RNA was used utilizing the Superscript II Transcriptase kit (New England Biolabs) according to the protocol provided. cDNA was stored at -20 °C until further usage.

6.4.6 Quantitative real-time PCR (qPCR)

Quantitative real-time PCR (qPCR) quantifies the amplification of nucleic acids in real-time as the thermocycler reaction progresses. The qPCR reaction was set using Applied Biosystems SYBR™ which contains a DNA binding green fluorescent dye, buffers, DNA polymerase and dNTPs together with qPCR-specific primers,

water and cDNA. The list of qPCR primers is listed in Table 6. The reaction mixtures were prepared for each target gene. The expression analysis of the target gene mRNA was normalized against the housekeeping gene GAPDH. The instrument used for the qPCR was the StepOnePlus™ real-time PCR system. The results were quantified using StepOnePlus™ software and the $2^{-\Delta\Delta C_t}$ method ($2^{\Delta C_t(\text{GAPDH}) - \Delta C_t(\text{target gene})}$).

6.5 Biochemistry

6.5.1 Protein extraction

Cells intended for protein extraction were grown in 10 cm dishes up to 80% confluency and trypsinized. The cell suspension was centrifuged to separate cells from the culture medium and the residual pellets were stored in 1 ml tubes at -80 °C until protein extraction. The pellets were dissolved in 500 µl of TENSIV or RIPA buffer with 1x protease inhibitor mix. The contents in tubes were vortexed, immediately kept on ice for 20 minutes and vortexed every 5 minutes. After 20 minutes, the tubes were centrifuged at 15000 rpm for 10 minutes at 4°C. The supernatant was carefully transferred to a fresh tube. Concentration was instantly determined and samples were stored at -80°C.

6.5.2 Protein Concentration Estimation

The estimation of protein concentration was determined by using the Pierce™ BCA Protein Assay Kit according to the protocol provided by the manufacturer. The assay was performed with samples of interest along with different concentrations of BSA to establish a standard curve. All samples were diluted in an assay reagent mixture at a 1:10 ratio and performed as triplicates in a 96-well plate. The plate was then incubated at 37°C for 30 minutes and the readings were measured by Multiskan™ FC microtiter plate photometer at 562 nm. The concentrations of samples were determined according to the values from the standard curve. The protein concentration was adjusted to 2 µg/µl with TENSIV/ RIPA buffer and

Laemmli buffer. The samples were then denatured at 95 °C for 10 minutes and stored at -20°C.

6.5.3 SDS Polyacrylamide gel electrophoresis (SDS-PAGE)

This method is used to segregate proteins in a sample based on their molecular weight where higher molecular weight proteins stay in the upper portion of the gel whereas lower molecular weight proteins migrate towards the bottom. The percentage of gel varied according to the molecular weight of the protein and as the percentage of gel increases from 7% to 15 %, the pore size decreases. The glass plates used were either 1 mm or 1.5 mm gel thickness and placed in a casting stand. The composition of reagents for casting the gel is listed in Tables 14 and 15. The gel consisted of two parts where first section contains the resolving gel and then the stacking gel. The contents of the resolving gel mixture were poured into the gap between the glass plate and layered with 1 ml of isopropanol to evenly distribute the contents. Once the gel was polymerized, the mixture for the stacking gel was poured on top of the resolving gel with an inserted 10-well or 15-well comb. The polymerized gel was immediately used for running the samples or kept at 4°C to use within a day. For loading samples to the gel, the gel casted within the glass plates was immersed in 1x running buffer containing bio-rad SDS running chamber. The comb was removed for loading the denatured protein samples. Each well was loaded with a volume corresponding to 50-60 µg of protein and a protein ladder was loaded in the last well. The chamber was then connected to a bio-rad power system set to 50V and ran until it reached the stacking gel. The voltage was then increased to 100 V till the dye front reached the bottom of the gel.

Table 17:Composition of running gel

The final concentration of acrylamide	7.50%	10%	12.50%
30% acrylamide	2.5 ml	3.3 ml	4.3 ml
TRIS (pH8.8, 1.5M)	2.5 ml	2.5 ml	2.5 ml
10% SDS	100 µl	100 µl	100 µl
TEMED	10 µl	10 µl	10 µl
10% APS	50 µl	50 µl	50 µl
distilled H ₂ O	4.84 ml	4.0 ml	3.0 ml

Table 18: Composition of stacking gel

Stacking gel	Volume
30 % Acrylamide	1.6 ml
TRIS (pH 6.8, 1 M)	1.3 ml
10 SDS	100 µl
TEMED	5 µl
10 % APS	75 µl
Distilled H ₂ O	6.9 ml

6.5.4 Western blot

The technique involves transferring proteins separated in an SDS-PAGE to a polyvinylidene difluoride (PVDF) membrane and quantifying the protein of interest by tracing it with antibodies. The PVDF membrane was activated in methanol for 30 seconds and transferred to a 1x transfer buffer. The gel was taken out from the glass plate once SDS-PAGE was finished and equilibrated in 1x transfer buffer for 10 to 15 minutes. The transfer was performed in a bio-rad transfer apparatus filled with 1x

transfer buffer and a sandwich of gel along with the blotting membrane prepared inside the cassette was immersed into the tank. The transfer was performed at 4°C for 2 hours at a constant current of 400 mA. The membrane was stained with Ponceau S solution to confirm the blotting and washed with water to remove the stain. The blot was then blocked with 5% skimmed milk prepared in 1x TBST buffer with shaking at room temperature for 45 minutes and washed thrice for 10 minutes each with 1x TBST buffer. The blot was incubated with the primary antibody at 4°C overnight for the protein of interest and the dilution factor varied for different proteins (Table. 8). The membrane was then washed thrice with 1x TBST buffer for 15 minutes each and incubated with a secondary antibody (1:2000) for 1 hour at room temperature. The membrane was again washed thrice with 1x TBST buffer for 15 minutes each. The secondary antibody is conjugated with horse radish peroxidase (HRP) which can be detected using Western Blotting Substrate or ECL prime for least expressed proteins on an ECL CL-XPosure™ Film by Pierce™ ECL. The developed film was scanned for quantification using ImageJ and it was normalized by the detection of loading control proteins (beta-TUBULIN, GAPDH or HSP90).

6.5.5 Statistical analysis

The software used for all statistical analysis was GraphPad Prism and all the experiments were repeated at least three times if not indicated otherwise. The data from all the experiments are represented as the average value \pm the standard error of the mean (SEM). A two-tailed Student's tests were used to determine the statistical significance of the results. For the human microarray data, a correlation analysis was performed using linear regression analysis.

7 Results

7.1 Positive correlation between CD44 and YAP in the *TKO* mouse model and other human HCC mouse models

Using initial data derived from the co-expression of CD44 and YAP in *TKO* pre-cancerous and tumor lesions, our primary goal focused on determining if there exists a positive correlation between CD44 and YAP target genes within *TKO* liver tumors. Analysis of the microarray gene expression profile revealed a favorable correlation between CD44 and YAP target genes, specifically *Gpc3* and *Ctgf* (Fig. 8).

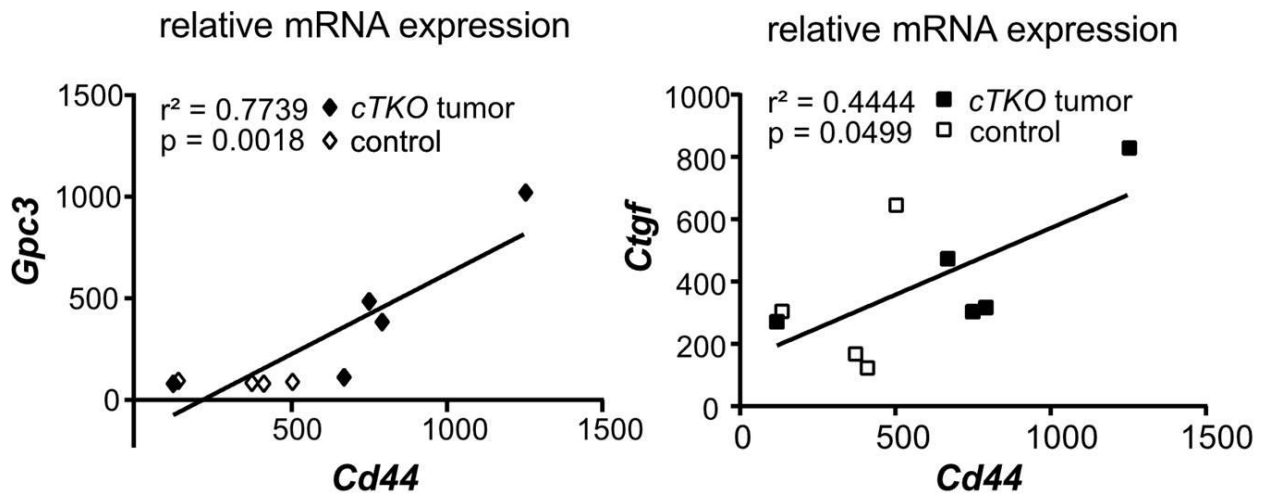


Figure 8: Microarray analysis of *TKO* tumor

Correlation analysis between CD44 and YAP target genes (*Gpc3* and *Ctgf*) mRNA expression in the *TKO* liver tumors- data from microarray analysis.

We next investigated, if the correlation of YAP and CD44 observed in the *TKO* model was conserved in other HCC models. To this aim, we conducted immunohistochemistry staining to assess the expression of YAP and CD44 in HCC mouse models, including chemically induced HCC in DEN-treated mice as well as genetic HCC models (*Mdr2*^{-/-}, and *Albumin-Lymphotoxin (AlbLTaβ)* mice). The

staining showed co-expression of CD44 and YAP in the DEN and *Mdr2*^{-/-} mouse model whereas, in the Albumin-Lymphotoxin model, both proteins were found to be absent in the *AlbLTαβ* model (Fig. 9).

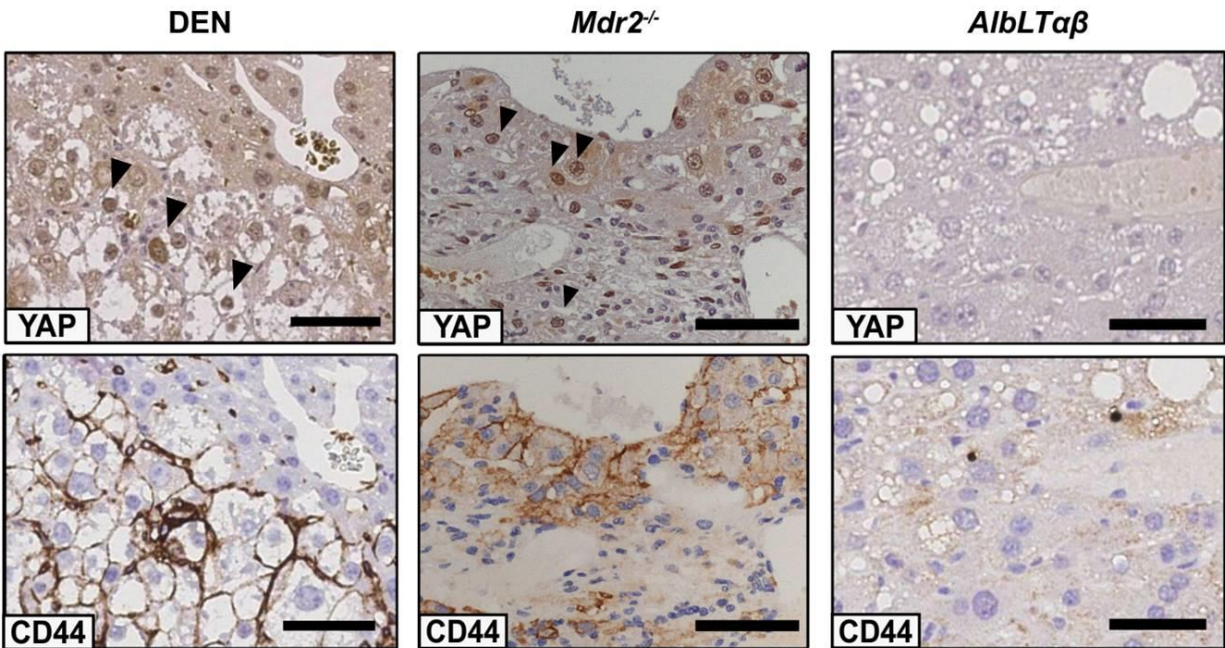


Figure 9: Immunohistochemistry staining of HCC mouse models

IHC staining of YAP (top) and CD44 (bottom) in mouse HCC models including DEN, *Mdr2*^{-/-} and *AlbLTαβ* models. The arrows denote nuclear expression of YAP. Scale bars 50 μ m

7.2 CRISPR/Cas9-based *Cd44* inactivation reduces *TKO* liver cancer cell proliferation

In order to gain a deeper understanding of the involvement of CD44 in YAP regulation, given the observed positive correlation in *TKO* tumors, we devised three distinct lentiCRISPRV2 constructs to specifically target *Cd44* in cell lines derived from *TKO* tumors. The guide RNA (*gRNA*) sequences, targeting Exon 4 of the *Cd44* gene, were designed using Benchling software. These sequences featured a 3bp PAM sequence at the 3' end and had an overall length of approximately 20 bp. The lentiCRISPRV2 functions as a unified vector system, encompassing both the Cas9 and chimeric *gRNA* expression systems. The vector underwent digestion with the

Bsmb1 enzyme, and subsequently, annealed oligos corresponding to the *gRNA* were cloned into a singular *gRNA* scaffold.

TKO2.1 cells then underwent lentiCRISPR viral transduction. Subsequently, puromycin treatment was employed to eliminate non-targeted cells. We then examined the proliferative characteristics of three distinct *Cd44*-mutant mixed populations in comparison to the TKO2.1 parental cell line. The cells were seeded in 96-well plates, and a viability assay using MTT was conducted after 96 hours (Fig. 10). Our findings revealed a reduced number of viable cells in all three *Cd44*-mutant cell sets when compared to the control group.

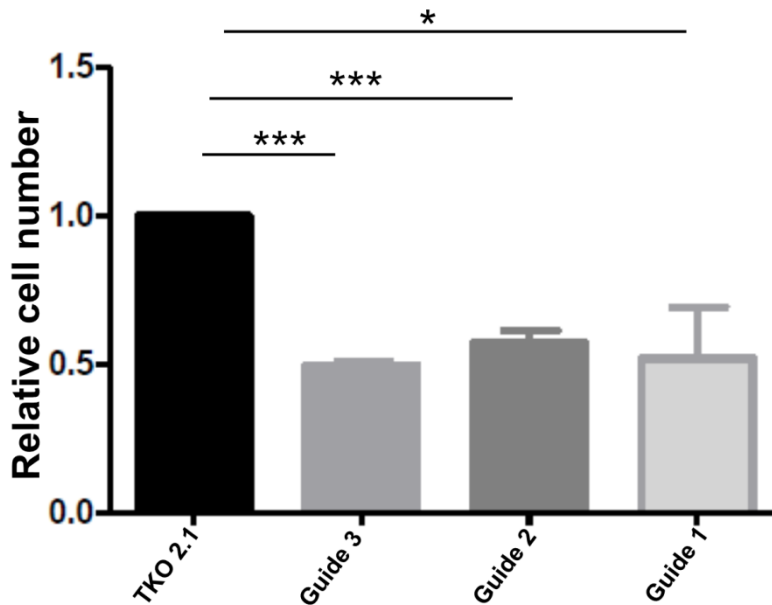


Figure 10 : MTT assay in mixed population of *TKO* liver cancer cell line after *Cd44* CRISPR edition.

Relative cell number in *Cd44*-targeted TKO2.1 cells (Guide 1 – 3, grey) in comparison to TKO2.1 control cells (black). Error bars indicate the S.E.M of three independent experiments. (*, $p < 0.05$; ***, $p < 0.001$)

Subsequently, we conducted a serial dilution of each distinct *Cd44* mutated mixed population to generate single-cell clones. Genomic DNA was extracted from these clones and subjected to sequencing for indel distribution analysis using TIDE analysis (Fig. 11). TIDE software was utilized to assess genomic editing efficiency

and identify the prevalent types of insertions and deletions (indels) within the DNA of the targeted cell pool. The selection of single-cell clones was then based on the insights obtained from the TIDE data (Brinkman, Chen et al. 2014).

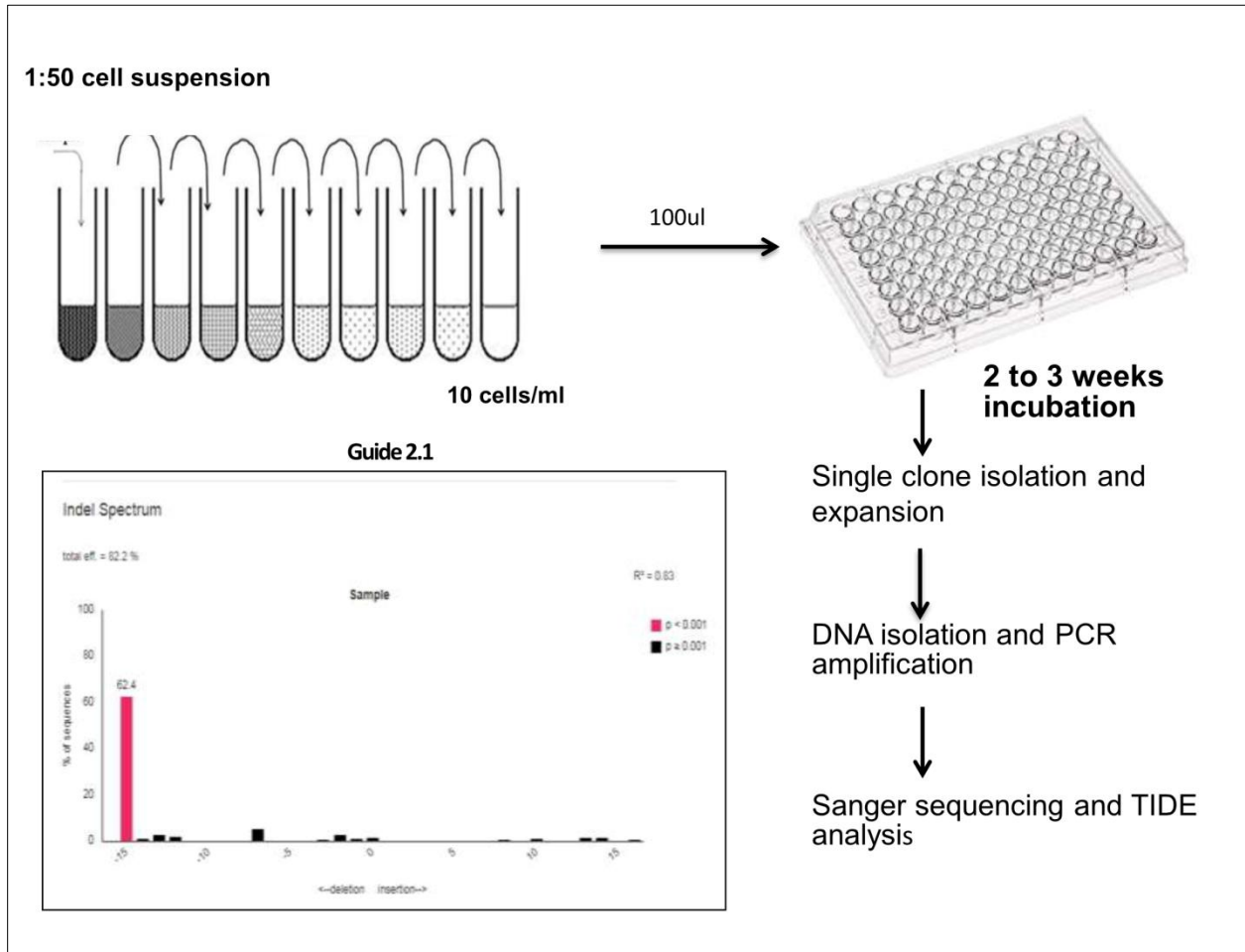


Figure 11: Schematic representation of single cell clone derivation from *Cd44* mutant mixed populations.

We then confirmed the lack of or severely reduced CD44 expression in previously selected single-cell clones through western blot analysis. The *Cd44* mutants exhibited minimal to no CD44 expression when compared to control cell lines (Fig. 12B). Additionally, we conducted a proliferation assay using MTT and a colony formation assay for the *Cd44* single-cell clones,

alongside the non-transfected TKO2.1 cells and CRISPR-derived mouse non-targeting control cells. In both experiments, we observed diminished cell proliferation in *Cd44* mutants when compared to the control groups (Fig. 13).

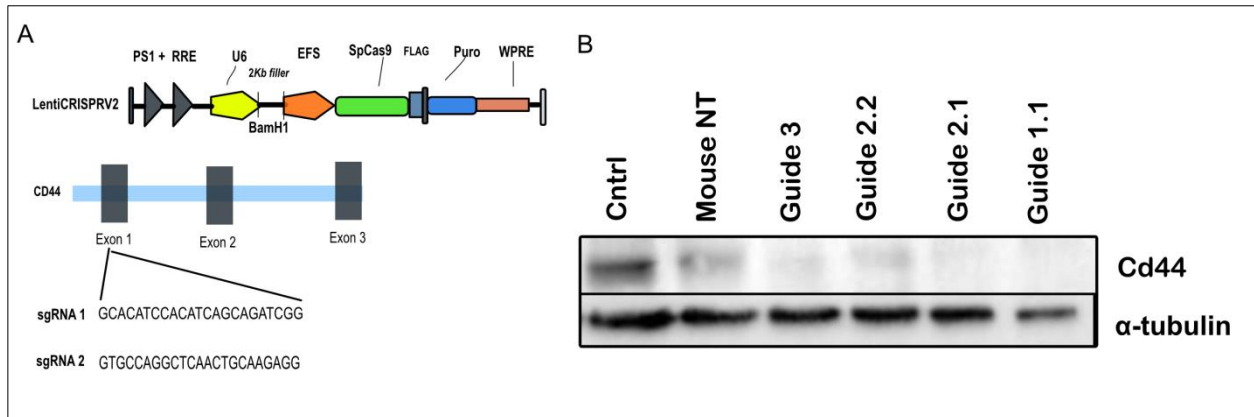


Figure 12: *Cd44* inactivation in TKO2.1 cells derived from *TKO* tumor

(A) Representation of cloning *gRNA* targeting *Cd44* gene into LentiCRISPR V2 backbone
 (B) Western blot analysis of CD44 expression in control and CRISPR/Cas9 mediated *Cd44* inactivated TKO cell line.

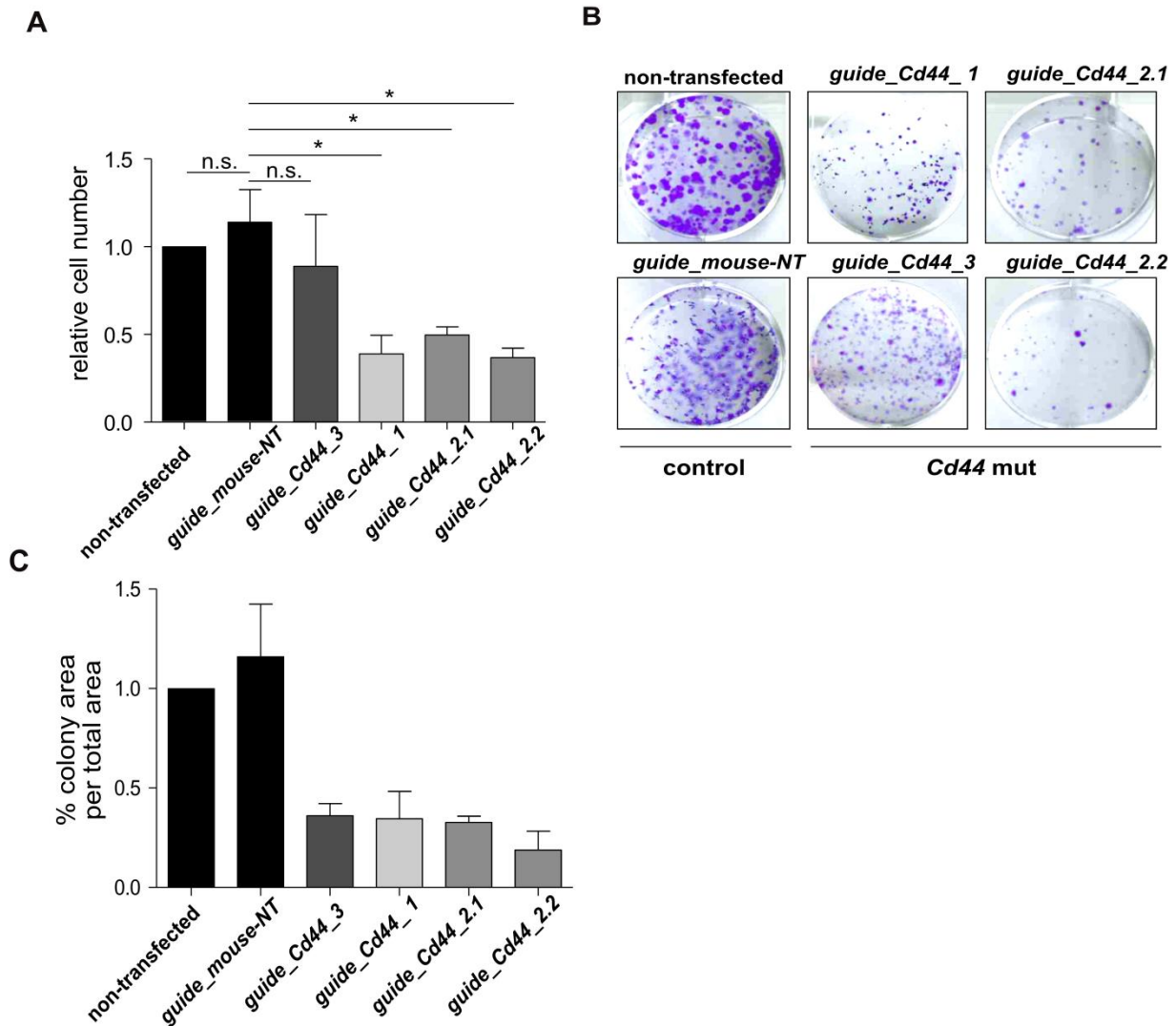


Figure 13: Cell viability analysis of *Cd44*-mutant cells by MTT assay

A) Cell viability test by MTT assay of TKO cells after CRISPR-mediated inactivation of the *Cd44* gene. Error bars indicate the S.E.M of three independent experiments. (*, $p < 0.05$; **, $p < 0.01$). (B) Colony formation assay of TKO cells after CRISPR-based *Cd44* gene edition. (C) Quantification of colony formation assays from two independent experiments. Error bars indicate the S.E.M of three independent experiments. (*, $P < 0.05$; **, $P < 0.01$)

7.3 *Cd44* ablation in *TKO* cell lines negatively regulates YAP expression

In light of the preliminary observation of a positive correlation between CD44 and YAP in *TKO* mouse liver tumors, we explored the YAP regulation in CRISPR-edited *Cd44* mutant cells. The active and inactive YAP (phosphorylated YAP, P-YAP) protein expression in *Cd44*-mutant cells and control cells was determined by western blot. Importantly, the loss of CD44 in *Cd44* mutant cells resulted in the downregulation of YAP and P-YAP protein expression (Fig. 14A). Furthermore, RNA sequencing analysis utilizing Gene Set Enrichment Analysis (GSEA) confirmed the downregulation of genes associated with YAP canonical signaling in a specific single-cell clone; Guide 1, in comparison to the control cell line (Fig. 14 B).

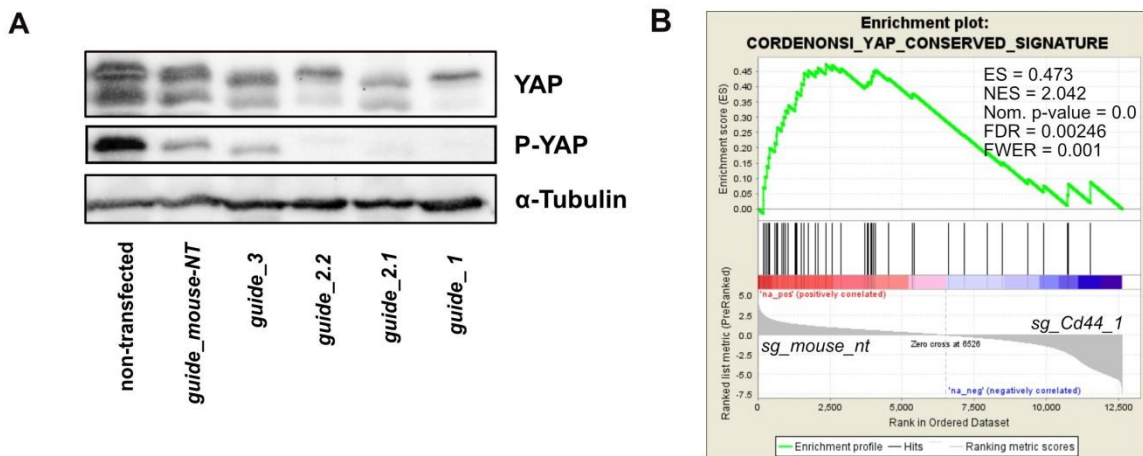


Figure 14: *Cd44* inactivation downregulates YAP expression

(A) Western blot analysis of YAP expression in *TKO* control and CRISPR edited cells. α -tubulin serves as loading control. (B) Enrichment plot generated by GSEA bioinformatics tool showing enrichment of a YAP signature in control vs a *Cd44*-mutant cells using a gene set generated from prominent YAP targets (Cordenonsi, Zanconato et al. 2011).

Subsequently, we examined the mRNA expression of YAP target genes in both *Cd44*-mutant cells and control cells using quantitative PCR (qPCR). The results revealed a significant downregulation of YAP target genes, including *Ankrd1*, *Amotl2*, and *Ctgf* in *Cd44*-mutant cell lines in comparison to the control cell lines (Fig. 15).

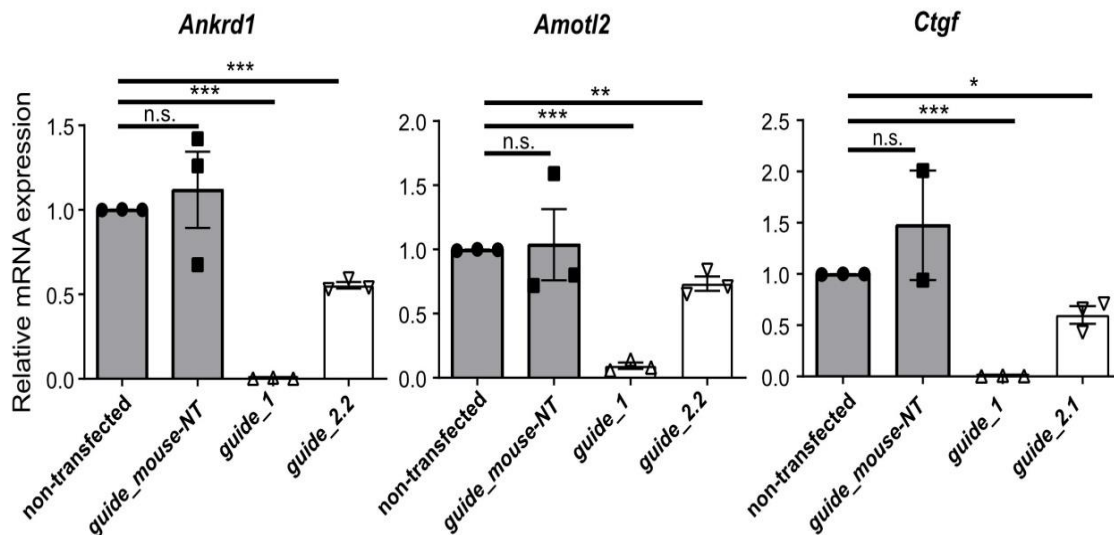
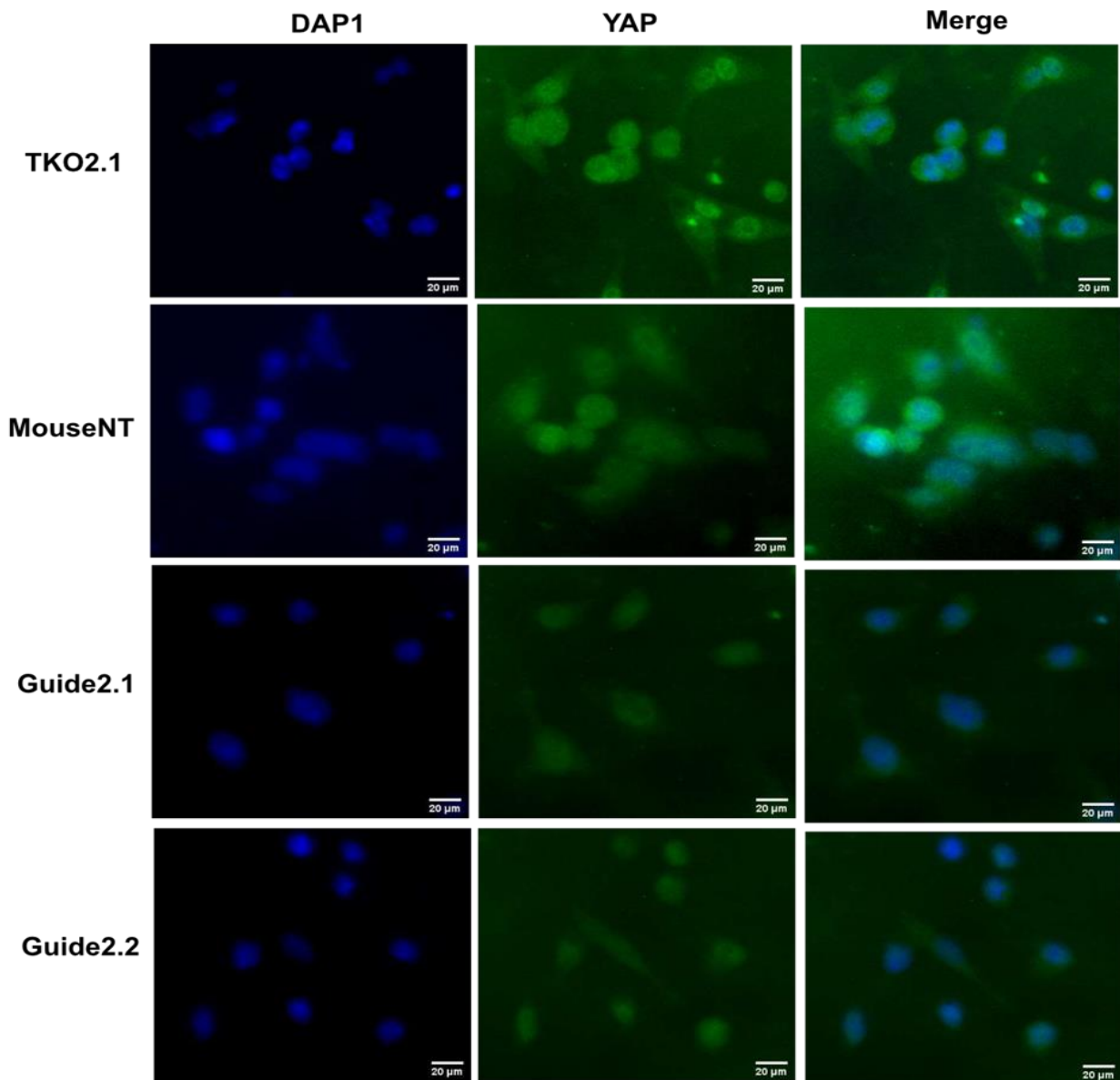


Figure 15: Relative mRNA expression of YAP target genes

The mRNA expression of indicated YAP target genes: *Ankrd1*, *Amotl2* and *Ctgf* in *TKO2.1* control and *Cd44*-mutant cell lines were quantified by RT-PCR. Data represents SEM of three independent experiments (*, $p < 0.05$; **, $p < 0.01$; ***, $p < 0.001$; n.s., not significant).

7.4 *Cd44*-mutant TKO cells showed nuclear exclusion of YAP

Cd44-mutant cells showed a downregulation of YAP compared to control cell lines, as evident from western blot analysis (Fig. 12). However, since YAP expression was not entirely absent in *Cd44*-mutant cells, we investigated the cellular localization of YAP using immunofluorescence. The actively dividing cells were initially fixed and stained with an anti-YAP antibody. Co-staining with DAPI was performed to visualize the nuclear region. Immunofluorescent staining showed significantly reduced nuclear YAP expression in *Cd44*-mutant cells compared to control cells (Fig. 16). Additionally, there was a concomitant increase in the percentage of cells with expression of inactive cytoplasmic YAP in *Cd44*-mutant cells compared to control cells, suggesting a potential nuclear export of YAP. The sequestration of YAP into the cytoplasmic compartment hinders its ability to transcribe downstream target genes and ultimately leads to degradation of YAP in the cytoplasm.



63 X oil immersion

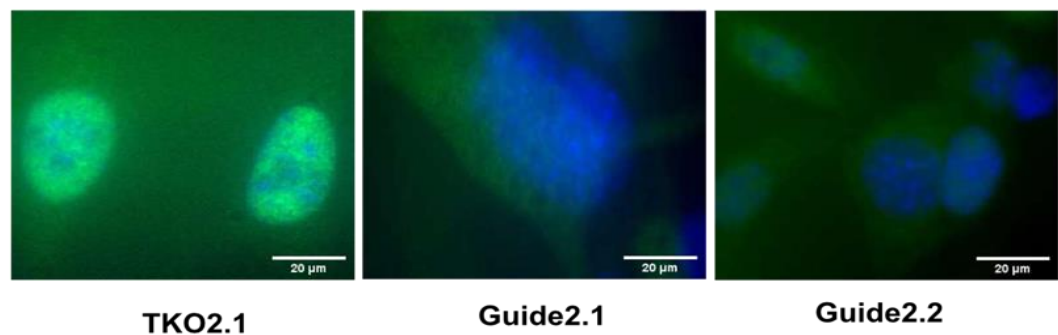


Figure 16: Immunofluorescence staining of YAP in *Cd44* mutant cells and control TKO2.1 cell lines

((Top): Immunofluorescent staining of *TKO* control and *Cd44* mutant cell lines. The cells were incubated for 24 hours and were stained with YAP antibody (green) and DAPI (blue). (Bottom): The magnified images of YAP immunofluorescent staining showing nuclear localization of YAP in *TKO* control cells and cytoplasmic YAP in *Cd44*-mutant cell lines. Scale bars 20 μ m.

The nuclear and cytoplasmic YAP distribution was manually analyzed from the YAP-positive images. Five distinct images were examined for each cell line (Fig. 17A). The overall YAP intensity in each image was classified as high, intermediate, or low, determined by visual inspection for each line (Fig. 17B).

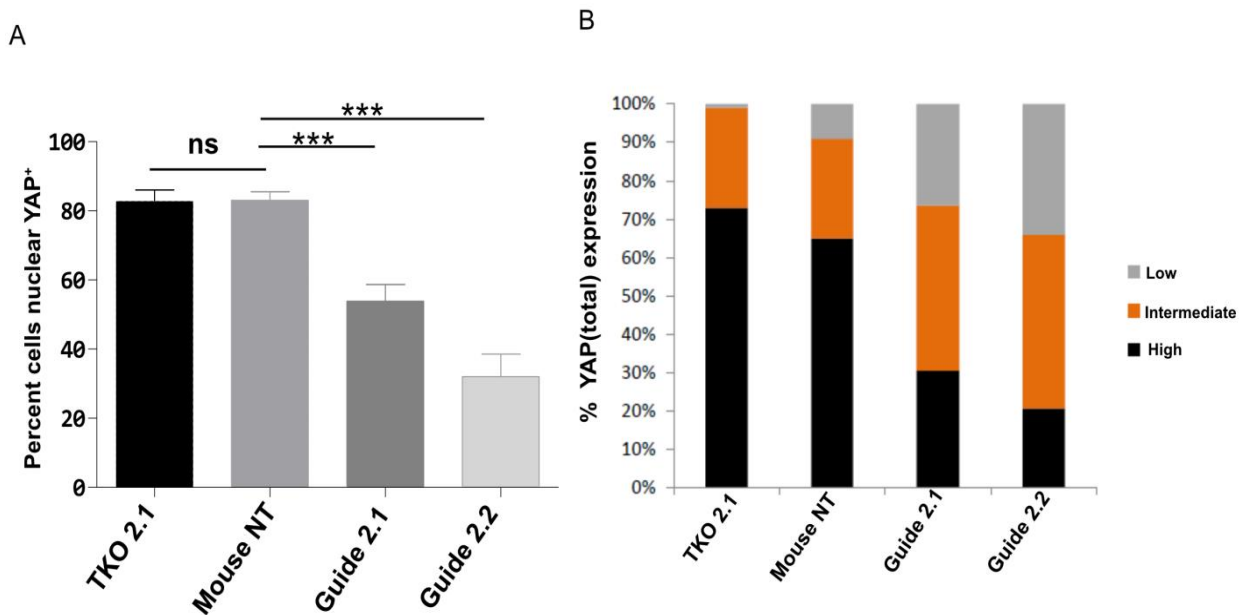


Figure 17: Quantification of YAP staining

(A): Quantification of YAP immunofluorescent staining in *TKO2.1* control and *Cd44* mutant cell lines. The data represent the percentage of nuclear YAP+ cells. (B): data represents the intensity of YAP expression in each cell line. Statistical analysis is performed by student t-test (***, $p < 0.001$; n.s, not significant).

7.5 *Cd44* mutation increased expression of senescence marker p16

Tumor cells attain uncontrollable cell proliferation by bypassing mechanisms of cellular homeostasis. The activation of tumor suppressors such as p53 ensures the controlled cellular proliferation by a variety of cellular mechanisms which includes

the promotion of irreversible cell cycle arrest mediated by cyclin-dependent kinase inhibitors p16 and p21. The cell cycle phase G1-S is controlled by the p16-Rb pathway. The prevention of Rb phosphorylation by p16 makes Rb remain associated with E2F1 and prevents it from the downstream transcription of its target genes that support the G1/S transition (Rubin, Gall et al. 2005).

Flattened and enlarged cells were observed in certain *Cd44* cell lines that were generated. To understand if the phenotype is associated with cellular senescence, we checked the p16 expression in all our *Cd44*-mutant cells by immunofluorescence staining. Interestingly, *Cd44*-inactivated cell lines exhibited increased expression of p16 compared to the non-transfected cells (Fig. 18). As p16-mediated cellular senescence is *Rb* dependent and *TKO* cell lines lack the *Rb* family, we speculate the cell undergoes senescence independent of the *Rb* family.

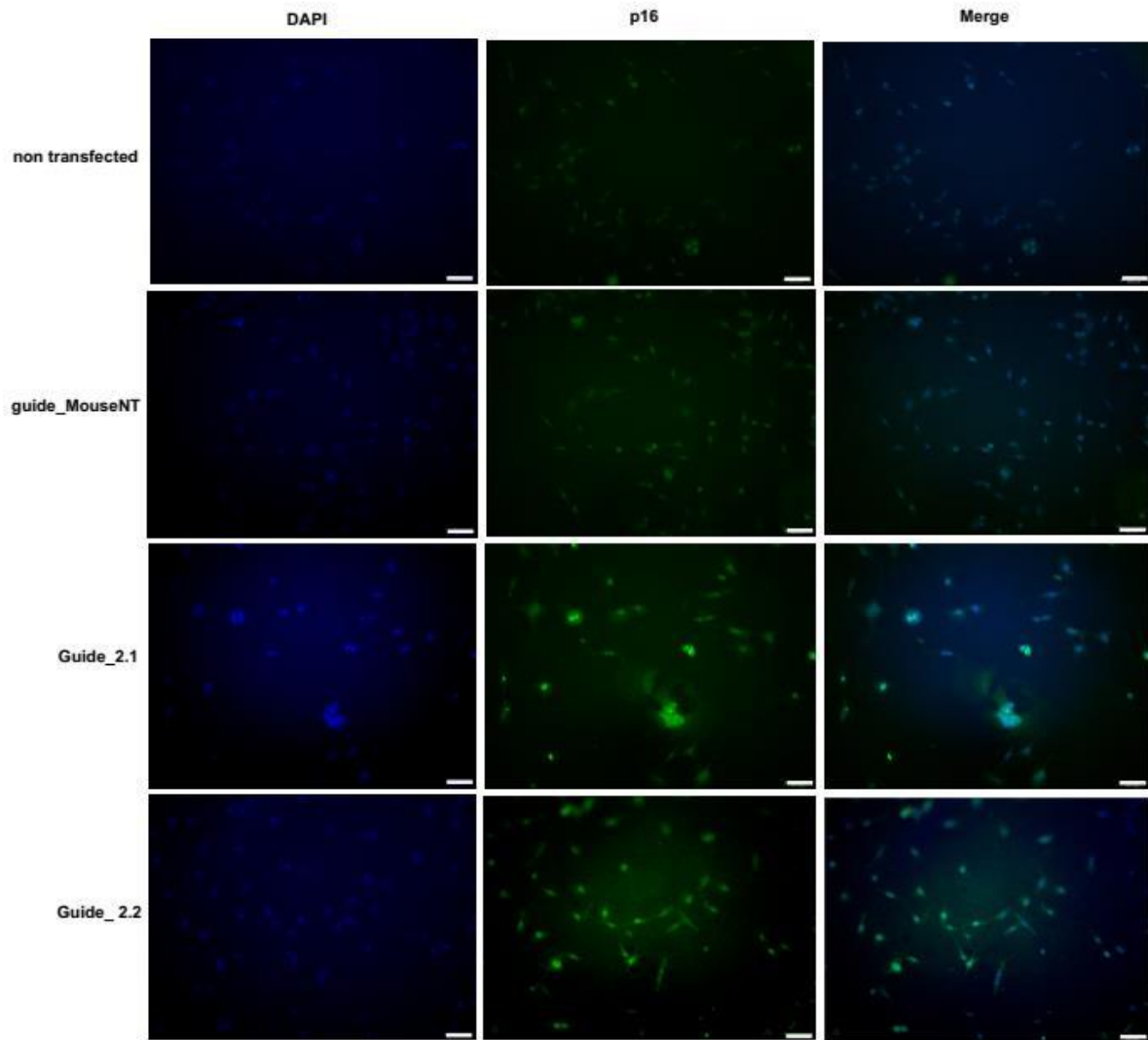


Figure 18: Immunofluorescence staining for p16 in control and *Cd44*-mutant TKO2.1 cells

Control and *Cd44*-mutant cells were seeded and incubated for 24 hours and stained with p16 (green) antibody and DAPI (blue). The upper two rows are control cell lines and lower rows are *Cd44*-mutant cells. Scale bar corresponds to 20 μm .

7.6 Mechanism of action within the CD44-YAP axis

The inactivation of *Cd44* in *TKO* liver cancer cells has effectively reduced expression of YAP and its downstream target genes and had a functional effect by reducing cell proliferation. We now aimed to investigate the mechanism by which CD44 regulates YAP from RNA sequencing and western blot expression analysis. The comparative analysis of RNA sequencing suggested possible downregulation of Src pathway components in *Cd44* mutants (Fig. 19A). We also found a decreased protein expression of STAT-3 and RhoA in two of the *Cd44* mutant cell lines (Fig. 19B). Although there is no evidence suggesting the direct regulation of YAP by both Src and STAT-3, the cross-talk between them has been identified in HCC as well as other types of cancers (Lamar, Xiao et al. 2019). However, the role of RhoA as a mediator of YAP regulation through CD44 has been found in a previous study based on *in vitro* assays in human lung and liver cancer cell lines (Zhang, Xia et al. 2014).

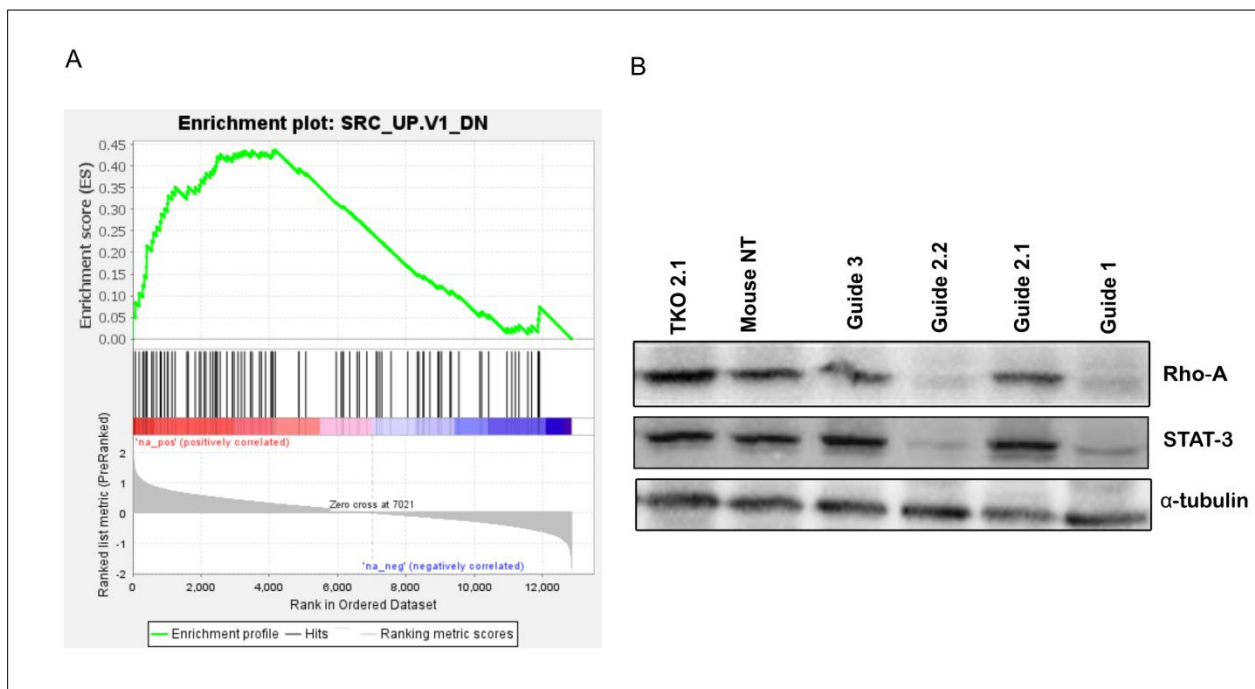


Figure 19: Candidate signaling pathways are downregulated in *Cd44*-mutant cells

(A) GSEA enrichment plot showing genes downregulated upon Src overexpression in control vs *Cd44* single cell mutant using gene set generated from (Bild, Yao et al. 2006)
(B) Western blot analysis of Rho-A and STAT-3 expression in *TKO2.1* control and *Cd44* mutant cells. α -tubulin serves as loading control.

For a better understanding of the functional relevance of these pathways, we performed inhibition assays in TKO2.1 control cells using specific inhibitors: H0-3867 (STAT-3 inhibitor), saracatinib, dasatinib (Src inhibitors) and rhosin (Rho-A inhibitor). Importantly, we did not observe any changes in proliferation when cells were treated with H0-3867 and saracatinib (Fig. 20A). On the other hand, cells treated with dasatinib showed reduced cell numbers. However, dasatinib effects were inconsistent and – most importantly – comparable between TKO2.1 and *Cd44*-mutant cells, indicating that dasatinib-mediated Src inhibition is independent of the CD44-YAP axis (Fig. 20B). However, the TKO2.1 cells treated with rhosin showed a consistent reduction in cell numbers (Fig. 20A).

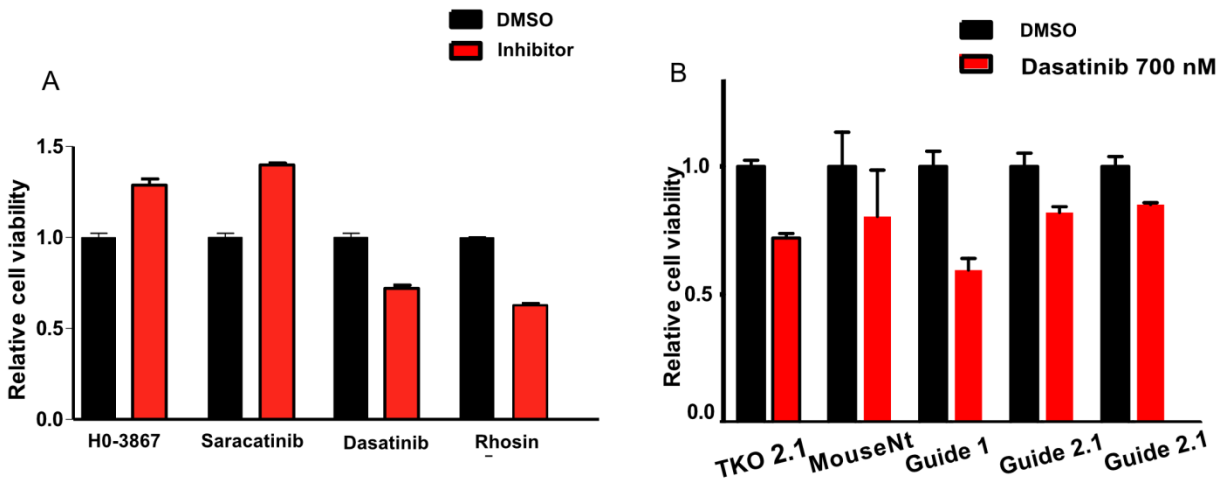


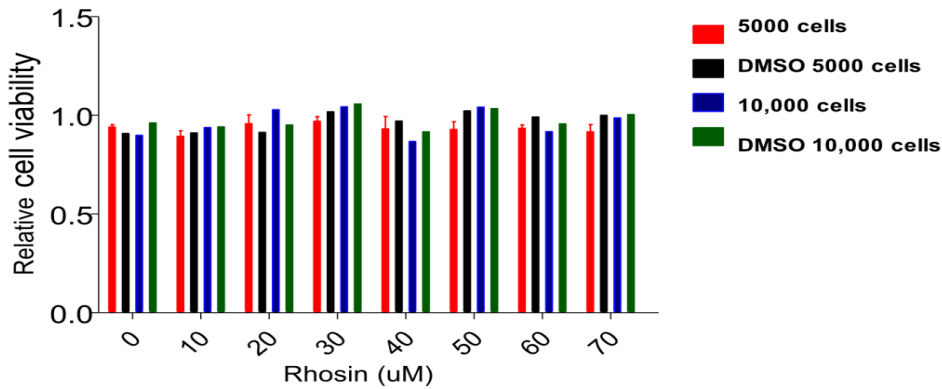
Figure 20: Proliferation analysis of TKO control cells and *Cd44*-mutant cells after inhibitor treatments

(A) MTT assay of TKO2.1 control cells after treatment with inhibitors: STAT-3 (H0-3867-15 μ M), Src: saracatinib (20 μ M), dasatinib (700 nM) and RhoA (rhosin, 60 μ M). (B) MTT assay of TKO2.1 control cells and *Cd44*-mutant cells after treatment with dasatinib.

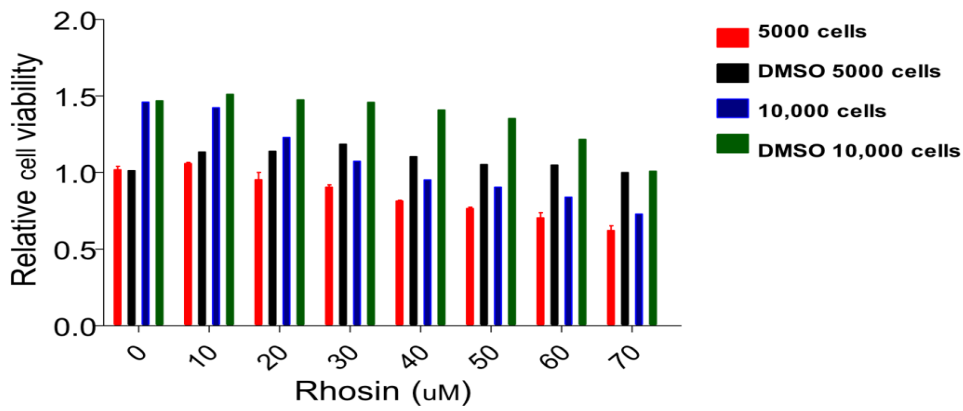
7.7 Rho-A is crucial for CD44-mediated YAP regulation

Rhosin serves as a potent inhibitor specifically targeting the RhoA subfamily of Rho GTPases. It binds specifically to RhoA, inhibiting the interaction between RhoA and RhoA-GEF. In the RhoA inhibition assay conducted using rhosin in non-transfected cells, a noticeable decrease in cell proliferation was observed. To validate this outcome, we conducted the assay with varied cell densities and time points in 96-well plates. Cell viability was assessed by MTT assay after treating cells with rhosin and DMSO-treated controls at 24 hours, 48 hours, and 72 hours, using both 5000 cells per well and 10,000 cells per well (Fig. 21). We noticed a decline in cell viability with increasing concentrations of rhosin and prolonged incubation time. This effect was particularly pronounced in cells sparsely seeded at 5000 cells per well. Subsequently, we extended our rhosin inhibition experiments to *Cd44*-mutant cells, using 60 µg of rhosin with 5000 cells per well for a 72-hour incubation period. Importantly, a reduction in cell proliferation was observed solely in the non-transfected cell lines and not in the *Cd44*-mutant cells indicating that RhoA has an important function within the CD44-YAP axis (Fig. 22A).

A



B



C

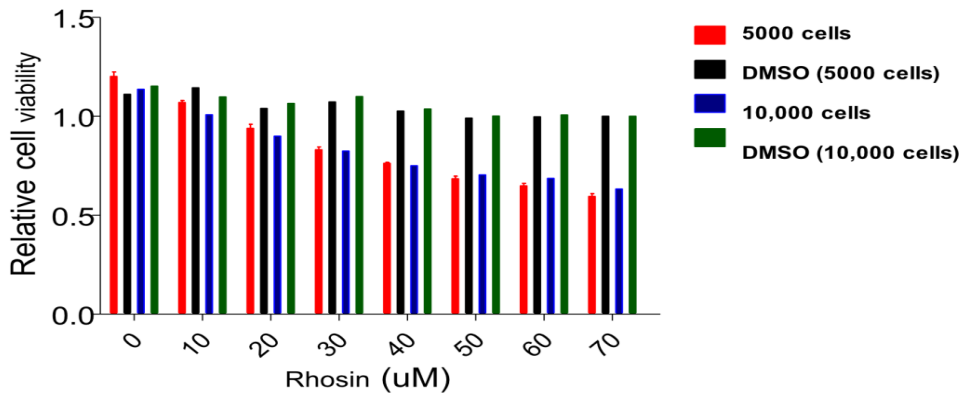


Figure 21 : Rhosin treatment in *TKO2.1* liver cancer cells in varied concentrations.

The cells were seeded in 96 well plates a day before rhosin treatment. The cells were treated with DMSO as control and increasing concentration of rhosin ranging from 10 μM to 70 μM for 24 hours (A), 48 hours (B) and 72 hours (C), respectively.

The comparative analysis of RNA sequencing data also confirmed the enrichment of genes corresponding to RHO-A GTPases signaling in control cell lines compared to *Cd44*-mutant cells (Fig. 22 B).

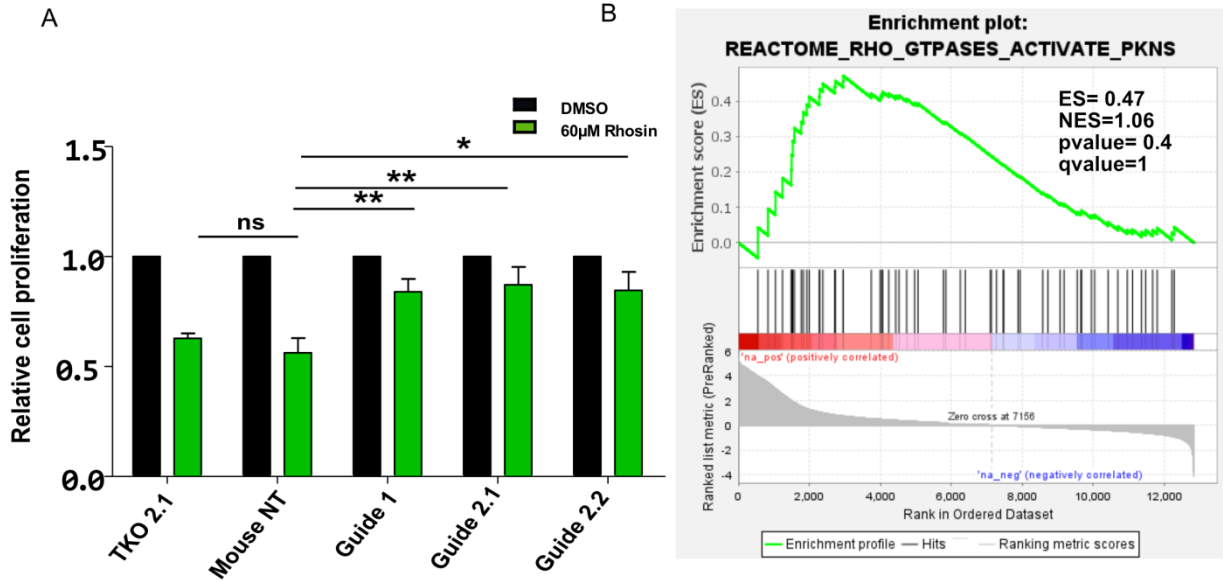


Figure 22: CD44 mediated YAP regulation is Rho-A dependent

(A) Cell viability test by MTT assay of control and *Cd44*-mutant cells after 72 hours incubation with the RhoA-inhibitor rhosin (60 µM). The error bar denotes SEM of three independent experiments (*, $p < 0.05$; **, $p < 0.01$; ns, not significant). (B) GSEA plot showing enrichment of a Rho-GTPase activation gene set in control vs *Cd44*-mutant cells.

We then assessed the expression of YAP in both control and *Cd44*-mutant cells after rhosin treatment at various time points – 3 hours, 6 hours, and 9 hours by western blot analysis. Notably, we observed a substantial downregulation of YAP protein expression 3 hours and 6 hours after rhosin treatment in TKO2.1 liver cancer cell lines, confirming that RhoA influences YAP expression in TKO cells (Fig. 23 A,B).

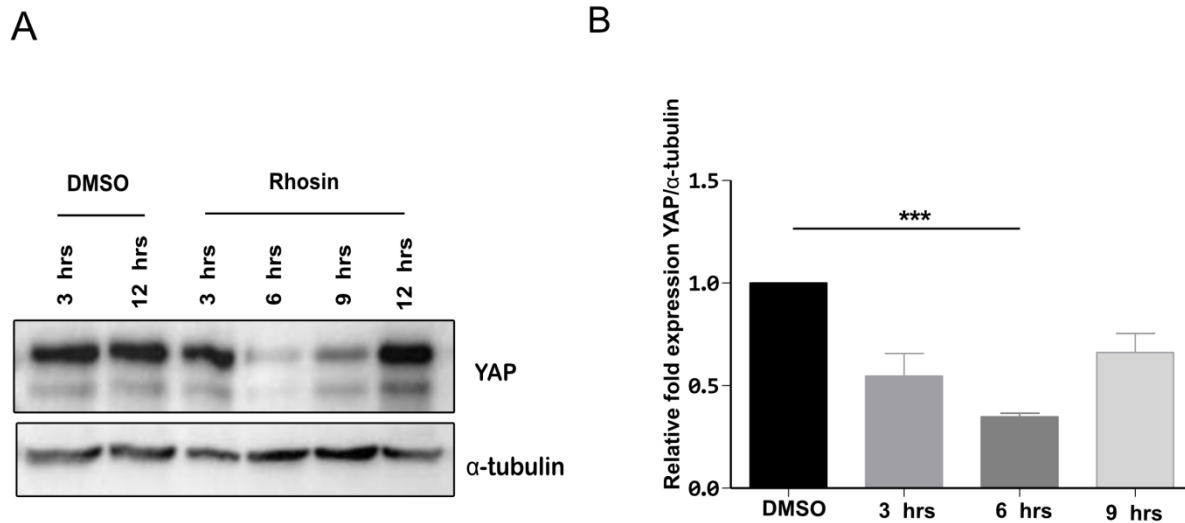


Figure 23: YAP protein expression analysis after rhosin treatment in *TKO* liver cancer cells

(A) Western blot analysis of YAP expression in TKO2.1 cells at different time points after rhosin treatment. α -tubulin serves as loading control. (B) Quantification of YAP protein expression by western blot after rhosin treatment from three independent experiments. Error bar shows SEM (***, $P < 0.001$)

7.8 CD44 mutation in *TKO* liver cancer cells induces changes in cell morphology and adhesion

Cell morphology and adhesion depend on a plethora of extra- and intracellular factors including extracellular matrix protein interaction and cytoskeleton-mediated cellular downstream signaling. In line with our observation of reduced cell proliferation in *Cd44*-mutant cells, we found that reduced expression of CD44 also altered cell morphology in comparison to TKO2.1 control cells. *Cd44*-mutant cells had a long, thin spindle-shaped appearance with membrane extensions in contrast to the control cells with a more triangular epithelial morphology (Fig. 24). We also found the *Cd44* mutants were less adhesive in the cell culture dishes compared to other mutants and control cell lines.

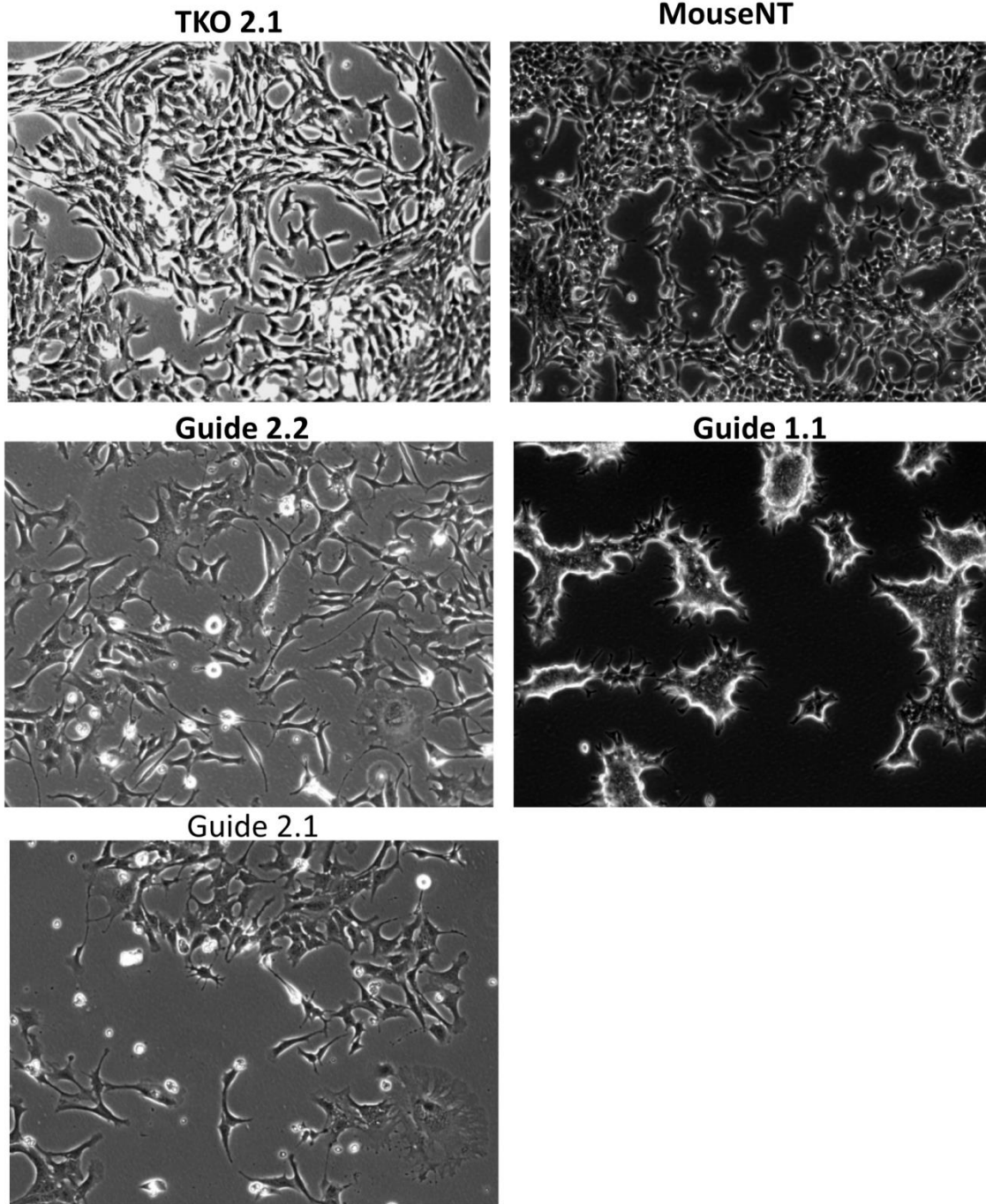


Figure 24: Cell morphology of *TKO* control cells and *Cd44*-mutants cells.

TKO 2.1 and control cells transfected with a non-targeting (nt) control *sgRNA* display a triangular epithelial-like morphology, while *Cd44*-mutant cells (Guide 2.1, Guide 2.2, and Guide 1.1) have a long spindle-shaped appearance.

7.9 The chemical induction of HCC in *Cd44*^{-/-} mice demonstrated reduced tumor burden

Di-ethyl nitrosamine (DEN)-mediated chemical induction of liver cancer is the most commonly used HCC model in mice. Usually, a single dose of 5 mg/kg DEN efficiently induces hepatic mutations in young mice and approximately 80% of them develop visible tumors after 9 months (Teoh, Dan et al. 2008). The hepatic alterations caused by DEN are similar to those found in of human hepatocellular carcinomas. To analyze the role of CD44 in HCC development, we intraperitoneally injected *Cd44*^{-/-} and C57/Bl6 control mice (n= 7 per group) with DEN at day 12 after birth (Fig. 25 top). The mice subjected to treatment were allowed to age and were sacrificed at 12 months of age. We subsequently compared tumor burden between *Cd44*^{-/-} mice and the control group in extracted livers. Notably, tumor burden in the control group of C57/Bl6 mice was significantly higher compared to Cd44-deficient mice (Fig. 25).

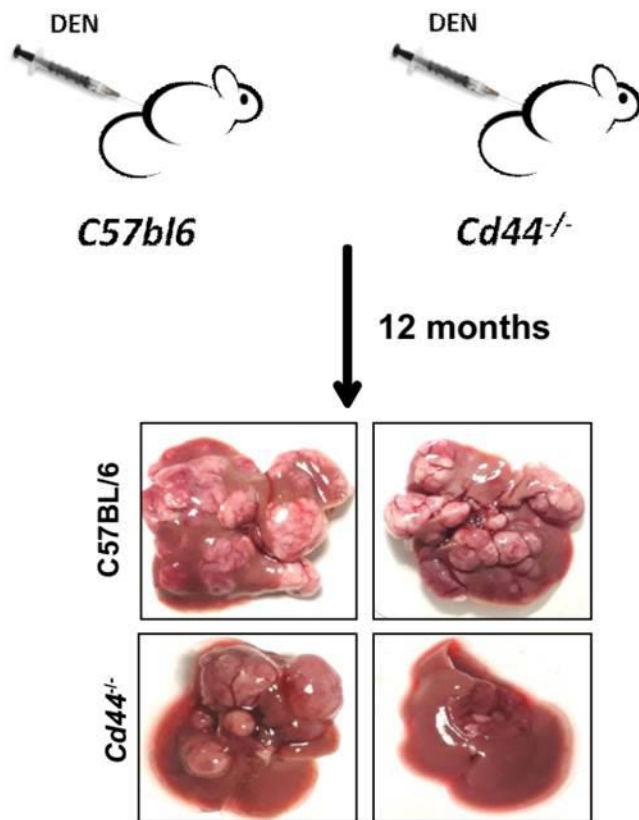


Figure 25: Chemical induction of HCC in C57/Bl6 and *Cd44^{-/-}* mice using DEN

Representation of DEN intraperitoneal injection in C57/Bl6 and *Cd44^{-/-}* animals and representative pictures of livers from 12- months old mice.

Additionally, we performed immunostaining for YAP and CD44 on liver tumors section extracted from DEN-treated mice (Fig. 26). However, we could not visualize any difference in the intensities of YAP expression between control and test cohorts, indicating that YAP in late tumor development is upregulated in a CD44-independent fashion.

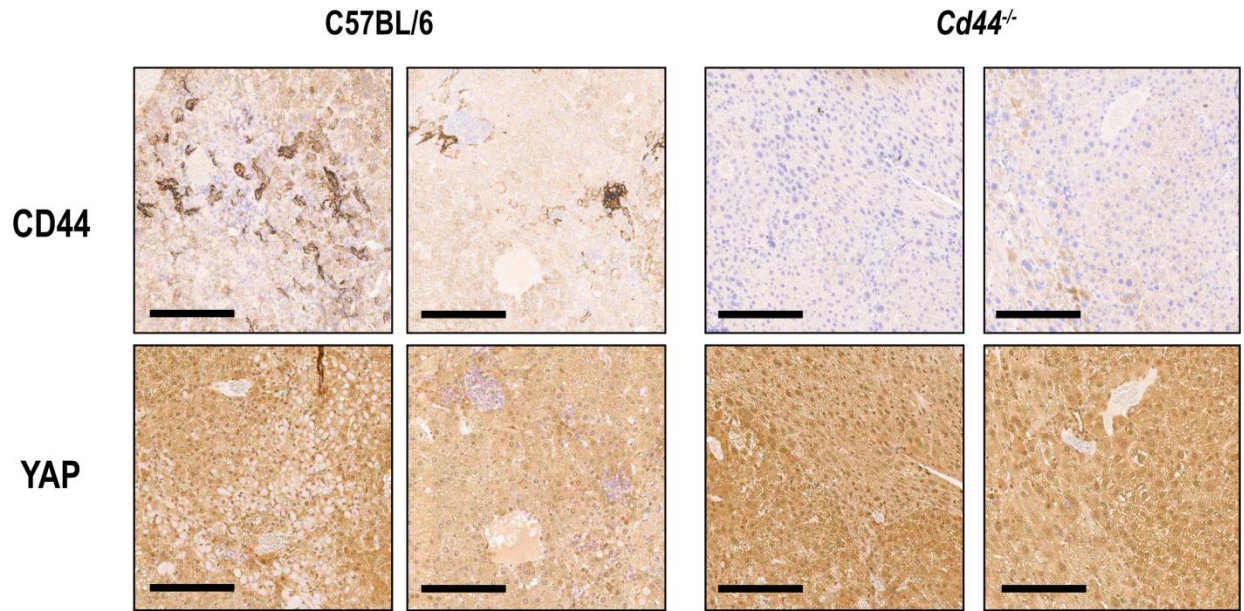


Figure 26: IHC Staining of CD44 and YAP in liver extracted from DEN mice.

The scale bar is 200 μ m.

Furthermore, we assessed both the tumor area and number of tumor nodules in both control and CD44-deficient animals. Reduced tumor burden observed in *Cd44*^{-/-} mice in comparison to C57/B6 control mice therefore suggest a significant role for CD44 in tumor development (Fig. 27).

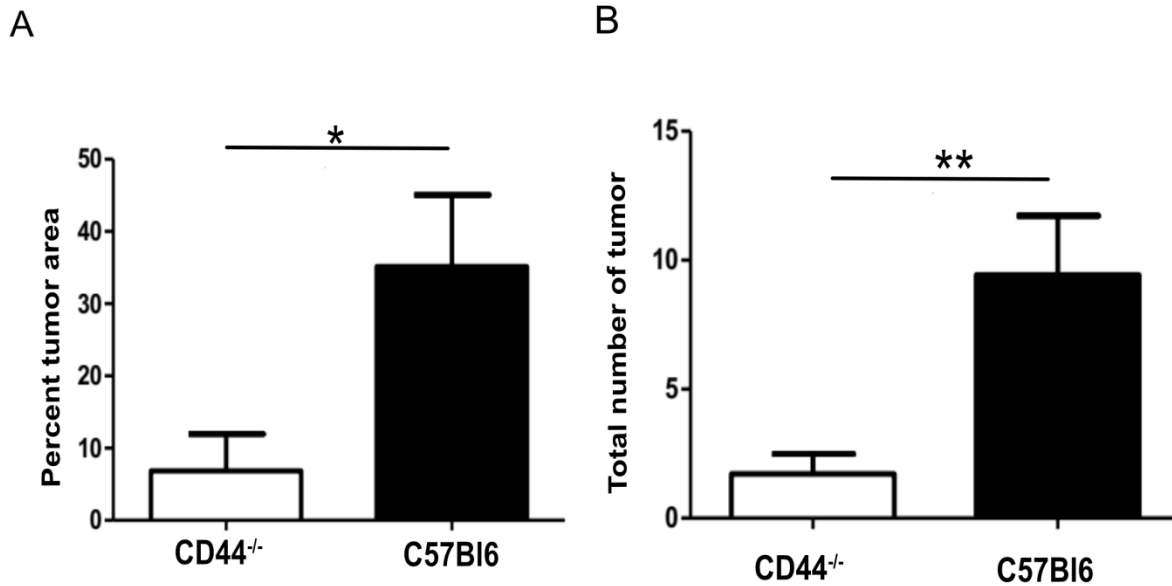


Figure 27: Quantification of liver tumor burden in livers of DEN-treated mice

(A) Quantification of tumor area per liver surface in C57/BI6 and *Cd44*^{-/-} mice. (B) Quantification of tumor nodules (n=7 per group). Error bars show SEM (*, p < 0.05; **, p < 0.01)

7.10 Adeno-Cre injection into *TKO* and *TKO; Cd44*^{-/-} mice

To understand the functional role of *Cd44* in tumor formation in our mouse model, we generated *TKO;Cd44*^{-/-} mice by breeding *TKO* with *Cd44*^{-/-} animals. In both cohorts, the presence of a *Rosa26*^{mTmG} reporter (*TKO* mice) or *Rosa26*^{LSL-YFP} reporter (*TKO;Cd44*^{-/-} mice) allowed for determination of recombination efficiency by immunostaining. In adult male mice (8-12 weeks of age), we then performed intrasplenic injection of an adeno-Cre virus in both cohorts and extracted liver tissues 4 weeks after injection. Liver tissue was analyzed by immunohistopathology for the presence and extent of pre-cancerous lesions in both *TKO* and *TKO;Cd44*^{-/-} animals. The liver extracted from the first set of experimental animals from both groups demonstrated few pre-cancerous lesions and sufficient gene recombination was

verified by immunostaining for the *Rosa26*-driven GFP or YFP reporter, respectively (Fig. 28). However, in the subsequent set of experiments with an equal number of animals from both cohorts, the tumor lesions were not formed at low rates or not at all and immunostaining for GFP or YFP revealed insufficient gene recombination in all livers analyzed. Therefore, we did not pursue this experimental approach any further.

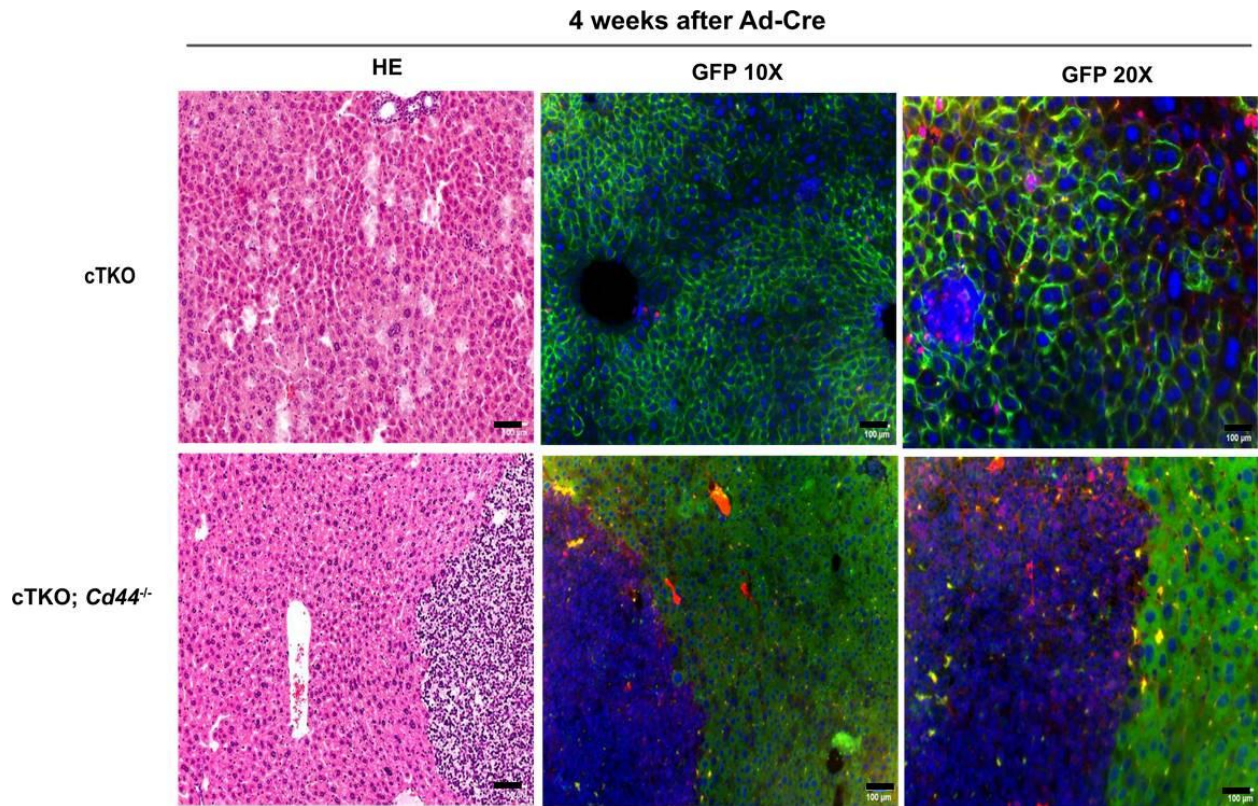


Figure 28 : Histological staining of liver sections of Ad-Cre injected mice

HE and GFP/YFP immunofluorescence staining of *TKO* livers (upper panel) and *TKO;Cd44^{-/-}* (lower panel) after 4 weeks of Ad-Cre injections. Scale bars are 100 μ m

7.11 Correlation of CD44 and YAP expression in human HCC samples

The majority of human HCC show upregulation of CD44 (Haramaki, Yano et al. 1995). We now aimed to investigate, if the correlation of CD44 and YAP expression found in mouse HCC models is conserved in human HCC samples. We used

samples from surgically resected HCC. The local ethics committee of Klinikum rechts der Isar, Munich, reviewed and approved the protocols for sampling and analysis (protocol number 5886/13). Interestingly, the presence of CD44 was significantly observed in the fibrous tissue made up of hepatocyte like cells near to tumor nodules. In these areas associated with the tumor, there was no observed link between the expression levels of CD44 and YAP. Nonetheless, the appearance of CD44 on the membranes of tumor cells in the parenchyma showed a correlation with the expression of YAP in both the cytoplasm and nucleus (Fig. 29).

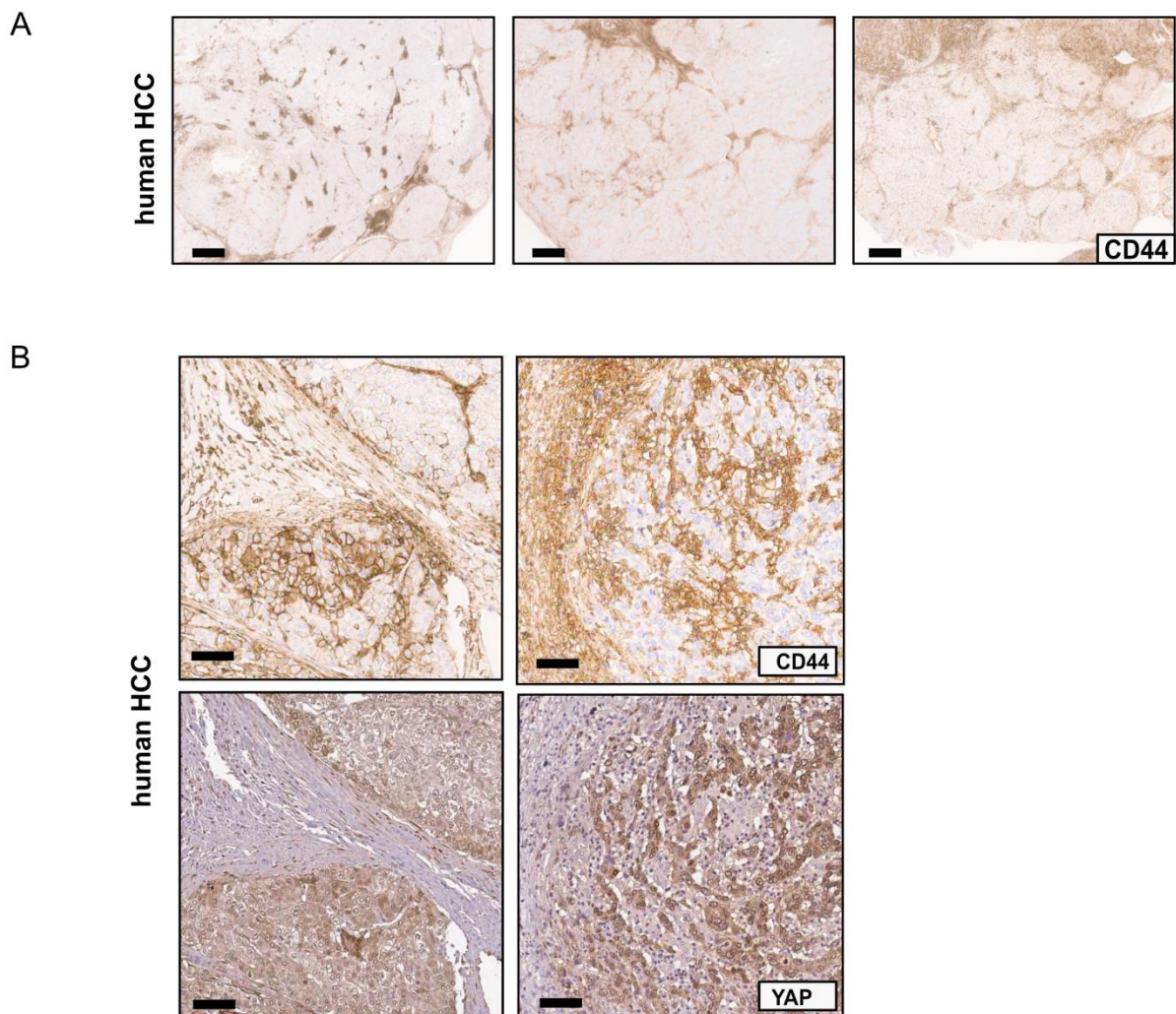


Figure 29: immunohistochemical staining of human HCC tissue

- (A) Immunostaining for CD44 in human hepatocellular carcinoma. Scale bars are 1 mm.
- (B) Immunostaining for CD44 (top) and YAP (bottom) in human HCC. Scale bars are 100 μm.

8 Discussion

When it comes to the prediction of treatment strategies for HCC, there are numerous factors to be considered. Most importantly, liver function, size and extend of the tumor as well as the overall condition of the patient. Although there are many treatment strategies such as surgical resection, locoregional therapies, and various systemic therapies, prognosis of HCC is still poor with low 5-year survival rates, especially in more advanced stages of the disease (Shannon, Ruff et al. 2022, Tumen, Heumann et al. 2022, Ducreux, Abou-Alfa et al. 2023).

On the genetic level, HCC develops due to the accumulation of various genetic aberrations (Tumen, Heumann et al. 2022). The mutational profile of HCC is highly heterogeneous, which is like contributing to the variability in prognosis of individuals with HCC and thereby suggesting a spectrum of biologically distinct phenotypes. There are several pathways that are commonly altered by these mutations, including p53, Rb, and β -catenin signaling (Liu, Al-Adra et al. 2022, Takeda, Takai et al. 2022). However, individual mutations occur in less than one third of HCC cases and there are no known driver mutations. The heterogenous mutation profile results in several subtypes of HCC. At least six distinct subgroups of hepatocellular carcinoma (HCC), labeled G1 to G6, have been identified, each displaying unique genetic and clinical features (Ahn, Haq et al. 2018, Montironi, Castet et al. 2023).

The use of next-generation sequencing on samples from HCC patients who have received systemic treatments is starting to shed light on how altered signaling pathways can influence disease management. For example, in HCC patients undergoing treatment with immune checkpoint inhibitors, mutations that activate the Wnt/ β -catenin signaling pathway have been linked to lower rates of disease control and survival (Huang, Skanderup et al. 2018, Harding, Nandakumar et al. 2019). Meanwhile, the Hippo signaling pathway has been recognized as a critical inhibitory mechanism against hepatocellular carcinoma. While mutations in tumor suppressive upstream Hippo signaling components are rare, an overexpression of the main

oncogenic Hippo signaling targets, YAP/TAZ, is frequently observed in HCC (Liu, Wang et al. 2020). Numerous studies are being conducted to understand the exact phenomenon. It is now well accepted that YAP/TAZ activation does not always occur via the traditional Hippo pathway, but rather through alternative routes (Zhu, Wu et al. 2023).

8.1 CD44- mediated YAP regulation in HCC

One alternative regulatory mechanism is YAP regulation by CD44 (Zhang, Xia et al. 2014). The impact of CD44 expression in YAP mediated liver hepatic carcinogenesis is not much explored. Although overexpression of CD44 and YAP is found in the majority of human HCC samples according to data from independent studies, data supporting a direct regulation of YAP by CD44 in HCC is scarce (Zhang, He et al. 2021). However, *in vitro* findings from our own research, as well as evidence from other studies, indicate that CD44 may serve as an important upstream regulator of YAP in HCC (Zhang, Xia et al. 2014, Fan, Xia et al. 2018). For a better insight into how CD44 regulates YAP in the HCC microenvironment, it is necessary to generate reliable data from animal studies. Intriguingly, our analysis revealed a significant correlation between *Cd44* expression and the mRNA levels of YAP target genes in liver tumors extracted from *TKO* mice. This observation is supported by findings in HCC mouse models, such as those involving diethylnitrosamine (DEN) treatment and *Mdr2* knockout (*Mdr2*^{-/-}), which also demonstrate a positive correlation between CD44 and YAP in HCC, aligning with what we observed in our *TKO* model. Moreover, it is noteworthy that the inflammation-associated *AlbLTαβ* model does not demonstrate expression of either CD44 or YAP (Haybaeck, Zeller et al. 2009). This observation suggests that the CD44 may not exert a universal influence across all HCC subtypes, implying subtype-specific mechanisms at play.

8.2 TKO hepatoma cell lines as tools for delineating CD44 and YAP correlation in HCC

The CD44S and CD44v6 are highly expressed in small hepatic cells around the portal triad compared to mature hepatocytes in regenerating murine livers (Mitaka, Ichinohe et al. 2023). Both variants of CD44 are found in the majority of human HCC samples and are associated with metastasis and vascular invasiveness (Mima, Okabe et al. 2012). It is already known that hepatocytes that have undergone genotoxic/carcinogenic insults depend on excess CD44 expression to escape major tumor suppressor checkpoints such as p53 for survival, proliferation, and accumulation of secondary mutations (Dhar, Antonucci et al. 2018).

Hepatoma cell lines are invaluable for *in vitro* investigations into liver tumor progression and for screening the potentiality of therapeutic compounds. It is a common practice to apply genetic modifications to these cell lines to enhance their functionality (Schicht, Seidemann et al. 2022). In our experiments, we targeted hepatoma cell lines derived from TKO tumors for *Cd44* gene inactivation through CRISPR/Cas9 technology, reduced cell viability was noted in the populations with inactivated *Cd44* (Fig. 10). Furthermore, the loss of *Cd44* led to remarkable changes in cell morphology and adhesion in all the *Cd44*-mutant clones (Fig. 24). Mechanistically, comparative analyses of the levels of active versus inactive (phosphorylated) YAP, and of the expression of YAP target genes at the mRNA level, and overall transcriptome profiles in the *Cd44*-mutant cells versus control cells reinforced a significant association between CD44 expression and YAP activity (Fig. 14, 15).

8.3 CD44 might act as an upstream regulator of YAP in HCC likely through RhoA

The mechanisms through which CD44 regulates YAP are not completely understood to date. To identify candidate mechanisms linking CD44 to YAP, we selected targetable candidate pathways - STAT-3, Src Kinase and Rho-A – from

RNAseq results in *Cd44*-mutant *TKO* cells and performed inhibition assays *TKO* cells (Fig. 19, 22). Our primary targets were STAT-3, Src Kinase and Rho-A.

STAT-3, Src kinase and RhoA expression has been found to be elevated in the majority of cancer types, including HCC (Yadav, Kashaninejad et al. 2020, Pelaz and Tabernero 2022, Tan and Feng 2023). In our studies, GSEA indicated STAT-3 and Src pathway activation in control cells compared to *Cd44* mutants. However, inhibition assays using the STAT-3 inhibitor HO-3867 and Src inhibitors such as saracatinib and dasatinib did not show a significant difference in cell proliferation between the control and *Cd44*-mutant cells. Interestingly, the *TKO* cells treated with RhoA inhibitor (Rhosin) not only showed significantly reduced proliferation, but also reduced YAP expression. Importantly, *Cd44*-mutant cells did not exhibit any difference in cell proliferation or YAP expression levels following Rhosin treatment, indicating that CD44 and RhoA work through the same mechanism to reduce YAP-dependent proliferation. RhoA, belonging to the Rho family of GTPases, plays a crucial role in regulating the cytoskeleton. The movement of YAP between the nucleus and cytoplasm in developmental and regenerative processes is significantly influenced by alterations in cytoskeletal structures due to contact inhibition (Schollenberger, Gronemeyer et al. 2010). It has been demonstrated in past research that RhoA influences the activity of YAP/TAZ via F-actin, a principal conductor of mechanical signals (Aragona, Panciera et al. 2013, Feng, Degese et al. 2014). Our finding is consistent with the observation made by Zhang et al. based on two independent experiments executed both by CD44 inactivation and/or RhoA inhibition, demonstrating comparable YAP downregulation in lung and liver cancer cell lines. This evidence supports the notion that CD44 regulates YAP through a mechanism independent of the Hippo signaling pathway, and likely dependent on RhoA (Li, Li et al. 2019).

8.4 HCC development in mice might depend on CD44 expression

Genetically engineered mouse models hold undeniable role in the pre-clinical and translational HCC research. However, the mouse models are often limited to one

specific driver mutation and limits mimicking the tumor microenvironment (de Ruiter, Wessels et al. 2018). To enhance the comprehension of the role of CD44 in regulating YAP in the context of HCC progression, we conducted an *in vivo* assessment of tumor formation in *Cd44*^{-/-} mice and wild type mice in a C57/Bl6 background. Upon DEN-mediated chemical induction of tumors, the livers of *Cd44*^{-/-} mice showed a significantly lower hepatic tumor burden with a smaller number of tumor nodules on the liver surface in comparison to the control mice (Fig. 25).

The findings from DEN-induced tumors provide valuable insights into the potential dynamics of the impact of CD44 on tumor development. While the absence of CD44 in the DEN model results in reduced tumor burden, nuclear YAP expression in hepatic tumor nodules or hepatocytes remained unaltered (Fig.26). While these findings could indicate that the effects of CD44 in the DEN model might be independent of YAP, another possible explanation is that CD44-YAP axis might be an important mechanism to activate oncogenic YAP in hepatocellular carcinoma, but not the only one. This observation also points to the notion of YAP regulation through multiple means (Pocaterra, Romani et al. 2020). This includes mechano-transduction pathways involving direct or indirect interactions with actin, mediated by G protein-coupled receptors (GPCRs), c-Jun N-terminal kinase (JNK), E-cadherins, and mitogen-activated protein kinase 4 (MAPK4), among various other contributing factors (Heng, Zhang et al. 2021). Additionally, it is necessary to acknowledge the complex interplay between Hippo signaling and multiple other signaling pathways, such as PI3K/AKT, Notch, and Wnt (Kim, Khan et al. 2017). These pathways contribute to the complex regulation of YAP/TAZ activity by influencing their phosphorylation. Furthermore, the YAP regulation does not completely dependent on its phosphorylation state. It is influenced by various post-translational modifications including ubiquitylation and methylation, thereby highlighting the complex involvement of multiple factors in YAP regulation in the context of HCC (Zhu, Yan et al. 2020).

In the next phase of our research, it will be important to conduct further studies that address the downstream functions of CD44 and how it regulates YAP *in vivo*. The *in vitro* assays conducted in mouse hepatoma cell lines, especially the selective inhibition of RhoA using Rhosin, provided certain level of understanding on the driving mechanism of CD44-mediated YAP-regulation. Testing the effect of RhoA inhibition by Rhosin *in vivo* in different HCC models will further help in our understanding of the functional relevance of the proposed CD44-RhoA-YAP axis in liver cancer. While no inhibitors of RhoA are being employed in clinical trials at present, this strategy has undergone thorough exploration and examination in preclinical experiments (Dyberg, Fransson et al. 2017). The systemic application of Rhosin has been shown to decrease tumor metastasis by blocking the RhoA and YAP pathways in mouse models of melanoma and breast cancer (Tsubaki, Genno et al. 2021). Another important aspect is to understand the specific cell types in which this interaction occurs. However, establishing a mechanistic interplay that mediates YAP dependency of CD44 can be challenging due to various oncogenic signaling pathways at play. This urges the need for an extensive study addressing different questions to unveil the precise mechanism.

9 Conclusions

We have been able to show a positive correlation between CD44 expression and YAP in hepatocellular cancer using different HCC mouse models. CRISPR/Cas9-mediated CD44 inactivation downregulated the expression of both YAP and its target genes in a mouse liver cancer cell line. Moreover, we were able to show an alternative mechanism of YAP regulation independent of the Hippo signaling pathway wherein a CD44-RhoA axis regulates YAP. Correspondingly, we showed the DEN-induced HCC in *Cd44*^{-/-} mice were characterized by a reduction in tumor load compared to the wild-type controls. Further studies will be needed to investigate if targeting of a CD44-RhoA-YAP axis could be a promising treatment option in hepatocellular carcinoma.

Acknowledgments

I would like to sincerely thank PD. Dr. Ursula Ehmer for accepting me as a doctoral student in her research group at department of Internal Medicine II and for supporting me throughout the 3.5 years of my doctoral research. Her belief in my abilities and constant motivation helped me to evolve as a scientist. Her valuable guidance helped me find the right direction for the project leading to its successful completion.

I would like to thank Prof. Dr. Roland M. Schmid for accepting me as a part of department of Internal Medicine II. I would also like to thank Prof. Dr. Gabriele Multhoff and PD. Dr. Fabian Geisler for all the scientific advice and input for the betterment of the project as part of the thesis advisory committee.

I would like to thank all my colleagues especially Magalie, Julia, Birgit Kohke-Ertel, Carina, Pooya, and Uli Bauer. All of them were an integral part of my Ph.D. life at my working group and have helped me one or the other way in the completion of my project.

I would like to thank the FAZIT organization for granting me the PhD finishing scholarship and for supporting me in the last few months in winding up my project.

I would like to thank my friends Sruthi, Hilansi, Raphela and Steffi for always being with me through thick and thin during my PhD. I would be always grateful for all the discussions, scientific or non-scientific and for cheering me up during the tougher times.

Last but not least, I would like to thank all my family members who constantly supported me morally and otherwise. I would like to individually thank my amma, Sukumary Manmadhan and achacha, K Manmadhan for everything from the moment I was born until now because nothing would have been possible without them. I would like to thank my brother Saurabh for always being at my side.

References

- Ahn, S. M., F. Haq, I. Park, J. C. Nault, J. Zucman-Rossi and E. Yu (2018). "The clinical implications of G1-G6 transcriptomic signature and 5-gene score in Korean patients with hepatocellular carcinoma." *BMC Cancer* **18**(1): 571.
- Ang, C., A. Shields, J. Xiu, Z. Gatalica, S. Reddy, M. E. Salem, C. Farhangfar, J. Hwang, I. Astsaturov and J. L. Marshall (2017). "Molecular characteristics of hepatocellular carcinomas from different age groups." *Oncotarget* **8**(60): 101591-101598.
- Aragona, M., T. Panciera, A. Manfrin, S. Giulitti, F. Michielin, N. Elvassore, S. Dupont and S. Piccolo (2013). "A mechanical checkpoint controls multicellular growth through YAP/TAZ regulation by actin-processing factors." *Cell* **154**(5): 1047-1059.
- Bagi, C. M. and C. J. Andresen (2010). "Models of hepatocellular carcinoma and biomarker strategy." *Cancers (Basel)* **2**(3): 1441-1452.
- Batlle, E. and H. Clevers (2017). "Cancer stem cells revisited." *Nat Med* **23**(10): 1124-1134.
- Bild, A. H., G. Yao, J. T. Chang, Q. Wang, A. Potti, D. Chasse, M. B. Joshi, D. Harpole, J. M. Lancaster, A. Berchuck, J. A. Olson, Jr., J. R. Marks, H. K. Dressman, M. West and J. R. Nevins (2006). "Oncogenic pathway signatures in human cancers as a guide to targeted therapies." *Nature* **439**(7074): 353-357.
- Blidisel, A., I. Marcovici, D. Coricovac, F. Hut, C. A. Dehelean and O. M. Cretu (2021). "Experimental Models of Hepatocellular Carcinoma-A Preclinical Perspective." *Cancers (Basel)* **13**(15).
- Brar, G., T. F. Greten, B. I. Graubard, T. S. McNeel, J. L. Petrick, K. A. McGlynn and S. F. Altekruse (2020). "Hepatocellular Carcinoma Survival by Etiology: A SEER-Medicare Database Analysis." *Hepatol Commun* **4**(10): 1541-1551.
- Brinkman, E. K., T. Chen, M. Amendola and B. van Steensel (2014). "Easy quantitative assessment of genome editing by sequence trace decomposition." *Nucleic Acids Res* **42**(22): e168.
- Bruix, J. and J. M. Llovet (2002). "Prognostic prediction and treatment strategy in hepatocellular carcinoma." *Hepatology* **35**(3): 519-524.
- Budzinska, M. A., T. Tu, W. M. d'Avigdor, G. W. McCaughan, F. Luciani and N. A. Shackel (2016). "Accumulation of Deleterious Passenger Mutations Is Associated with the Progression of Hepatocellular Carcinoma." *PLoS One* **11**(9): e0162586.
- Calvisi, D. F. and S. S. Thorgeirsson (2005). "Molecular mechanisms of hepatocarcinogenesis in transgenic mouse models of liver cancer." *Toxicol Pathol* **33**(1): 181-184.
- Camargo, F. D., S. Gokhale, J. B. Johnnidis, D. Fu, G. W. Bell, R. Jaenisch and T. R. Brummelkamp (2007). "YAP1 increases organ size and expands undifferentiated progenitor cells." *Curr Biol* **17**(23): 2054-2060.
- Chan, S. W., C. J. Lim, Y. F. Chong, A. V. Pobbati, C. Huang and W. Hong (2011). "Hippo pathway-independent restriction of TAZ and YAP by angiotensin." *J Biol Chem* **286**(9): 7018-7026.
- Chang, P. H., K. Sekine, H. M. Chao, S. H. Hsu and E. Chern (2017). "Chitosan promotes cancer progression and stem cell properties in association with Wnt signaling in colon and hepatocellular carcinoma cells." *Sci Rep* **8**: 45751.
- Chen, C., S. Zhao, A. Karnad and J. W. Freeman (2018). "The biology and role of CD44 in cancer progression: therapeutic implications." *J Hematol Oncol* **11**(1): 64.
- Clara, J. A., C. Monge, Y. Yang and N. Takebe (2020). "Targeting signalling pathways and the immune microenvironment of cancer stem cells - a clinical update." *Nat Rev Clin Oncol* **17**(4): 204-232.
- Cordenonsi, M., F. Zanconato, L. Azzolin, M. Forcato, A. Rosato, C. Frasson, M. Inui, M. Montagner, A. R. Parenti, A. Poletti, M. G. Daidone, S. Dupont, G. Basso, S. Bicciato and S. Piccolo (2011). "The Hippo transducer TAZ confers cancer stem cell-related traits on breast cancer cells." *Cell* **147**(4): 759-772.
- Dasgupta, P., C. Henshaw, D. R. Youlden, P. J. Clark, J. F. Aitken and P. D. Baade (2020). "Global Trends in Incidence Rates of Primary Adult Liver Cancers: A Systematic Review and Meta-Analysis." *Front Oncol* **10**: 171.

Day, C. P., G. Merlino and T. Van Dyke (2015). "Preclinical mouse cancer models: a maze of opportunities and challenges." *Cell* **163**(1): 39-53.

de La Coste, A., B. Romagnolo, P. Billuart, C. A. Renard, M. A. Buendia, O. Soubrane, M. Fabre, J. Chelly, C. Beldjord, A. Kahn and C. Perret (1998). "Somatic mutations of the beta-catenin gene are frequent in mouse and human hepatocellular carcinomas." *Proc Natl Acad Sci U S A* **95**(15): 8847-8851.

de Ruiter, J. R., L. F. A. Wessels and J. Jonkers (2018). "Mouse models in the era of large human tumour sequencing studies." *Open Biol* **8**(8).

Donaires, F. S., N. F. Scatena, R. M. Alves-Paiva, J. D. Podlevsky, D. Logeswaran, B. A. Santana, A. C. Teixeira, J. J. Chen, R. T. Calado and A. L. C. Martinelli (2017). "Telomere biology and telomerase mutations in cirrhotic patients with hepatocellular carcinoma." *PLoS One* **12**(8): e0183287.

Dong, J., G. Feldmann, J. Huang, S. Wu, N. Zhang, S. A. Comerford, M. F. Gayyed, R. A. Anders, A. Maitra and D. Pan (2007). "Elucidation of a universal size-control mechanism in Drosophila and mammals." *Cell* **130**(6): 1120-1133.

Ducieux, M., G. K. Abou-Alfa, T. Bekaii-Saab, J. Berlin, A. Cervantes, T. de Baere, C. Eng, P. Galle, S. Gill, T. Gruenberger, K. Haustermans, A. Lamarca, P. Laurent-Puig, J. M. Llovet, F. Lordick, T. Macarulla, D. Mukherji, K. Muro, R. Obermannova, J. M. O'Connor, E. M. O'Reilly, P. Osterlund, P. Philip, G. Prager, E. Ruiz-Garcia, B. Sangro, T. Seufferlein, J. Tabernero, C. Verslype, H. Wasan and E. Van Cutsem (2023). "The management of hepatocellular carcinoma. Current expert opinion and recommendations derived from the 24th ESMO/World Congress on Gastrointestinal Cancer, Barcelona, 2022." *ESMO Open* **8**(3): 101567.

Dupont, S., L. Morsut, M. Aragona, E. Enzo, S. Giullitti, M. Cordenonsi, F. Zanconato, J. Le Digabel, M. Forcato, S. Bicciato, N. Elvassore and S. Piccolo (2011). "Role of YAP/TAZ in mechanotransduction." *Nature* **474**(7350): 179-183.

Dyberg, C., S. Fransson, T. Andonova, B. Sveinbjornsson, J. Lannerholm-Palm, T. K. Olsen, D. Forsberg, E. Herlenius, T. Martinsson, B. Brodin, P. Kogner, J. I. Johnsen and M. Wickstrom (2017). "Rho-associated kinase is a therapeutic target in neuroblastoma." *Proc Natl Acad Sci U S A* **114**(32): E6603-E6612.

Ege, N., A. M. Dowbaj, M. Jiang, M. Howell, S. Hooper, C. Foster, R. P. Jenkins and E. Sahai (2018). "Quantitative Analysis Reveals that Actin and Src-Family Kinases Regulate Nuclear YAP1 and Its Export." *Cell Syst* **6**(6): 692-708 e613.

Ehmer, U., A. F. Zmoos, R. K. Auerbach, D. Vaka, A. J. Butte, M. A. Kay and J. Sage (2014). "Organ size control is dominant over Rb family inactivation to restrict proliferation in vivo." *Cell Rep* **8**(2): 371-381.

Elosegui-Artola, A., I. Andreu, A. E. M. Beedle, A. Lezamiz, M. Uroz, A. J. Kosmalska, R. Oria, J. Z. Kechagia, P. Rico-Lastres, A. L. Le Roux, C. M. Shanahan, X. Trepas, D. Navajas, S. Garcia-Manyes and P. Roca-Cusachs (2017). "Force Triggers YAP Nuclear Entry by Regulating Transport across Nuclear Pores." *Cell* **171**(6): 1397-1410 e1314.

Enzo, E., G. Santinon, A. Pocaterra, M. Aragona, S. Bresolin, M. Forcato, D. Grifoni, A. Pession, F. Zanconato, G. Guzzo, S. Bicciato and S. Dupont (2015). "Aerobic glycolysis tunes YAP/TAZ transcriptional activity." *EMBO J* **34**(10): 1349-1370.

Fan, Z., J. Duan, L. Wang, S. Xiao, L. Li, X. Yan, W. Yao, L. Wu, S. Zhang, Y. Zhang, Y. Li, X. Zhu, Y. Hu, D. Zhang, S. Jiao and X. Xu (2019). "PTK2 promotes cancer stem cell traits in hepatocellular carcinoma by activating Wnt/beta-catenin signaling." *Cancer Lett* **450**: 132-143.

Fan, Z., H. Xia, H. Xu, J. Ma, S. Zhou, W. Hou, Q. Tang, Q. Gong, Y. Nie and F. Bi (2018). "Standard CD44 modulates YAP1 through a positive feedback loop in hepatocellular carcinoma." *Biomed Pharmacother* **103**: 147-156.

Farinati, F., A. Sergio, A. Baldan, A. Giacomini, M. A. Di Nolfo, P. Del Poggio, L. Benvegna, G. Rapaccini, M. Zoli, F. Borzio, E. G. Giannini, E. Caturelli and F. Trevisani (2009). "Early and very early hepatocellular

carcinoma: when and how much do staging and choice of treatment really matter? A multi-center study." *BMC Cancer* **9**: 33.

Feng, X., M. S. Degese, R. Iglesias-Bartolome, J. P. Vaque, A. A. Molinolo, M. Rodrigues, M. R. Zaidi, B. R. Ksander, G. Merlino, A. Sodhi, Q. Chen and J. S. Gutkind (2014). "Hippo-independent activation of YAP by the GNAQ uveal melanoma oncogene through a trio-regulated rho GTPase signaling circuitry." *Cancer Cell* **25**(6): 831-845.

Fitamant, J., F. Kottakis, S. Benhamouche, H. S. Tian, N. Chuvin, C. A. Parachoniak, J. M. Nagle, R. M. Perera, M. Lapouge, V. Deshpande, A. X. Zhu, A. Lai, B. Min, Y. Hoshida, J. Avruch, D. Sia, G. Camprecios, A. I. McClatchey, J. M. Llovet, D. Morrissey, L. Raj and N. Bardeesy (2015). "YAP Inhibition Restores Hepatocyte Differentiation in Advanced HCC, Leading to Tumor Regression." *Cell Rep* **10**(10): 1692-1707.

Fouad, Y. A. and C. Aanei (2017). "Revisiting the hallmarks of cancer." *Am J Cancer Res* **7**(5): 1016-1036.

Fujimoto, A., Y. Totoki, T. Abe, K. A. Boroevich, F. Hosoda, H. H. Nguyen, M. Aoki, N. Hosono, M. Kubo, F. Miya, Y. Arai, H. Takahashi, T. Shirakihara, M. Nagasaki, T. Shibuya, K. Nakano, K. Watanabe-Makino, H. Tanaka, H. Nakamura, J. Kusuda, H. Ojima, K. Shimada, T. Okusaka, M. Ueno, Y. Shigekawa, Y. Kawakami, K. Arihiro, H. Ohdan, K. Gotoh, O. Ishikawa, S. Ariizumi, M. Yamamoto, T. Yamada, K. Chayama, T. Kosuge, H. Yamaue, N. Kamatani, S. Miyano, H. Nakagama, Y. Nakamura, T. Tsunoda, T. Shibata and H. Nakagawa (2012). "Whole-genome sequencing of liver cancers identifies etiological influences on mutation patterns and recurrent mutations in chromatin regulators." *Nat Genet* **44**(7): 760-764.

Futakuchi, M., K. Lami, Y. Tachibana, Y. Yamamoto, M. Furukawa and J. Fukuoka (2019). "The Effects of TGF-beta Signaling on Cancer Cells and Cancer Stem Cells in the Bone Microenvironment." *Int J Mol Sci* **20**(20).

Global Burden of Disease Liver Cancer, C., T. Akinyemiju, S. Abera, M. Ahmed, N. Alam, M. A. Alemayohu, C. Allen, R. Al-Raddadi, N. Alvis-Guzman, Y. Amoako, A. Artaman, T. A. Ayele, A. Barac, I. Bensenor, A. Berhane, Z. Bhutta, J. Castillo-Rivas, A. Chittheer, J. Y. Choi, B. Cowie, L. Dandona, R. Dandona, S. Dey, D. Dicker, H. Phuc, D. U. Ekwueme, M. S. Zaki, F. Fischer, T. Furst, J. Hancock, S. I. Hay, P. Hotez, S. H. Jee, A. Kasaeian, Y. Khader, Y. H. Khang, A. Kumar, M. Kutz, H. Larson, A. Lopez, R. Lunevicius, R. Malekzadeh, C. McAlinden, T. Meier, W. Mendoza, A. Mokdad, M. Moradi-Lakeh, G. Nagel, Q. Nguyen, G. Nguyen, F. Ogbo, G. Patton, D. M. Pereira, F. Pourmalek, M. Qorbani, A. Radfar, G. Roshandel, J. A. Salomon, J. Sanabria, B. Sartorius, M. Satpathy, M. Sawhney, S. Sepanlou, K. Shackelford, H. Shore, J. Sun, D. T. Mengistu, R. Topor-Madry, B. Tran, K. N. Ukwaja, V. Vlassov, S. E. Vollset, T. Vos, T. Wakayo, E. Weiderpass, A. Werdecker, N. Yonemoto, M. Younis, C. Yu, Z. Zaidi, L. Zhu, C. J. L. Murray, M. Naghavi and C. Fitzmaurice (2017). "The Burden of Primary Liver Cancer and Underlying Etiologies From 1990 to 2015 at the Global, Regional, and National Level: Results From the Global Burden of Disease Study 2015." *JAMA Oncol* **3**(12): 1683-1691.

Grijalva, J. L., M. Huizenga, K. Mueller, S. Rodriguez, J. Brazzo, F. Camargo, G. Sadri-Vakili and K. Vakili (2014). "Dynamic alterations in Hippo signaling pathway and YAP activation during liver regeneration." *Am J Physiol Gastrointest Liver Physiol* **307**(2): G196-204.

Guicciardi, M. E., C. E. Trussoni, A. Krishnan, S. F. Bronk, M. J. Lorenzo Pisarello, S. P. O'Hara, P. L. Splinter, Y. Gao, P. Vig, A. Revzin, N. F. LaRusso and G. J. Gores (2018). "Macrophages contribute to the pathogenesis of sclerosing cholangitis in mice." *J Hepatol* **69**(3): 676-686.

Guichard, C., G. Amaddeo, S. Imbeaud, Y. Ladeiro, L. Pelletier, I. B. Maad, J. Calderaro, P. Bioulac-Sage, M. Letexier, F. Degos, B. Clement, C. Balabaud, E. Chevet, A. Laurent, G. Couchy, E. Letouze, F. Calvo and J. Zucman-Rossi (2012). "Integrated analysis of somatic mutations and focal copy-number changes identifies key genes and pathways in hepatocellular carcinoma." *Nat Genet* **44**(6): 694-698.

Hanahan, D. and R. A. Weinberg (2011). "Hallmarks of cancer: the next generation." *Cell* **144**(5): 646-674.

Hao, Y., D. Baker and P. Ten Dijke (2019). "TGF-beta-Mediated Epithelial-Mesenchymal Transition and Cancer Metastasis." *Int J Mol Sci* **20**(11).

Haramaki, M., H. Yano, K. Fukuda, S. Momosaki, S. Ogasawara and M. Kojiro (1995). "Expression of CD44 in human hepatocellular carcinoma cell lines." *Hepatology* **21**(5): 1276-1284.

Harding, J. J., S. Nandakumar, J. Armenia, D. N. Khalil, M. Albano, M. Ly, J. Shia, J. F. Hechtman, R. Kundra, I. El Dika, R. K. Do, Y. Sun, T. P. Kingham, M. I. D'Angelica, M. F. Berger, D. M. Hyman, W. Jarnagin, D. S. Klimstra, Y. Y. Janjigian, D. B. Solit, N. Schultz and G. K. Abou-Alfa (2019). "Prospective Genotyping of Hepatocellular Carcinoma: Clinical Implications of Next-Generation Sequencing for Matching Patients to Targeted and Immune Therapies." *Clin Cancer Res* **25**(7): 2116-2126.

Haybaeck, J., N. Zeller, M. J. Wolf, A. Weber, U. Wagner, M. O. Kurrer, J. Bremer, G. Iezzi, R. Graf, P. A. Clavien, R. Thimme, H. Blum, S. A. Nedospasov, K. Zatloukal, M. Ramzan, S. Ciesek, T. Pietschmann, P. N. Marche, M. Karin, M. Kopf, J. L. Browning, A. Aguzzi and M. Heikenwalder (2009). "A lymphotoxin-driven pathway to hepatocellular carcinoma." *Cancer Cell* **16**(4): 295-308.

He, L., D. A. Tian, P. Y. Li and X. X. He (2015). "Mouse models of liver cancer: Progress and recommendations." *Oncotarget* **6**(27): 23306-23322.

He, M., Z. Zhou, A. A. Shah, H. Zou, J. Tao, Q. Chen and Y. Wan (2016). "The emerging role of deubiquitinating enzymes in genomic integrity, diseases, and therapeutics." *Cell Biosci* **6**: 62.

Heindryckx, F., I. Colle and H. Van Vlierberghe (2009). "Experimental mouse models for hepatocellular carcinoma research." *Int J Exp Pathol* **90**(4): 367-386.

Hoshida, Y., S. M. Nijman, M. Kobayashi, J. A. Chan, J. P. Brunet, D. Y. Chiang, A. Villanueva, P. Newell, K. Ikeda, M. Hashimoto, G. Watanabe, S. Gabriel, S. L. Friedman, H. Kumada, J. M. Llovet and T. R. Golub (2009). "Integrative transcriptome analysis reveals common molecular subclasses of human hepatocellular carcinoma." *Cancer Res* **69**(18): 7385-7392.

Huang, J., S. Wu, J. Barrera, K. Matthews and D. Pan (2005). "The Hippo signaling pathway coordinately regulates cell proliferation and apoptosis by inactivating Yorkie, the Drosophila Homolog of YAP." *Cell* **122**(3): 421-434.

Huang, W., A. J. Skanderup and C. G. Lee (2018). "Advances in genomic hepatocellular carcinoma research." *Gigascience* **7**(11).

Hubner, E. K., C. Lechler, T. N. Rosner, B. Kohnke-Ertel, R. M. Schmid and U. Ehmer (2018). "Constitutive and Inducible Systems for Genetic In Vivo Modification of Mouse Hepatocytes Using Hydrodynamic Tail Vein Injection." *J Vis Exp*(132).

Ikenaga, N., S. B. Liu, D. Y. Sverdlov, S. Yoshida, I. Nasser, Q. Ke, P. M. Kang and Y. Popov (2015). "A new Mdr2(-/-) mouse model of sclerosing cholangitis with rapid fibrosis progression, early-onset portal hypertension, and liver cancer." *Am J Pathol* **185**(2): 325-334.

Ishii, S., R. Ford, P. Thomas, A. Nachman, G. Steele, Jr. and J. M. Jessup (1993). "CD44 participates in the adhesion of human colorectal carcinoma cells to laminin and type IV collagen." *Surg Oncol* **2**(4): 255-264.

Jhappan, C., C. Stahle, R. N. Harkins, N. Fausto, G. H. Smith and G. T. Merlino (1990). "TGF alpha overexpression in transgenic mice induces liver neoplasia and abnormal development of the mammary gland and pancreas." *Cell* **61**(6): 1137-1146.

Ju, H. L., S. H. Ahn, D. Y. Kim, S. Baek, S. I. Chung, J. Seong, K. H. Han and S. W. Ro (2013). "Investigation of oncogenic cooperation in simple liver-specific transgenic mouse models using noninvasive in vivo imaging." *PLoS One* **8**(3): e59869.

Ju, H. L., K. H. Han, J. D. Lee and S. W. Ro (2016). "Transgenic mouse models generated by hydrodynamic transfection for genetic studies of liver cancer and preclinical testing of anti-cancer therapy." *Int J Cancer* **138**(7): 1601-1608.

Jung, J. (2014). "Human tumor xenograft models for preclinical assessment of anticancer drug development." *Toxicol Res* **30**(1): 1-5.

Kapoor, A., W. Yao, H. Ying, S. Hua, A. Liewen, Q. Wang, Y. Zhong, C. J. Wu, A. Sadanandam, B. Hu, Q. Chang, G. C. Chu, R. Al-Khalil, S. Jiang, H. Xia, E. Fletcher-Sananikone, C. Lim, G. I. Horwitz, A. Viale, P. Pettazzoni, N. Sanchez, H. Wang, A. Protopopov, J. Zhang, T. Heffernan, R. L. Johnson, L. Chin, Y. A. Wang, G. Draetta and R. A. DePinho (2014). "Yap1 activation enables bypass of oncogenic Kras addiction in pancreatic cancer." *Cell* **158**(1): 185-197.

Katt, M. E., A. L. Placone, A. D. Wong, Z. S. Xu and P. C. Searson (2016). "In Vitro Tumor Models: Advantages, Disadvantages, Variables, and Selecting the Right Platform." *Front Bioeng Biotechnol* **4**: 12.

Kim, C. M., K. Koike, I. Saito, T. Miyamura and G. Jay (1991). "HBx gene of hepatitis B virus induces liver cancer in transgenic mice." *Nature* **351**(6324): 317-320.

Kim, E., A. Lisby, C. Ma, N. Lo, U. Ehmer, K. E. Hayer, E. E. Furth and P. Viatour (2019). "Promotion of growth factor signaling as a critical function of beta-catenin during HCC progression." *Nat Commun* **10**(1): 1909.

Kim, W., S. K. Khan, J. Gvozdenovic-Jeremic, Y. Kim, J. Dahlman, H. Kim, O. Park, T. Ishitani, E. H. Jho, B. Gao and Y. Yang (2017). "Hippo signaling interactions with Wnt/beta-catenin and Notch signaling repress liver tumorigenesis." *J Clin Invest* **127**(1): 137-152.

Kim, W., S. K. Khan, Y. Liu, R. Xu, O. Park, Y. He, B. Cha, B. Gao and Y. Yang (2018). "Hepatic Hippo signaling inhibits protumoural microenvironment to suppress hepatocellular carcinoma." *Gut* **67**(9): 1692-1703.

Kinoshita, A., H. Onoda, N. Fushiya, K. Koike, H. Nishino and H. Tajiri (2015). "Staging systems for hepatocellular carcinoma: Current status and future perspectives." *World J Hepatol* **7**(3): 406-424.

Kofler, M., P. Speight, D. Little, C. Di Ciano-Oliveira, K. Szaszi and A. Kapus (2018). "Mediated nuclear import and export of TAZ and the underlying molecular requirements." *Nat Commun* **9**(1): 4966.

Lamar, J. M., Y. Xiao, E. Norton, Z. G. Jiang, G. M. Gerhard, S. Kooner, J. S. A. Warren and R. O. Hynes (2019). "SRC tyrosine kinase activates the YAP/TAZ axis and thereby drives tumor growth and metastasis." *J Biol Chem* **294**(7): 2302-2317.

Lambert, A. W., D. R. Pattabiraman and R. A. Weinberg (2017). "Emerging Biological Principles of Metastasis." *Cell* **168**(4): 670-691.

Laurent-Puig, P., P. Legoix, O. Bluteau, J. Belghiti, D. Franco, F. Binot, G. Monges, G. Thomas, P. Bioulac-Sage and J. Zucman-Rossi (2001). "Genetic alterations associated with hepatocellular carcinomas define distinct pathways of hepatocarcinogenesis." *Gastroenterology* **120**(7): 1763-1773.

Lee, J. S. (2015). "The mutational landscape of hepatocellular carcinoma." *Clin Mol Hepatol* **21**(3): 220-229.

Li, S., C. Li, Y. Zhang, X. He, X. Chen, X. Zeng, F. Liu, Y. Chen and J. Chen (2019). "Targeting Mechanics-Induced Fibroblast Activation through CD44-RhoA-YAP Pathway Ameliorates Crystalline Silica-Induced Silicosis." *Theranostics* **9**(17): 4993-5008.

Li, X., D. Liu, Y. Ma, X. Du, J. Jing, L. Wang, B. Xie, D. Sun, S. Sun, X. Jin, X. Zhang, T. Zhao, J. Guan, Z. Yi, W. Lai, P. Zheng, Z. Huang, Y. Chang, Z. Chai, J. Xu and H. Deng (2017). "Direct Reprogramming of Fibroblasts via a Chemically Induced XEN-like State." *Cell Stem Cell* **21**(2): 264-273 e267.

Li, X., J. Tao, A. Cigliano, M. Sini, J. Calderaro, D. Azoulay, C. Wang, Y. Liu, L. Jiang, K. Evert, M. I. Demartis, S. Ribback, K. Utpatel, F. Dombrowski, M. Evert, D. F. Calvisi and X. Chen (2015). "Co-activation of PIK3CA and Yap promotes development of hepatocellular and cholangiocellular tumors in mouse and human liver." *Oncotarget* **6**(12): 10102-10115.

Liao, Y. J., T. S. Lee, Y. C. Twu, S. M. Hsu, C. P. Yang, C. K. Wang, Y. C. Liang and Y. A. Chen (2016). "Glycine N-methyltransferase deficiency in female mice impairs insulin signaling and promotes gluconeogenesis by modulating the PI3K/Akt pathway in the liver." *J Biomed Sci* **23**(1): 69.

Lin, L., R. Amin, G. I. Gallicano, E. Glasgow, W. Jogunoori, J. M. Jessup, M. Zasloff, J. L. Marshall, K. Shetty, L. Johnson, L. Mishra and A. R. He (2009). "The STAT3 inhibitor NSC 74859 is effective in hepatocellular cancers with disrupted TGF-beta signaling." *Oncogene* **28**(7): 961-972.

Liu, F., G. Wang, X. Wang, Z. Che, W. Dong, X. Guo, Z. Wang, P. Chen, D. Hou, Q. Zhang, W. Zhang, Y. Pan, D. Yang and H. Liu (2017). "Targeting high Aurora kinases expression as an innovative therapy for hepatocellular carcinoma." *Oncotarget* **8**(17): 27953-27965.

Liu, H. H., K. H. Chen, Y. P. Shih, W. Y. Lui, F. H. Wong and Y. M. Chen (2003). "Characterization of reduced expression of glycine N-methyltransferase in cancerous hepatic tissues using two newly developed monoclonal antibodies." *J Biomed Sci* **10**(1): 87-97.

Liu, Y., D. P. Al-Adra, R. Lan, G. Jung, H. Li, M. M. Yeh and Y. Z. Liu (2022). "RNA sequencing analysis of hepatocellular carcinoma identified oxidative phosphorylation as a major pathologic feature." *Hepatol Commun* **6**(8): 2170-2181.

Liu, Y., X. Wang and Y. Yang (2020). "Hepatic Hippo signaling inhibits development of hepatocellular carcinoma." *Clin Mol Hepatol* **26**(4): 742-750.

Lokeshwar, B. L., V. B. Lokeshwar and N. L. Block (1995). "Expression of CD44 in prostate cancer cells: association with cell proliferation and invasive potential." *Anticancer Res* **15**(4): 1191-1198.

Lu, L., M. J. Finegold and R. L. Johnson (2018). "Hippo pathway coactivators Yap and Taz are required to coordinate mammalian liver regeneration." *Exp Mol Med* **50**(1): e423.

Malumbres, M., E. Harlow, T. Hunt, T. Hunter, J. M. Lahti, G. Manning, D. O. Morgan, L. H. Tsai and D. J. Wolgemuth (2009). "Cyclin-dependent kinases: a family portrait." *Nat Cell Biol* **11**(11): 1275-1276.

Margherita Correnti, R. Booiijink, G. D. Maira, C. Raggi and F. Marra (2018). "Stemness features in liver cancer." *Hepatoma Res* **2018**;4:69.

Marhaba, R. and M. Zoller (2004). "CD44 in cancer progression: adhesion, migration and growth regulation." *J Mol Histol* **35**(3): 211-231.

Marrero, J. A., R. J. Fontana, A. Barrat, F. Askari, H. S. Conjeevaram, G. L. Su and A. S. Lok (2005). "Prognosis of hepatocellular carcinoma: comparison of 7 staging systems in an American cohort." *Hepatology* **41**(4): 707-716.

Marrero, J. A., H. K. Hussain, H. V. Nghiem, R. Umar, R. J. Fontana and A. S. Lok (2005). "Improving the prediction of hepatocellular carcinoma in cirrhotic patients with an arterially-enhancing liver mass." *Liver Transpl* **11**(3): 281-289.

Mauad, T. H., C. M. van Nieuwkerk, K. P. Dingemans, J. J. Smit, A. H. Schinkel, R. G. Notenboom, M. A. van den Bergh Weerman, R. P. Verkruijsen, A. K. Groen, R. P. Oude Elferink and et al. (1994). "Mice with homozygous disruption of the *mdr2* P-glycoprotein gene. A novel animal model for studies of nonsuppurative inflammatory cholangitis and hepatocarcinogenesis." *Am J Pathol* **145**(5): 1237-1245.

Mercer, K. E., L. Hennings and M. J. Ronis (2015). "Alcohol consumption, Wnt/beta-catenin signaling, and hepatocarcinogenesis." *Adv Exp Med Biol* **815**: 185-195.

Miletti-Gonzalez, K. E., K. Murphy, M. N. Kumaran, A. K. Ravindranath, R. P. Wernyj, S. Kaur, G. D. Miles, E. Lim, R. Chan, M. Chekmareva, D. S. Heller, D. Foran, W. Chen, M. Reiss, E. V. Bandera, K. Scotto and L. Rodriguez-Rodriguez (2012). "Identification of function for CD44 intracytoplasmic domain (CD44-ICD): modulation of matrix metalloproteinase 9 (MMP-9) transcription via novel promoter response element." *J Biol Chem* **287**(23): 18995-19007.

Mima, K., H. Okabe, T. Ishimoto, H. Hayashi, S. Nakagawa, H. Kuroki, K. Miyake, H. Takamori, T. Beppu and H. Baba (2012). "The expression levels of CD44v6 are correlated with the invasiveness of hepatocellular carcinoma in vitro, but do not appear to be clinically significant." *Oncol Lett* **3**(5): 1047-1051.

Mirabelli, P., L. Coppola and M. Salvatore (2019). "Cancer Cell Lines Are Useful Model Systems for Medical Research." *Cancers (Basel)* **11**(8).

Mitaka, T., N. Ichinohe and N. Tanimizu (2023). "Small Hepatocytes" in the Liver." *Cells* **12**(23).

Mondal, T., G. N. Shivange, R. G. Tihagam, E. Lyerly, M. Battista, D. Talwar, R. Mosavian, K. Urbanek, N. S. Rashid, J. C. Harrell, P. D. Bos, E. B. Stelow, M. S. Stack, S. Bhatnagar and J. Tushir-Singh (2021). "Unexpected PD-L1 immune evasion mechanism in TNBC, ovarian, and other solid tumors by DR5 agonist antibodies." *EMBO Mol Med* **13**(3): e12716.

Montironi, C., F. Castet, P. K. Haber, R. Pinyol, M. Torres-Martin, L. Torrens, A. Mesropian, H. Wang, M. Puigvehi, M. Maeda, W. Q. Leow, E. Harrod, P. Taik, J. Chinburen, E. Taivanbaatar, E. Chinbold, M. Sole Arques, M. Donovan, S. Thung, J. Neely, V. Mazzaferro, J. Anderson, S. Roayaie, M. Schwartz, A. Villanueva, S. L. Friedman, A. Uzilov, D. Sia and J. M. Llovet (2023). "Inflamed and non-inflamed classes of HCC: a revised immunogenomic classification." *Gut* **72**(1): 129-140.

Morton, J. J., G. Bird, Y. Refaeli and A. Jimeno (2016). "Humanized Mouse Xenograft Models: Narrowing the Tumor-Microenvironment Gap." *Cancer Res* **76**(21): 6153-6158.

Murakami, H., N. D. Sanderson, P. Nagy, P. A. Marino, G. Merlino and S. S. Thorgeirsson (1993). "Transgenic mouse model for synergistic effects of nuclear oncogenes and growth factors in tumorigenesis: interaction of c-myc and transforming growth factor alpha in hepatic oncogenesis." *Cancer Res* **53**(8): 1719-1723.

Nault, J. C., M. Ningarhari, S. Rebouissou and J. Zucman-Rossi (2019). "The role of telomeres and telomerase in cirrhosis and liver cancer." *Nat Rev Gastroenterol Hepatol* **16**(9): 544-558.

Pavel, M., M. Renna, S. J. Park, F. M. Menzies, T. Ricketts, J. Fullgrabe, A. Ashkenazi, R. A. Frake, A. C. Lombarte, C. F. Bento, K. Franze and D. C. Rubinsztein (2018). "Contact inhibition controls cell survival and proliferation via YAP/TAZ-autophagy axis." *Nat Commun* **9**(1): 2961.

Petrick, J. L., A. A. Florio, A. Znaor, D. Ruggieri, M. Laversanne, C. S. Alvarez, J. Ferlay, P. C. Valery, F. Bray and K. A. McGlynn (2020). "International trends in hepatocellular carcinoma incidence, 1978-2012." *Int J Cancer* **147**(2): 317-330.

Ponta, H., L. Sherman and P. A. Herrlich (2003). "CD44: from adhesion molecules to signalling regulators." *Nat Rev Mol Cell Biol* **4**(1): 33-45.

Reig, M., A. Forner, J. Rimola, J. Ferrer-Fabrega, M. Burrel, A. Garcia-Criado, R. K. Kelley, P. R. Galle, V. Mazzaferro, R. Salem, B. Sangro, A. G. Singal, A. Vogel, J. Fuster, C. Ayuso and J. Bruix (2022). "BCLC strategy for prognosis prediction and treatment recommendation: The 2022 update." *J Hepatol* **76**(3): 681-693.

Reuven, N., M. Shanzer and Y. Shaul (2019). "Hippo Pathway Regulation by Tyrosine Kinases." *Methods Mol Biol* **1893**: 215-236.

Richmond, A. and Y. Su (2008). "Mouse xenograft models vs GEM models for human cancer therapeutics." *Dis Model Mech* **1**(2-3): 78-82.

Rosenbluh, J., D. Nijhawan, A. G. Cox, X. Li, J. T. Neal, E. J. Schafer, T. I. Zack, X. Wang, A. Tsherniak, A. C. Schinzel, D. D. Shao, S. E. Schumacher, B. A. Weir, F. Vazquez, G. S. Cowley, D. E. Root, J. P. Mesirov, R. Beroukhim, C. J. Kuo, W. Goessling and W. C. Hahn (2012). "beta-Catenin-driven cancers require a YAP1 transcriptional complex for survival and tumorigenesis." *Cell* **151**(7): 1457-1473.

Rozeik, M. S., O. A. Hammam, A. I. Ali, M. Magdy, H. Khalil, A. Anas, A. A. Abo El Hassan, A. A. Rahim and A. I. El-Shabasy (2017). "Evaluation of CD44 and CD133 as markers of liver cancer stem cells in Egyptian patients with HCV-induced chronic liver diseases versus hepatocellular carcinoma." *Electron Physician* **9**(7): 4708-4717.

Rubin, S. M., A. L. Gall, N. Zheng and N. P. Pavletich (2005). "Structure of the Rb C-terminal domain bound to E2F1-DP1: a mechanism for phosphorylation-induced E2F release." *Cell* **123**(6): 1093-1106.

Sandgren, E. P., C. J. Quaife, C. A. Pinkert, R. D. Palmiter and R. L. Brinster (1989). "Oncogene-induced liver neoplasia in transgenic mice." *Oncogene* **4**(6): 715-724.

Schollenberger, L., T. Gronemeyer, C. M. Huber, D. Lay, S. Wiese, H. E. Meyer, B. Warscheid, R. Saffrich, J. Peranen, K. Gorgas and W. W. Just (2010). "RhoA regulates peroxisome association to microtubules and the actin cytoskeleton." *PLoS One* **5**(11): e13886.

Schulze, K., S. Imbeaud, E. Letouze, L. B. Alexandrov, J. Calderaro, S. Rebouissou, G. Couchy, C. Meiller, J. Shinde, F. Soysouvanh, A. L. Calatayud, R. Pinyol, L. Pelletier, C. Balabaud, A. Laurent, J. F. Blanc, V. Mazzaferro, F. Calvo, A. Villanueva, J. C. Nault, P. Bioulac-Sage, M. R. Stratton, J. M. Llovet and J. Zucman-Rossi (2015). "Exome sequencing of hepatocellular carcinomas identifies new mutational signatures and potential therapeutic targets." *Nat Genet* **47**(5): 505-511.

Shannon, A. H., S. M. Ruff and T. M. Pawlik (2022). "Expert Insights on Current Treatments for Hepatocellular Carcinoma: Clinical and Molecular Approaches and Bottlenecks to Progress." *J Hepatocell Carcinoma* **9**: 1247-1261.

Shen, S., D. C. Dean, Z. Yu and Z. Duan (2019). "Role of cyclin-dependent kinases (CDKs) in hepatocellular carcinoma: Therapeutic potential of targeting the CDK signaling pathway." *Hepatol Res* **49**(10): 1097-1108.

Shiao, S. L., A. P. Ganesan, H. S. Rugo and L. M. Coussens (2011). "Immune microenvironments in solid tumors: new targets for therapy." *Genes Dev* **25**(24): 2559-2572.

Song, S., M. Xie, A. W. Scott, J. Jin, L. Ma, X. Dong, H. D. Skinner, R. L. Johnson, S. Ding and J. A. Ajani (2018). "A Novel YAP1 Inhibitor Targets CSC-Enriched Radiation-Resistant Cells and Exerts Strong Antitumor Activity in Esophageal Adenocarcinoma." *Mol Cancer Ther* **17**(2): 443-454.

Strassburger, K., M. Tiebe, F. Pinna, K. Breuhahn and A. A. Teleman (2012). "Insulin/IGF signaling drives cell proliferation in part via Yorkie/YAP." *Dev Biol* **367**(2): 187-196.

Sugihara, T., N. W. Werneburg, M. C. Hernandez, L. Yang, A. Kabashima, P. Hirsova, L. Yohanathan, C. Sosa, M. J. Truty, G. Vasmatzis, G. J. Gores and R. L. Smoot (2018). "YAP Tyrosine Phosphorylation and Nuclear Localization in Cholangiocarcinoma Cells Are Regulated by LCK and Independent of LATS Activity." *Mol Cancer Res* **16**(10): 1556-1567.

Sullivan, N. J., A. K. Sasser, A. E. Axel, F. Vesuna, V. Raman, N. Ramirez, T. M. Oberyszyn and B. M. Hall (2009). "Interleukin-6 induces an epithelial-mesenchymal transition phenotype in human breast cancer cells." *Oncogene* **28**(33): 2940-2947.

Suwannakul, N., N. Ma, R. Thanan, S. Pinlaor, P. Ungarreevittaya, K. Midorikawa, Y. Hiraku, S. Oikawa, S. Kawanishi and M. Murata (2018). "Overexpression of CD44 Variant 9: A Novel Cancer Stem Cell Marker in Human Cholangiocarcinoma in Relation to Inflammation." *Mediators Inflamm* **2018**: 4867234.

Takeda, H., A. Takai, Y. Eso, K. Takahashi, H. Marusawa and H. Seno (2022). "Genetic Landscape of Multistep Hepatocarcinogenesis." *Cancers (Basel)* **14**(3).

Tamm, C., N. Bower and C. Anneren (2011). "Regulation of mouse embryonic stem cell self-renewal by a Yes-YAP-TEAD2 signaling pathway downstream of LIF." *J Cell Sci* **124**(Pt 7): 1136-1144.

Tang, A., O. Hallouch, V. Chernyak, A. Kamaya and C. B. Sirlin (2018). "Epidemiology of hepatocellular carcinoma: target population for surveillance and diagnosis." *Abdom Radiol (NY)* **43**(1): 13-25.

Taniguchi, K., T. Moroishi, P. R. de Jong, M. Krawczyk, B. M. Grebbin, H. Luo, R. H. Xu, N. Golob-Schwarzl, C. Schweiger, K. Wang, G. Di Caro, Y. Feng, E. R. Fearon, E. Raz, L. Kenner, H. F. Farin, K. L. Guan, J. Haybaeck, C. Datz, K. Zhang and M. Karin (2017). "YAP-IL-6ST autoregulatory loop activated on APC loss controls colonic tumorigenesis." *Proc Natl Acad Sci U S A* **114**(7): 1643-1648.

Tao, J., D. F. Calvisi, S. Ranganathan, A. Cigliano, L. Zhou, S. Singh, L. Jiang, B. Fan, L. Terracciano, S. Armeanu-Ebinger, S. Ribback, F. Dombrowski, M. Evert, X. Chen and S. P. S. Monga (2014). "Activation of beta-catenin and Yap1 in human hepatoblastoma and induction of hepatocarcinogenesis in mice." *Gastroenterology* **147**(3): 690-701.

Tsubaki, M., S. Genno, T. Takeda, T. Matsuda, N. Kimura, Y. Yamashita, Y. Morii, K. Shimomura and S. Nishida (2021). "Rhosin Suppressed Tumor Cell Metastasis through Inhibition of Rho/YAP Pathway and Expression of RHAMM and CXCR4 in Melanoma and Breast Cancer Cells." *Biomedicines* **9**(1).

Tumen, D., P. Heumann, K. Gulow, C. N. Demirci, L. S. Cosma, M. Muller and A. Kandulski (2022). "Pathogenesis and Current Treatment Strategies of Hepatocellular Carcinoma." *Biomedicines* **10**(12).

Viatour, P., U. Ehmer, L. A. Saddic, C. Dorrell, J. B. Andersen, C. Lin, A. F. Zmoos, P. K. Mazur, B. E. Schaffer, A. Ostermeier, H. Vogel, K. G. Sylvester, S. S. Thorgeirsson, M. Grompe and J. Sage (2011). "Notch signaling inhibits hepatocellular carcinoma following inactivation of the RB pathway." *J Exp Med* **208**(10): 1963-1976.

Wang, J., B. Zhang, H. Wu, J. Cai, X. Sui, Y. Wang, H. Li, Y. Qiu, T. Wang, Z. Chen, Q. Zhu, H. Xia, W. Song and A. P. Xiang (2017). "CD51 correlates with the TGF-beta pathway and is a functional marker for colorectal cancer stem cells." *Oncogene* **36**(10): 1351-1363.

Watanabe, S., Y. Horie, E. Kataoka, W. Sato, T. Dohmen, S. Ohshima, T. Goto and A. Suzuki (2007). "Non-alcoholic steatohepatitis and hepatocellular carcinoma: lessons from hepatocyte-specific phosphatase and tensin homolog (PTEN)-deficient mice." *J Gastroenterol Hepatol* **22 Suppl 1**: S96-S100.

Wei, Y., Y. Jiang, F. Zou, Y. Liu, S. Wang, N. Xu, W. Xu, C. Cui, Y. Xing, Y. Liu, B. Cao, C. Liu, G. Wu, H. Ao, X. Zhang and J. Jiang (2013). "Activation of PI3K/Akt pathway by CD133-p85 interaction promotes tumorigenic capacity of glioma stem cells." *Proc Natl Acad Sci U S A* **110**(17): 6829-6834.

Weiler, S. M. E., F. Pinna, T. Wolf, T. Lutz, A. Geldiyev, C. Sticht, M. Knaub, S. Thomann, M. Bissinger, S. Wan, S. Rossler, D. Becker, N. Gretz, H. Lang, F. Bergmann, V. Ustiyani, T. V. Kalin, S. Singer, J. S. Lee, J. U. Marquardt, P. Schirmacher, V. V. Kalinichenko and K. Breuhahn (2017). "Induction of Chromosome Instability by Activation of Yes-Associated Protein and Forkhead Box M1 in Liver Cancer." *Gastroenterology* **152**(8): 2037-2051 e2022.

Woerner, S. M., M. Givchian, M. Durst, A. Schneider, S. Costa, P. Melsheimer, J. Lacroix, M. Zoller and M. K. Doeberitz (1995). "Expression of CD44 splice variants in normal, dysplastic, and neoplastic cervical epithelium." *Clin Cancer Res* **1**(10): 1125-1132.

Xiao, Y. S., Zeng, Y. K. Liang, Y. Wu, M. F. Li, Y. Z. Qi, X. L. Wei, W. H. Huang, M. Chen and G. J. Zhang (2019). "Major vault protein is a direct target of Notch1 signaling and contributes to chemoresistance in triple-negative breast cancer cells." *Cancer Lett* **440-441**: 156-167.

Xin, B., Y. Cui, Y. Wang, L. Wang, J. Yin, L. Zhang, H. Pang, H. Zhang and R. A. Wang (2017). "Combined use of alcohol in conventional chemical-induced mouse liver cancer model improves the simulation of clinical characteristics of human hepatocellular carcinoma." *Oncol Lett* **14**(4): 4722-4728.

Xu, Y., I. Stamenkovic and Q. Yu (2010). "CD44 attenuates activation of the hippo signaling pathway and is a prime therapeutic target for glioblastoma." *Cancer Res* **70**(6): 2455-2464.

Yamashita, T. and X. W. Wang (2013). "Cancer stem cells in the development of liver cancer." *J Clin Invest* **123**(5): 1911-1918.

Yan, Y., Q. Song, L. Yao, L. Zhao and H. Cai (2022). "YAP Overexpression in Breast Cancer Cells Promotes Angiogenesis through Activating YAP Signaling in Vascular Endothelial Cells." *Anal Cell Pathol (Amst)* **2022**: 5942379.

Yimlamai, D., C. Christodoulou, G. G. Galli, K. Yanger, B. Pepe-Mooney, B. Gurung, K. Shrestha, P. Cahan, B. Z. Stanger and F. D. Camargo (2014). "Hippo pathway activity influences liver cell fate." *Cell* **157**(6): 1324-1338.

Zhang, H. E., J. M. Henderson and M. D. Gorrell (2019). "Animal models for hepatocellular carcinoma." *Biochim Biophys Acta Mol Basis Dis* **1865**(5): 993-1002.

Zhang, S. and D. Zhou (2019). "Role of the transcriptional coactivators YAP/TAZ in liver cancer." *Curr Opin Cell Biol* **61**: 64-71.

Zhang, Y., H. Xia, X. Ge, Q. Chen, D. Yuan, Q. Chen, W. Leng, L. Chen, Q. Tang and F. Bi (2014). "CD44 acts through RhoA to regulate YAP signaling." *Cell Signal* **26**(11): 2504-2513.

Zhang, Z., J. Du, S. Wang, L. Shao, K. Jin, F. Li, B. Wei, W. Ding, P. Fu, H. van Dam, A. Wang, J. Jin, C. Ding, B. Yang, M. Zheng, X. H. Feng, K. L. Guan and L. Zhang (2019). "OTUB2 Promotes Cancer Metastasis via Hippo-Independent Activation of YAP and TAZ." *Mol Cell* **73**(1): 7-21 e27.

Zhao, B., X. Wei, W. Li, R. S. Udan, Q. Yang, J. Kim, J. Xie, T. Ikenoue, J. Yu, L. Li, P. Zheng, K. Ye, A. Chinnaiyan, G. Halder, Z. C. Lai and K. L. Guan (2007). "Inactivation of YAP oncoprotein by the Hippo pathway is involved in cell contact inhibition and tissue growth control." *Genes Dev* **21**(21): 2747-2761.

Zhu, H., F. Yan, T. Yuan, M. Qian, T. Zhou, X. Dai, J. Cao, M. Ying, X. Dong, Q. He and B. Yang (2020). "USP10 Promotes Proliferation of Hepatocellular Carcinoma by Deubiquitinating and Stabilizing YAP/TAZ." *Cancer Res* **80**(11): 2204-2216.

Zhu, J., T. Wu and Q. Lin (2023). "Non-hippo kinases: indispensable roles in YAP/TAZ signaling and implications in cancer therapy." *Mol Biol Rep* **50**(5): 4565-4578.